Charge Separation and Transfer in Hybrid Type II Tunneling Structures of CdTe and CdSe Nanocrystals

Dieter GROSS

Dissertation
an der Fakultät für Physik
Ludwig-Maximilians-Universität München

Vorgelegt von
Dieter Konrad Michael Groß
aus Feuchtwangen

München, im August 2013

Erstgutachter: Professor Dr. Jochen Feldmann
Zweitgutachter: Privatdozent Dr. Thomas Dittrich
Tag der mündlichen Prüfung: 08. November 2013

Scientific Publications of Results Presented in this Thesis

- **Dieter Gross**, Ivan Mora-Sero, Thomas Dittrich, Abdelhak Belaidi, Christian Mauser, Arjan J. Houtepen, Enrico Da Como, Andrey L. Rogach, Jochen Feldmann.
  Charge separation in type II tunneling multilayered structures of CdTe and CdSe nanocrystals directly proven by surface photovoltage spectroscopy.
  Journal of the American Chemical Society, 132(17):5981-5983, 2010.

- **Dieter Gross**, Andrei S. Susha, Thomas A. Klar, Enrico Da Como, Andrey L. Rogach, Jochen Feldmann.
  Charge separation in type II tunneling structures of close-packed CdTe and CdSe nanocrystals.
  Nano Letters, 8(5):1482-1485, 2008.

Additional Publications

- Sixto Giménez, Andrey L. Rogach, Andrey A. Lutich, **Dieter Gross**, Andreas Pöschl, Andrei S. Susha, Iván Mora-Seró, Teresa Lana-Villarreal, Juan Bisquert.
  Energy transfer versus charge separation in hybrid systems of semiconductor quantum dots and Ru-dyes as potential co-sensitizers of TiO2-based solar cells.
  Journal of Applied Physics, 110(1):014314, 2011.

- Iván Mora-Seró, **Dieter Gross**, Tobias Mittereder, Andrey A. Lutich, Andrei S. Susha, Thomas Dittrich, Abdelhak Belaidi, Ruben Caballero, Fernando Langa, Juan Bisquert, Andrey L. Rogach.
  Nanoscale interaction between CdSe or CdTe nanocrystals and molecular dyes fostering or hindering directional charge separation.
  Small, 6(2):221-225, 2010.

- L. Weinhardt, O. Fuchs, **D. Groß**, E. Umbach, C. Heske, N. G. Dhere, A. A. Kadam, and S. S. Kulkarni. *Surface modifications of Cu(In,Ga)S_2 thin film solar cell absorbers by KCN and H_2O_2/H_2SO_4 treatments.* Journal of applied physics, 100:024907, 2006.

- L. Weinhardt, O. Fuchs, **D. Groß**, G. Storch, E. Umbach, N. G. Dhere, A. A. Kadam, S. S. Kulkarni, and C. Heske. *Band alignment at the CdS/Cu(In,Ga)S_2 interface in thin-film solar cells.*
  Applied Physics Letters, 86(6):062109, 2005.

Contributions to Conferences and Workshops

- **Dieter Gross**, Iván Mora Seró, Thomas Dittrich, Andrei S. Susha, Enrico Da Como, Andrey L. Rogach, Jochen Feldmann.
  Charge diffusion in layered structures of CdTe and CdSe nanocrystals evidenced by surface photovoltage experiments.
  Conference: Nanax 4, Munich/Tutzing (Germany), A24, April 2010.

- **Dieter Groß**.
  Energy and charge transfer in layered nanocrystal structures.
  Workshop: New Concepts in Nanophotonics, Garmisch-Partenkirchen (Germany), November 2009.

- **Dieter Gross**, Iván Mora Seró, Thomas Dittrich, Andrei S. Susha, Enrico Da Como, Andrey L. Rogach, Jochen Feldmann.
  Charge separation in self-assembled type II tunneling structures of CdTe and CdSe nanocrystals.
  Conference: Spie Optics and Photonics 2009, San Diego (Carlifornia, USA), 7393-01, August 2009.

- **Dieter Gross**, Sergiy Mayilo, Iván Mora-Seró, Thomas Dittrich, Andrei S. Susha, Andrey L. Rogach, Enrico Da Como, Jochen Feldmann.
  Light harvesting, charge separation and diffusion in self-assembled nanostructures of CdTe and CdSe nanocrystals.
  Conference: Light-Harvesting Processes 2009, Banz (Germany), P19, March 2009.

- **Dieter Gross**, Iván Mora Seró, Thomas Dittrich, Andrei S. Susha, Andrey L. Rogach, Enrico Da Como, Jochen Feldmann.
  Charge delocalization and separation in type II tunneling structures of CdTe and CdSe nanocrystals by surface photovoltage spectroscopy.
  Conference: The 237th ACS National Meeting, Salt Lake City (Utah, USA), PHYS 394, March 2009

- **Dieter Groß**, Andrei S. Susha, Thomas A. Klar, Enrico Da Como, Andrey L. Rogach, Jochen Feldmann.
  Charge separation between type II aligned closed packed CdTe and CdSe nanocrystals.
  Workshop: Interactions in Hybrid Nanosystems, Frauenwörth (Germany), May 2008

- **Dieter Groß**, Andrei S. Susha, Thomas A. Klar, Andrey L. Rogach, Jochen Feldmann.
  Charge separation between type II aligned closed packed CdTe and CdSe nanocrystals.
  Conference: DPG-Frühjahrstagung 2008, Berlin (Germany), MM 23.38, Febuary 2008.

- **Dieter Groß**.
  Closed packed nano crystals for cascaded energy transfer and charge separation.
  Workshop: Nano for Lifescience, Riezlern (Austria), June 2007.

Contents

Publication List iii

Contents vii

Zusammenfassung ix

1 Introduction 1

2 Fundamental Concepts in Nanosciences 5

2.1 Type II Tunneling Structure 5

2.2 Semiconductor Nanocrystals 7

2.2.1 Quantum Confinement 8

2.2.2 Crystal Structure for CdTe and CdSe Semiconductors 9

2.2.3 CdTe and CdSe Nanocrystals 12

2.3 Physical Processes in Nanostructures 16

2.3.1 Photo-Excitation 17

2.3.2 Radiative and Non-Radiative Decay 18

2.3.3 Charge Transfer between Nanocrystals 20

2.3.4 Energy Transfer 21

2.3.5 Diffusion 23

3 Experimental Details and Methods 26

3.1 Experimental Details on Semiconductor Nanocrystals 26

3.1.1 Water Based Synthesis of CdTe and CdSe Nanocrystals 26

3.1.2 Size Characterization of CdTe and CdSe Nanocrystals 27

3.1.3 Stokes Shift for the CdTe Nanocrystals Used 30

3.2 Assembly Methods 30

3.2.1 Layer-by-Layer Assembly 31

3.2.2 Colloidal Clustering 34

3.3 Spectroscopy 35

3.3.1 Extinction Spectroscopy 35

3.3.2 Photoluminescence Spectroscopy 37

3.3.3 Surface Photovoltage 40

4 Charge Separation between CdTe and CdSe Nanocrystals 44
4.1 Experimental System 44
4.2 Photoluminescence Quenching Indicating Charge Separation 45
4.2.1 Clustered System 46
4.2.2 Layered System 49
4.3 Correlation of PL-Quenching and Energetic Offset of Electron States . . 56
4.4 Discussion 60

5 Directional Charge Separation and Diffusion for Layered CdTe and CdSe Nanocrystals 64
5.1 Experimental System 64
5.2 Directional Charge Separation 65
5.3 Suppression of Charge Separation at Increased Barrier Width 70
5.4 Diffusion in Layered Semiconductor Nanocrystal Assemblies 72
5.5 Discussion 76

6 Conclusions and Outlook 82

Bibliography 84

Acknowledgments 98

Zusammenfassung

Halbleiter-Nanokristalle sind eine besondere Materialklasse in den Nanowissenschaften. Sie sind kleinste Halbleiter-Kristalle, die an ihrer Oberfläche mittels organischer Chemie passiviert wurden. Damit können Sie auf völlig neue Arten produziert, prozessiert und zu größeren hybriden Überstrukturen zusammengesetzt werden. In diesen Nanomaterialien treten neue Effekte insbesondere durch die Größeneinschränkung auf. Es stellt sich vielfach die Frage, welche Eigenschaften von den Halbleiter-Materialien übernommen werden und was alleine aufgrund der geometrischen Größenordnung im Nanometerbereich von 1-10 nm zustande kommt.

Diese Arbeit beschäftigt sich mit dem Nachweis von elektronischem Transfer über eine quantenmechanische Tunnelbarriere aus organischen Materialien zwischen dicht gepackten Halbleiternanokristallen. Diese Barriere besteht aus Molekülen der Oberflächenpassivierung und Material für die gewählten Selbstorganisationsmethoden, so dass eine organische Tunnelbarriere von ca. 1 nm zwischen den Nanokristallen der Größe von ca. 3 nm entsteht. Um elektronischen Tunnel-Transfer nachzuweisen, wird erfolgreich der intrinsische Typ-II-Bandversatz der klassischen ausgedehnten CdTe- und CdSe-Volumenhalbleitern ausgenutzt, der bedeutet, dass das globale Valenzbandmaximum in CdSe und das Leitungsbandminium in CdTe liegen. Es ist daher Hauptziel der Arbeit, Ladungstrennung in Hybridstrukturen aus dicht gepackten Typ-II-angeordneten CdTe- und CdSe- Halbleiternanokristallen nachzuweisen.

Mittels Photolumineszenzspektroskopie wurde indirekt der Elektronenübergang von CdTe- zu CdSe-Nanokristallen untersucht. Es wurden zwei verschiedene Methoden zur Selbstorganisation überprüft: ungeordnete Cluster aus CdTe- und CdSe-Nanokristallen in wässriger Lösung sowie trockene geschichtete Systeme aus Nanokristall-Monolagen auf Glassubstraten. In beiden Probensystemen deutet eine Photolumineszenzunterdrückung um bis zu 70 % bei den CdTe-Nanokristallen Ladungstrennung durch Elektronenübergang von CdTe- zu CdSe-Nanokristallen an. Eine maximale Transferrate von um 1/100 ps wurde in geschichteten Proben ermittelt. Neben dem Elektronentransfer wurde gezeigt, dass Energietransfer von CdSe- zu CdTe-Nanokristallen stattfindet, der nicht die beobachtete Photolumineszenzunterdrückung erklärt, da er ihr entgegenwirkt. Durch Variation der Nanokristallgrößen konnte eine Korrelation der Photolumineszenzunterdrückung mit dem Versatz der am Elektronentransfer beteiligten Energieniveaus der Nanokristalle aufgedeckt werden. Durch diese indirekten Beweise konnte die Ladungstrennung wie auch der intrinsische Typ-II-Versatz in den Hybridsystemen der verwendeten CdTe- und CdSe-Nanokristallen angezeigt werden.

Oberflächenphotospannungsmessungen bewiesen eindeutig die gerichtete Ladungs–trennung in geschichteten Systemen aus CdTe und CdSe Nanokristallen. Die Orientierung der Typ II-Grenzschicht aus CdTe- und CdSe-Nanokristalllagen bestimmte die Richtung der Ladungstrennung, so dass eine umgekehrte Schichtfolge die gemessene Polarität änderte. Der Ladungstransfer wird fast vollständig unterdrückt, wenn die Barrierendicke verdoppelt wird, was für Tunneltransfer erwartet wird. Weiterhin wurden Elektronendiffusion über CdSe-Nanokristallmultischichten und langsamerer Ladungstransfer über CdTe-Nanokristallmultischichten nachgewiesen.

Die Ergebnisse dieser Arbeit könnten für Anwendungen zur solaren Energiegewinnung wie Photovoltaik oder photokatalytischer Wasserspaltung relevant sein.

1 Introduction

Semiconductor nanocrystals are a unique type of material in nanosciences as they feature properties and concepts from both classical crystalline semiconductor physics and new nanomaterials such as organic molecules. Versatile processing and assembly capabilities offer great potential for a wide range of future applications such as solar energy conversion [1–9] as well as various other applications in optoelectronics particularly light-emitting diodes, lasers, or displays for instance. [10–16] Different semiconductor nanocrystals can be assembled into hybrid nanostructures by self-organization to study their interaction in order to customize new functionalities. Closely packed hybrid assembly of the semiconductor nanocrystals can be achieved particularly in dry layers [16–20] and as disordered assemblies in solutions [21, 22]. The semiconductor nanocrystals are surrounded by organic molecules which inhibit further chemical reaction on the surfaces of the semiconductor nanocrystals. Moreover, these surface ligands feature the ability for self-assembly techniques mentioned above. With respect to electronic transport properties these ligands are in principle isolating. However, their thin thickness in the range of 1 nm allows them to act as tunneling barriers for transport between two semiconductor nanoparticles. The main topic of my thesis was to observe efficient electronic transfer dynamics across the organic barriers of closely packed semiconductor nanocrystals.

A wide variety of semiconductor materials is available which are chemically synthesized as colloidal semiconductor nanocrystal solutions. II-VI materials in particular, such as CdS, CdSe, CdTe, CdHgTe, HgTe, ZnSe, PbS and PbSe [23–27] are used in many experiments. III-V materials such as InP, GaP, InAs, GaAs can also be produced. [28, 29] Assemblies of CdTe and CdSe nanocrystals are good prototype systems which can be used to study electronic interactions in their hybrid assembly. CdTe and CdSe bulk semiconductors exhibit intrinsically the so-called type II alignment, meaning that the lowest electronic state for excited electrons is in CdSe, and that for holes in CdTe. Thus, spacial charge separation can be observed in suitable assemblies of these materials. This concept is approved by sintered layered system of CdTe and CdSe nanoparticles [1] and direct chemically-assembled hybrid semiconductor nanostructures [30–34]. Such assemblies are often called ”hybrid” which means literally ”crossbreeds” of different materials. They are assembled so that advantage

can be taken of precisely selected properties of all the materials used. This allows new functional materials with new properties to be formed.

Charge-carrier transfer dynamics at a type II aligned interface of CdTe and CdSe nanocrystals leads to charge separation of photo-excited electron-hole pairs. [1] Charge separation together with absorption of the light is one of most important processes for solar energy conversion. There are several methods that can be used to reveal charge separation of photo-excited charge carriers in structures of semiconductor nanocrystals. The creation of a working solar cell with these materials is a clear indication. [1, 4] Also photo-current measurements already showed charge separation in hybrid systems with semiconductor nanocrystals. [12, 35] Moreover, transport, related to free charge carriers and photo-excited electron-hole pairs, was already observed across layers of semiconductor nanocrystals. [36–40] However, the experiments mentioned are direct measurements involving direct electrical contact with the nanosystems which interact with the semiconductor nanocrystals and disturb the whole nanoparticle system. Direct electric contacts are generally not applicable to nanosystems where charge separation occurs between semiconductor nanocrystals of about 3 nm in size which cannot be contacted easily. Surface photovoltage (SPV) spectroscopy is however a tool that allows contactless observation of photoinduced charge separation. [41–44] This is based on measuring the electric dipole fields of separated electrons and holes.

Nanocrystals feature highly efficient individual photoluminescence (PL) emission which can be customized due to the remarkable properties of quantum confinement. [10] Thus, PL-spectroscopy can be used to detect separation of photoexcited electron hole pairs since it quenches the characteristic PL-emission of these semiconductor nanocrystals. PL-spectroscopy has already been used to successfully prove energy transfer dynamics [45,46] in hybrid type I aligned assemblies of semiconductor nanocrystals. Using optical spectroscopy transfer rates of up to $1/50\ ps$ were observed. [17, 19, 20, 47, 48] Since the typical size of semiconductor nanocrystals is usually 2 - 5 nm Förster Resonant Energy Transfer (FRET) [45] appears in their closely packed assemblies. FRET is relevant for transfer distances of under 6 nm according to reference [49] and therefore is an alternative transfer dynamic that must be considered in hybrid closely packed semiconductor nanocrystal assemblies.

For this thesis we studied hybrid closely packed assemblies of CdTe nanocrystals and CdSe nanocrystals. I used the expected type II alignment of these materials to create a charge selective interface to promote charge separation across an organic tunneling barrier of about 1 nm. The purpose of my investigations was to prove unequivocally that efficient charge separation occurs in closely packed CdTe-CdSe assemblies. We proved the occurrence of charge separation via fast and efficient electronic transfer across the barrier, implying the relevance of electronic transfer between semiconductor nanocrys-

tals surrounded by a tiny isolating shell. This confirmed that relative energetic levels can be easily determined by the quantum confinement theory using the effective mass approach. During this work we observed that charge separation affects not just the small interface of one CdTe and one CdSe nanocrystal monolayer. In this connection, diffusion phenomena for self-assembled multilayers of semiconductor nanocrystals, passivated with ligands of thioglycolic acid (shell thickness 0.1 - 0.2 nm; [50]) are discussed in the end of my thesis.

PL-spectroscopy indicates efficient electron transfer from CdTe nanocrystals to CdSe nanocrystals with a maximum transfer rate of $1/100\ ps$. The results have been proved using SPV-spectroscopy where the directionality of the charge separation was clearly revealed on the interface of the CdTe-CdSe nanocrystal. Furthermore, the SPV-results indicate diffusion processes across multilayers of of CdSe and CdTe nanocrystals.

Chapter 2 describes the fundamental concepts required to understand the methods and results presented. First of all, the term "type II aligned tunneling structure" is defined. The difference between type I and type II alignment is explained, as only type II structures can lead to efficient charge separation. The CdTe and CdSe nanocrystals are introduced as size confined semiconductors before the physical processes in hybrid nano-assemblies are addressed: here, we describe photo-excitation, PL, electron transfer, energy transfer and diffusion dynamics including the formula on which the experimental data-evaluation is based.

Experimental details are provided in chapter 3. The synthesis and characteristics are documented for the semiconductor nanocrystals used. The following section is dedicated to the methods used to achieve closely packing of the colloidal semiconductor nanocrystals. The layer-by-layer method uses positively charged polyelectrolytes to form layer-by-layer assemblies with the negatively charged semiconductor nanocrystals. The negative charges come from the carboxyl groups of the surrounding ligands. Clustered assembly leads to disordered colloidal clusters by the use of the divalent Ca^{2+} ions. Both promote inter-particle distances of about 1 nm. The experimental methods are described in the next section. UV-vis transmission spectroscopy was used to characterize the sample and to ascertain the correct composition for the subsequent data analysis. The concentration of the single components was measured in each of our semi-transparent samples in order to correct the spectroscopy graphs for these typical minor concentration fluctuations. Details of the setups required for steady-state and time resolved PL-spectroscopy are provided. These techniques have been used in chapter 4. Last but not least, the SPV-setup for spectroscopy and transients used for the experiments described in chapter 5 is presented.

Chapter 4 relates to experiments where PL-spectroscopy has been applied as an indirect method to provide evidence of dominant charge separation dynamics in the

type II aligned tunneling structures of CdTe and CdSe nanocrystals. Both systems - the disordered hybrid clusters in solution and the dry layered samples on glass - proved PL-quenching on the luminescent CdTe nanocrystals through the transfer of electrons from CdTe to CdSe nanocrystals. In the case of the layered assembly, transfer rates of up to $1/100\,ps$ were observed. Results using different sizes of semiconductor nanocrystal prove a correlation of the theoretically calculated electron level offset between CdTe and CdSe nanocrystals. This indicates that the shifts of the electron and hole energy states can be approximated using the effective mass approach and that, in general, a type II alignment of the CdTe and CdSe nanocrystals can be expected. Energy transfer from CdSe to CdTe nanocrystals can also be observed for type II aligned CdTe and CdSe nanocrystals, although the PL-quenching of CdTe nanocrystals which is attributed to charge separation is dominant.

Chapter 5 provides information concerning SPV-techniques as a direct method clearly proving the charge separation properties of the selected CdTe-CdSe nanocrystal hybrids and thus providing independent confirmation of the results of chapter 4. All studies have been carried out on layered samples with only one CdTe-CdSe interface. Thus, changes in the directionality of this charge separating type II interface lead to a change in the sign of the SPV-signal. The SPV-signal is suppressed when the interlayer distance was increased from about 1 to about 2 nm by additional double polymer layers. This highlights the short interaction length required for the electronic transfer and is consistent with quantum mechanical tunneling being basically exponentially dependent on the barrier width. Last but not least, we obtained a strong indication of diffusion dynamics across CdSe and CdTe layers.

Chapter 6 summarizes the results of this work and provides a brief outlook.

2 Fundamental Concepts in Nanosciences

First, the fundamental background of the basic physical concepts for my thesis are discussed: the type II alignment leading to charge separation and charge transfer is introduced. The semiconductor nanocrystals are presented which combine the properties of classical semiconductor materials (such as the possibility of a type II alignment) with nanoscience concepts (such as quantum confinement). The CdTe and CdSe nanocrystals are introduced as approximation by spatial confinement of extended bulk semiconductors. Details of the essential physical concepts and processes in hybrid nanoassemblies are given at the end of this chapter: photo-excitation, PL-decays, charge transfer, energy transfer and diffusion dynamics.

2.1 Type II Tunneling Structure

This thesis concerns charge separation induced by charge transfer in self assembled systems of two types of semiconductor nanocrystals. Both processes depend crucially on the alignment of the energetic levels in the semiconductor nanocrystals. In this connection, the essential energetic configuration of type II alignment for charge separation and some basic considerations on the transport are also mentioned.

The systems investigated are basically static material assemblies where only pure electron and hole dynamics play a role. We discuss thus in general only the ground levels of the first excited states of electrons in semiconductor nanoparticles. Those states are the nearest to the Fermi-level (which is generally the benchmark between typical occupied and unoccupied electron levels [51]). They correspond to the lowest accessible excited states of electrons and holes. As this thesis addresses dynamic processes in particular we studied, in general, systems where far less than one electron hole pair per semiconductor nanocrystal is excited. In this thesis, we investigated the PL-decays by radiative recombination of excited-electron hole pairs to the relaxed ground states and the electric dipole field of separated charges.

Charge separation is expressed by collection of positively charged holes on one type of the semiconductor nanocrystals, negatively charged electrons are concentrated on the other semiconductor nanocrystals. Therefore, the lowest accessible energetic level for

the positive and negative charge must be on different particles. In classical crystalline bulk solar cells this is realized by doping, leading to a p-n-junction. [52] But a controlled fine tuning of the energetic positions of nanocrystals by doping is difficult. [53]. In any case, intrinsic materials also exist which provide more p-type or n-type behavior [54]. These can be used for charge transfer leading to charge separation similar to a p-n-junction. [55]

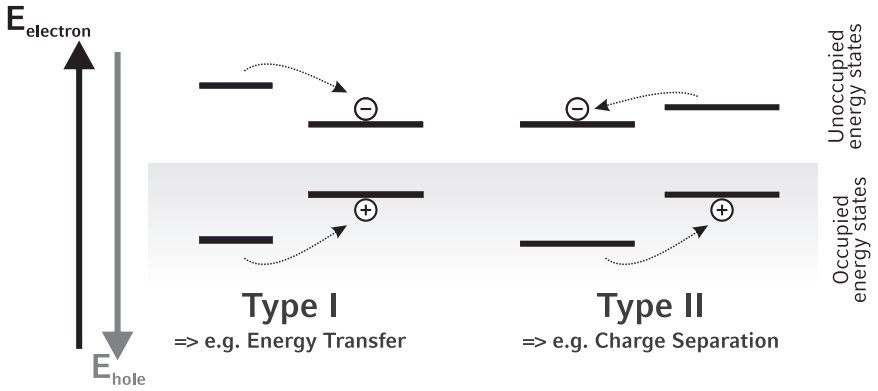

Figure 2.1: This illustrates the difference between type I and type II alignment. Only the energy ground levels are displayed for excited electrons (in the area for unoccupied states) and for excited holes (seen in the area shaded gray). The type I alignment concentrates electrons and holes on the side with the lowest energetic states; no charge separation can occur, only energy transfer. The type II alignment is the correct choice for long lasting charge separation. N.B. the energy scale of the holes is in reverse order to that of the electrons. In the remainder of this thesis only the electron energy scale is illustrated.

In general two different energetic alignments are possible for a two component system (fig. 2.1). The type I alignment concentrates both the lowest excited hole states and electron states on one and the same type of semiconductor nanocrystals. The type II alignment separates these excited ground states between the two nanocrystals. Hence, only a type II alignment can lead to an effective long-lasting charge separation. Energy transfer is observed especially in type I systems. However, it may also occur in type II assemblies when electron and hole are transferred together to the nanocrystal with the smaller energy gap. Nevertheless, observing energy transfer in type II structures does not prevent subsequent efficient charge separation. Type I alignment in nanocrystal assemblies has already been studied extensively. It leads to concentration of charges in one material and may thus serve as artificial antenna complexes. [19,21,47,48] For this work I shall concentrate on type II systems in order to study charge separation related phenomena.

Transfer dynamics between different nanocrystals depend crucially on the potential barrier between them (fig. 2.2 a), on the energetic offset of the corresponding energy levels between both particles as driving force (fig. 2.2 b) and on the overlap of the density of states to allow tunneling or hopping processes and to dissipate excess energy if needed (fig. 2.2 c). Any transfer can only take place when the corresponding energy state in the neighboring nanocrystal is empty. A typical barrier width is 1 nm for the system studied in this thesis. The energetic offset in the investigated hybrid nanocrystal assemblies is typically in the range of 0.0 - 0.5 eV for the relevant free electron states and of 0.5 - 0.7 eV for the hole states.

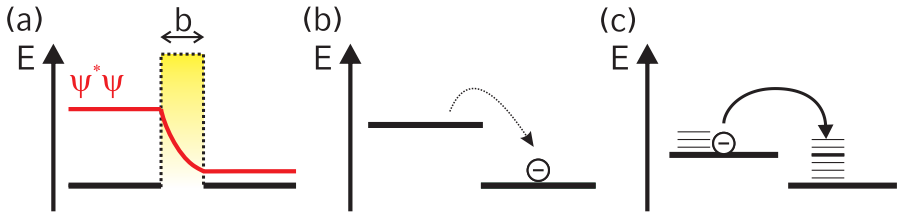

Figure 2.2: Three main concepts are relevant for charge carrier transfer between two particles: (a) The existence of a quantum mechanical barrier between the particles influences the local transfer probability ($\psi^*\psi$). (b) The energetic alignment is the driving force for permanent transfer without back transfer. (c) To transfer charge carriers it is important to have a sufficient the density of accessible states in the neighboring semiconductor nanocrystal.

In conclusion it can be said that the systems investigated are type II aligned materials which provide an intrinsic potential offset for electron and hole states leading to long-lasting charge separation. The material used provides quantum mechanical tunneling barriers. Hence, the system investigated is called "type II aligned tunneling structure" to emphasize that a tunneling barrier is involved which may lead to tunneling and hopping transfer dynamics.

2.2 Semiconductor Nanocrystals

Semiconductor nanocrystals are investigated in my thesis. First, the expression "nanostructure" is defined in this section and the quantum confinement is explained. This is the quantum mechanical effect of size quantization and one of the most prominent effects in the semiconductor nanocrystals. Then the semiconductor materials are introduced with emphasis on their periodic crystal structures before the CdTe and CdSe nanocrystals are discussed on the basis of size confined crystals.

2.2.1 Quantum Confinement

By definition nanostructures feature non-classical and especially quantum mechanical effects that are related to the size of the particles on the nanometer scale. The typical length scale ranges from under 1 nm up to 10 nm. This leads to the name "nanotechnology". [56]

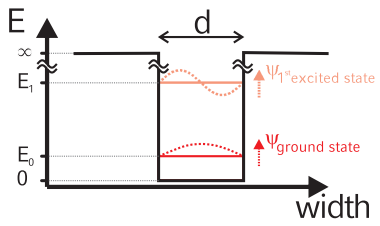

Figure 2.3: The illustrated quantum well has the confined width d in space and an infinite height of their potential barrier. All quantum states inside have a higher energy level than the minimum energy level of the quantum well. The ground state and the first excited state are shown together with their sinusoidal wave functions. [57–59]

One of the most important effects in semiconductor nanostructures is quantum confinement. Semiconductor nanocrystals are confined spatially in all three dimensions. Hence, energy states of particles (such as electrons, holes and phonons) are also spatially confined. Briefly, the introduction is made for one dimension using the "Heisenberg's uncertainty relation of position and momentum". [58, 60]

We may assume a one dimensional quantum well of the size d with infinite potential barriers on both sides (fig. 2.3). Then a quantum mechanical particle (like an electron) is confined to $\Delta x = d$. This can be inserted into "Heisenberg's uncertainty relation of position and momentum":

$$\Delta x \cdot \Delta p \geq h/2 \tag{2.1}$$

where h is the Planck constant and Δp. As the minimum momentum p_{min} in such a structure can only be $\pm\Delta p$ this gives:

$$\Delta p \geq p_{min} =: h/2d \tag{2.2}$$

The size quantization energy $E_{size}(d)$ in the ground state corresponds to the kinetic energy of a particle with the minimum momentum p_{min} (zero-point energy, e.g. reference [58]):

$$E_{size}(d) = E_{kin}(p_{min}) = \frac{p_{min}^2}{2m^*} = \frac{\hbar^2\pi^2}{2m^*d^2} \tag{2.3}$$

$$==> E_{size}(d) \propto \frac{1}{m \cdot d^2} \tag{2.4}$$

where m^* is the effective mass of the particle in the quantum well. Hence, the quantization energy is indirectly proportional to the square of the diameter of the semiconductor nanoparticles d and indirectly proportional to the mass of the particle. The same result can also easily be obtained using elementary quantum mechanical calculations based on Schrödinger's equation. [57, 58, 61] Such calculations are used to obtain the sinusoidal shape of the particles wave functions and higher excitation levels in the quantum well in fig. 2.3. [57–59] However in the context of the physical experiments performed in this thesis, it is sufficient to limit the discussion to the ground state only.

The quantization energy $E_{size}(d)$ of equation 2.3 is only introduced for one dimension. It must be calculated separately for all three dimensions and then totalled. Since we are investigating spherical nanocrystals with the same confinement d in all three dimensions this adds only a factor 3. Hence, the relation 2.4 stays unchanged since only the proportionality constant changes.

To conclude, semiconductor nanostructures are dominated by quantum mechanical effects due to their size which is typically under 10 nm. The size quantization effect was introduced. It leads to a quantization energy which is indirectly proportional to the mass of the particle and indirectly proportional to the squared width of the semiconductor nanoparticle.

2.2.2 Crystal Structure for CdTe and CdSe Semiconductors

The nanocrystals studied are of course crystalline in structure. The periodicity of any crystal lattice leads to delocalization of electron wave functions over the whole crystal. This implies new energetic levels for the electrons which are discussed in this section.

CdTe and CdSe materials occur in the zincblende structure in this work as shown in fig. 2.4. [62, 63] A tetrahedral arrangement of the next neighboring atoms may be seen. This atomic structure is also reflected in the shape of the nanocrystals which are terminated mainly by equivalent [111], [11$\bar{1}$], [1$\bar{1}$1] and [$\bar{1}$11] facettes. [64, 65]. The zincblende lattice belongs to the space group F$\bar{4}$3m (Hermann-Mauguin notation). [66]

Electrons tend to delocalize in the periodic structure of an extended crystal when neighboring wave functions overlap. [51,56]. This leads to new energy levels for the electrons which are reflected in the band structure (fig. 2.5). Since electrons are fermions, there is a variety of delocalized electronic wave functions which differ mainly in their periodicities and energetic levels.

The periodic structure of the crystals can be well expressed by Fourier transformation. Thus, the reciprocal lattice with its reciprocal wave vectors $\vec{k}$ is used which is a Fourier transformation of the real space lattice. The electron wave functions in crystal lattices can be associated with the reciprocal lattice vectors $\vec{k}$ in the Brillouin zone of the crystal lattice according to the Bloch-theorem: the electron wave functions in a

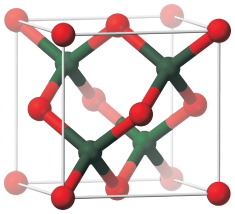

Figure 2.4: The unit cell of the CdTe and CdSe nanocrystals used is the zincblende. Red stands for Cd atoms and green for Se or Te. The tetrahedral coordination of the chemical bonds of each atom can be clearly seen. This figure has been adapted from reference [66].

crystal lattice can be approximated by the Bloch-waves $\psi_{\vec{n}\vec{k}}(\vec{x})$ [56]:

$$\psi_{\vec{n}\vec{k}}(\vec{x}) = e^{i\vec{k}\vec{x}} \cdot u_{\vec{n}\vec{k}}(\vec{x}) \tag{2.5}$$

The Bloch-waves $\psi_{\vec{n}\vec{k}}(\vec{x})$ are solutions of the stationary Schrödinger equation for non-interacting electrons in a crystal lattice with the lattice vectors $\vec{R}$ expressed by a periodic potential $V(\vec{x}) = V(\vec{x}+\vec{R})$. $\vec{k}$ is wave vector in the reciprocal space, $u_{\vec{k}}(\vec{x})$ the lattice periodical factor with $u_{\vec{n}\vec{k}}(\vec{x}) = u_{\vec{n}\vec{k}}(\vec{x}+\vec{R})$ and $\vec{n}$ is a wave vector standing for the multiplicity of the Bloch-solutions. The Bloch-waves $\psi_{\vec{x}\vec{k}}(\vec{x})$ depend on the wave vectors $\vec{k}$. Hence, all electron wave functions can be attributed to wave vectors $\vec{k}$.

The origin in the reciprocal space is the Γ-point where the reciprocal vectors are zero. Zero in the Fourier space signifies an infinite period length over the whole real space. The further away a point in the Fourier space is from the origin (Γ-point) the higher the periodicity of the corresponding envelop wave function is in the real space (see equation 2.5).

The lowest band gap in CdTe and CdSe is situated at the Γ-point for both electron and hole (fig. 2.5). Moreover, the states for the lowest band gap are at the Γ-point which means their electron wave functions expand over the whole crystal. Spatial confinement of the wave functions to a nanocrystal therefore augments its energy gap. This can be used for energy gap tuning in nanocrystals (as discussed below).

The global shape of the band structures in fig. 2.5 a and fig. 2.5 b is comparable, showing that the global electronic properties of CdTe and CdSe are quite similar. According to reference [67] the conduction band of CdTe is made in first approximation of the 5s-orbital of Cd and the valence band of the p-orbital of Te in the case of CdTe. This implies that the p-orbital of Se also form the valence band of CdSe due to strong chemical and physical similarities. Thus, optical selection rules are satisfied for photo-excitations and radiative decay between valence band and conduction band. This is

the basis for strong absorption and PL-emission efficiencies in these materials. The CdTe and CdSe studied are direct semiconductors.

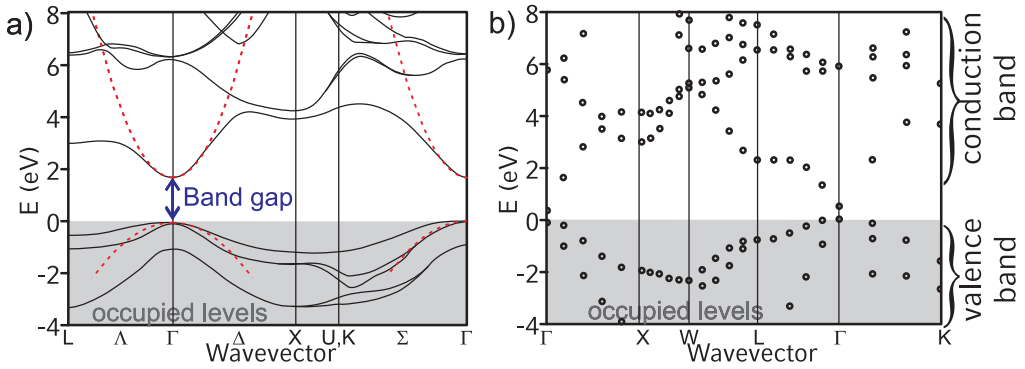

Figure 2.5: The band structure is displayed for bulk CdTe (a) [68,69] and bulk CdSe (b) [68,70] in zincblende structure. Both diagrams are based on theoretical calculations. The red broken-line curves in (a) illustrate effective masses in crystal lattices being a parabolic fit at the Γ-point to the maximum or minimum of the valence or conduction band. The occupied states are called "valence band", the unoccupied states "conduction band", the empty space in between "band gap". CdSe bulk crystals occur at standard conditions mostly in wurzite structure. Thus, less data are available in lower precision for its zincblende conformation.

The effective mass (as a parabolic fit to the band structure) can be introduced to characterize the charge carrier electrons and holes in conduction and valence band respectively :

$$m^* = \frac{\hbar^2}{\left(\frac{\partial^2 E}{\partial k^2}\right)} \tag{2.6}$$

where $\hbar$ is the reduced Planck constant and $\frac{\partial^2 E}{\partial k^2}$ the second derivative in the band structure (fig. 2.5) of the lowest accessible band at the Γ-point. This means that the effective mass m^* is indirectly proportional to the curvature of the band structure at the Γ-point as indicated in fig. 2.5. The fitted lines in fig. 2.5 a have an approximately three times higher curvature for the conduction band than for the valence band. Hence, the effective mass of electrons in CdTe (and CdSe) is about three times lower than the one of holes.

The interface between CdTe and CdSe presents a type II alignment. An offset of about 0.3 eV can be observed for the conduction band, 0.6 eV for the valence band [54]. Holes find their lowest energetic states in CdTe, electrons in CdSe. In this thesis, we used the following values for CdTe and CdSe bulk material in zincblende conformation (table 2.1).

	CdTe	CdSe
band gap [68]	1.48 eV	1.7 eV
lattice constant [68]	0.6481 nm	0.6052 nm
effective electron mass m_e^* [68]	0.14 $\cdot m_e$	0.13 $\cdot m_e$
effective hole mass m_h^* [68]	0.37 $\cdot m_e$	0.44$\cdot m_e$
conduction band level [54]	-3.86 eV	-4.2 eV
valence band level [54]	-5.33 eV	-5.9 eV

Table 2.1: Relevant physical parameters of CdTe and CdSe bulk crystals are shown in this table for the zincblende conformation at standard conditions. Energy levels are given relative to the vacuum level. m_e is the electron mass.

In conclusion, CdTe and CdSe are direct semiconductors which present a type II alignment. Electron wave functions in these crystals can be approximated by Bloch waves which have, in real space, the periodicities of the lattice or its multiples. This can be expressed in the reciprocal space by wave vectors. Energetic states of these electron wave functions in crystals are expressed in band diagrams as indicated above. The lowest band gap is realized only for wave functions which expand over the whole crystal.

2.2.3 CdTe and CdSe Nanocrystals

The semiconductor nanocrystals are described in this section. Their size quantization effect is discussed and illustrated for CdTe and CdSe nanocrystals. Finally, some of the limitations of the presented simplified introduction are mentioned.

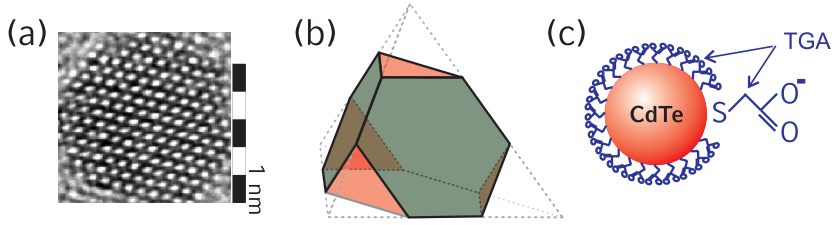

Figure 2.6: The microscopic shape of nanocrystals is illustrated. An electron micrograph shows (a) one CdSe nanocrystal of 6 nm diameter. [71] The precise 3-dimensional shape of the studied nanocrystals is described by a truncated tetrahedron (b). [64] Nevertheless, the nanocrystals are typically called and treated as spherical nanocrystals. Thus, we illustrate them as spheres for the remainder of this thesis(c). The organic ligand shell of TGA-ligands is also displayed (c).

Semiconductor nanocrystals are single crystals on the scale of several nanometers (fig. 2.6 a). The nanocrystals consist typically of several hundreds to thousands of atoms and are generally 2 - 4 nm in size. The crystal lattice of the CdTe and CdSe

nanocrystals studied is zincblende. The nano-scopic shape is a truncated tetrahedron (fig. 2.6 b). [64] It is however sufficient to describe them as spherical nanocrystals (fig. 2.6 c). We illustrate the nanocrystals for the remainder of this thesis simplified as spheres. Nanocrystals are passivated by an organic ligand shell to prevent their aggregation to an amorphous structure. For this work, we used only nanocrystals with water soluble thioglycolic acid (TGA) ligands.

The surfaces of the CdTe and CdSe nanocrystals are mainly covered by Cd atoms to which the thiol-groups of the organic ligand anchor. The TGA ligands used lead to a thin shell of organic ligands of only 0.1-0.2 nm thickness. [19] The acid group (-COOH) of TGA provides water solubility and is used for self-assembly methods.

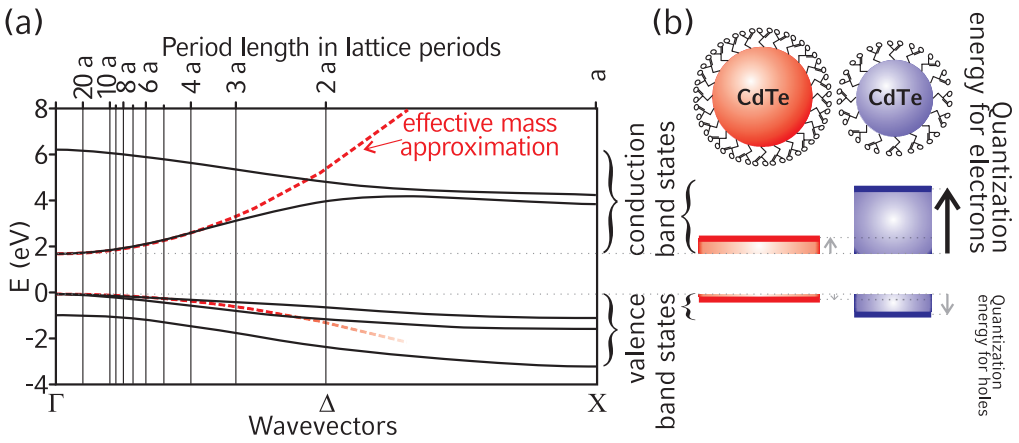

Figure 2.7: The size quantization effect is motivated for CdTe nanocrystals from the band structure (a) (extracted from references [68, 69]) and illustrated schematically (b). The X-Point in (a) corresponds to the electron wave function having an envelop function with the lattice periodicity $\vec{a}$. The Γ-point corresponds to an infinite period length and is thus only available for bulk crystals. In nanocrystals the maximum period length is limited to about the physical size of the nanocrystal. Hence, only certain states to the right of the corresponding nanocrystal sizes are accessible. The effective mass approximation simplifies the calculation of the energy levels of the nanocrystal, shown here as broken red lines. The quantization energy for electrons is about three times higher than for the holes as illustrated in (b) for two different nanocrystal diameters.

The size quantization effect can be understood on the basis of the band structure shown in fig. 2.5 a. An electron wave function in a nanocrystal cannot have a period length that is longer than the diameter of the nanocrystals. Since the Γ-point corresponds to bulk states and the X-point to wave functions of the lattice's period $\vec{a}$ the maximum period length possible for the nanocrystal must be determined. The corresponding energy levels can then be obtained from fig. 2.7 a. The difference between the

lowest energy levels in the nanocrystals and the levels at the Γ-point is the quantization energy (fig. 2.7 b).

Most of the quantization energy is related to the conduction band states (fig. 2.7). The curvature of the conduction band in the band-structure diagram (fig. 2.7 a) is higher than that of the valence band. Hence, the effective mass of electrons is lower than that of the holes. Thus, the quantum confinement leads to a higher energy shift for electrons than for holes.

The effective mass approach to determine the energy levels in nanocrystals is more effective in practice. The broken red lines in fig. 2.7 a illustrate the effective mass fits where we observe a good agreement of simplifying quadratic fit and the shown band-structure for a sufficiently wide range. Thus, the quantization formula 2.3 can be used for nanocrystals with the effective masses m_e^* or m_h^* for electrons and holes respectively. For the moment, only quantization in one dimension is discussed (fig. 2.7 a). However, the quantization energy must be determined for all three dimensions. Since zincblende is a cubic lattice, the quantization energy is the same for all three dimensions and leads to a factor 3. Thus, the formula to calculate the energy gap of nanocrystals $E_{NC}(d)$ is:

$$E_{NC}(d) = E_{gap}(Bulk) + 3 \cdot \frac{\hbar^2 \pi^2}{2 m_e^* d^2} + 3 \cdot \frac{\hbar^2 \pi^2}{2 m_h^* d^2} \tag{2.7}$$

where $E_{gap}(Bulk)$ is the band gap of the corresponding bulk material, $\hbar$ the reduced Planck's constant.

Solutions of nanocrystals are shown for CdTe nanocrystals under UV-illumination in fig. 2.8 a and for CdSe under daylight in fig. 2.8 b. The size of the nanocrystals increases from left to right. The energy gap of the CdTe nanocrystals is directly visible under UV light (fig. 2.8 a) since the nanocrystals emit the PL-light depending on their energy gap. The appearance of CdTe and CdSe nanocrystals under daylight is similar. Photons with higher energy than the energy gap are increasingly absorbed. Only longer wave lengths in the red regime pass the solutions so that the appearance of the solutions starts form yellowish-orange for very small nanocrystals and reaches dark red for large nanocrystals.

To be more precise, the absorption (fig. 2.8 c) and emission spectra of CdTe (fig. 2.8 d) are provided, as well as absorption and emission spectra of CdSe nanocrystals (fig. 2.8 e). Both absorption spectra are typical for the studied nanocrystals. The absorption starts from the low energy side with a first absorption peak. This peak is related to the energy gap of the corresponding nanocrystals (without exciton binding energy). [72] After this first absorption peak, the absorption continues to increase from visible to UV light and approaches the bulk material values in the UV range. Peaks for excitation of higher

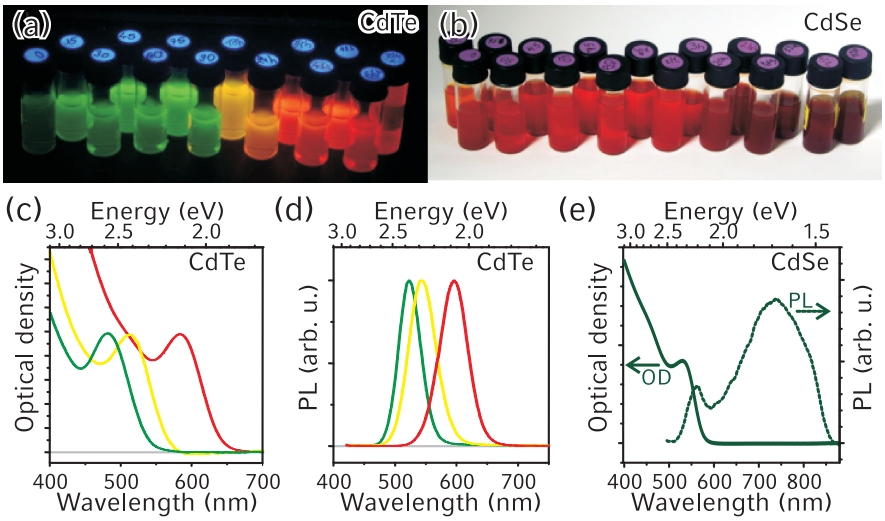

Figure 2.8: A variety of different nanocrystal sizes in colloidal solution is presented for CdTe nanocrystals under UV-illumination (a) and under normal light for different CdSe nanocrystals (b). The nanocrystal diameter increases from left to right. Some example spectra of the absorption (c) and emission (d) for CdTe nanocrystals and for CdSe nanocrystals (e) are illustrated.

order nanocrystal quantized levels (see reference [72]) are normally not resolved in the absorption spectra of TGA stabilized water soluble CdTe and CdSe nanocrystals. [63]

The emission spectra of the corresponding CdTe nanocrystals can be seen in fig. 2.8 d. The PL emission peak value is red-shifted with respect to the absorption peak especially due to the exciton binding energy. All nanocrystal spectra are quite broad since all presented spectra are taken on ensembles of nanocrystals of similar, but not identical, shape and size.

The absorption and emission spectra of CdSe nanocrystals are presented in fig. 2.8 e. The CdSe absorption spectrum is of similar shape (compared to CdTe spectra in fig. 2.8 c). The CdSe PL-emission in contrast is different to CdTe. A PL-peak close to the first absorption edge appears and is of the same type as shown in fig. 2.8 d. It is also called an excitonic peak or core emission. Moreover, a broad peak is observed in the near infrared (NIR) called trap emission. The PL-spectrum presented in fig. 2.8 e is typical for TGA stabilized CdSe nanocrystals in water. [24] The broad NIR-peak is related to trap states of CdSe nanocrystals capped with ligands containing thiol groups. [37] The binding to sulfur is supposed to induce trap states in the energy gap of the CdSe nanocrystals. However, it must be emphasized that no absorption can be observed in the NIR which can be related to direct optical excitation of these trap states.

The nanocrystals are labeled with their first absorption peak position in this work. The CdTe nanocrystals in fig. 2.8 c,d are labeled CdTe480 (green), CdTe 515 (yellow), CdTe580 (red), the CdSe in fig. 2.8 e is CdSe529. The PL-data are not used in labeling, as the PL may be affected by shifts caused by the environment or by quenching. [73]

The model presented above (equation 2.7) is quite simple as it describes a cubic nanocrystal instead of a spheric nanocrystal or a nanocrystal shaped like a truncated tetrahedron. There are further limitations which are addressed in the following. As mentioned the maxima of absorption and emission peaks differ due to the Stokes shift attributed to exciton binding (see also chapter 3.1.3). The CdTe480 (green) for instance shows a large red shift of about 40 nm or 200 meV as Stokes shift (fig. 2.8 c,d). The electrostatic interaction between photo-excited electrons and holes has to be taken into consideration here. Electrons and holes in nanocrystals interact and form excitons the more they are confined to a smaller space. [74–76]. The exciton binding energy of the CdTe nanocrystals used in this work is mainly (100±50) meV (fig. 3.3, except for the smallest green luminescent nanocrystals) and is therefore significantly smaller than reported in documentation referring to quantum dots. [74]

Moreover, when introducing quantum wells it is not realistic to assume an infinite barrier height. Thus, the electron wave functions also spread out into the barriers. Hence, the charge carriers are much less confined. This leads to a virtually increased nanocrystal with respect to the penetration of their electron wave functions in the barriers. It is shown later that this concept fits well to the experiments (section 3.1.2). As a consequence tunneling transfer dynamics become more likely.

Spherical CdTe and CdSe nanocrystals have been introduced. They are typically of 2 - 4 nm in size so that quantum confinement occurs. This leads to an increase in the energy gap in the nanocrystals. The size quantization effect can be approximated by the effective mass approach. The lowest energetic state of the conduction band levels shifts about three times more than the highest valence band state. Absorption and PL-spectra show very well the size dependent characteristics for nanocrystals.

2.3 Physical Processes in Nanostructures

Physical processes that are relevant to the studies presented are introduced in the following section. Their principles are explained together with cases and formula related to the experiments conducted for this thesis. Since optical analysis was used, photo-excitation and radiative and non-radiative decay dynamics are presented first. Then charge and energy transfer processes between nanocrystals are discussed. Formula related to diffusion are included at the end.

2.3.1 Photo-Excitation

Photo-excitation means that photons are absorbed by matter leading to excitation of electron-hole pairs. In the cases presented, visible and ultra-violet (UV) light was absorbed by the nanocrystals. This leads to the excitation of electrons which reach higher energy levels and leave behind so-called holes. Also the additional excitation of other particles, quasi-particles or modes, such as vibrations or phonons is possible. However, these states generally decay quickly after internal conversion. Therefore, in this thesis we concentrate only on excitation of electrons and holes. The photo-excitation is necessary to promote charge carriers to unoccupied energetic states where their dynamics can be investigated. It is therefore the basis for all studies in this thesis.

A clear separation of occupied electronic levels and unoccupied electronic levels exists for the structures studied at T=300K when all electrons are completely relaxed (this is the relaxed initial ground state). Upon photo-excitation an electron is shifted to a higher energy level that lies in the unoccupied electronic states (fig. 2.9 a). Thus, an empty space called a hole is left behind (A hole behaves similar to a positively charged particle and can therefore be treated as a quasi particle in description). The excited electrons and holes relax to their lowest excited state due to fast internal relaxation or thermalization involving other low energy excitations, for instance vibrations (fig. 2.9 b).

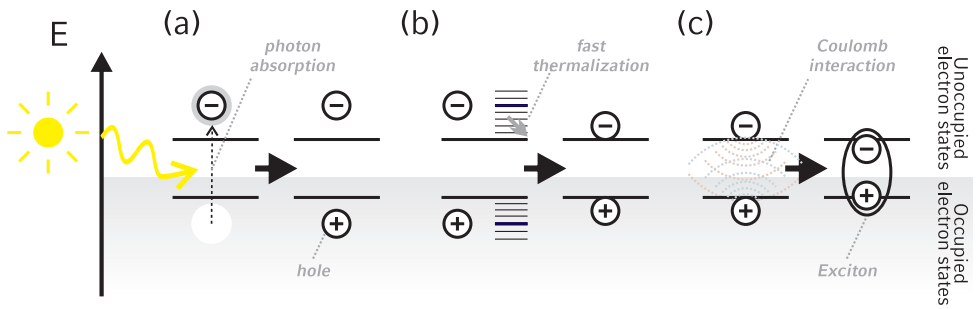

Figure 2.9: The photo-excitation process is illustrated. Electronic energy levels (black lines) exist which are in the completely relaxed situation either fully occupied with electrons (shaded gray) or unoccupied. In case of photo-absorption one electron is excited to a higher energy level (a). Thus, it leaves behind a hole with virtual positive charge as an empty place. Fast thermalization processes lead to relaxation of the electron and the hole to their excited ground state (b). Coulomb attraction of electron and hole leads to the formation of an exciton. As a result, their energy is lowered even further (c).

Another effect is Coulomb attraction between the negatively charged electron and the positively charged hole leading to the creation of an uncharged quasi-particle called exciton. This again has a lower energetic level compared to the excited ground states

of electron and hole (fig. 2.9 c). Charge separation mainly needs to break this exciton binding energy before one charge carrier can be transferred out of the interaction range with the other particle. We assume a typical exciton binding energy in the range of (100±50) meV for the water soluble CdTe nanocrystals used in this work (see chapter 3.1.3). The exciton binding energy increases for smaller semiconductor nanocrystals. [75, 77]

Electrons and holes relax by recombination to the initial ground state. It is the opposite process to the absorption. However, its probability is generally significantly lower than the fast thermalization which involves phonons. Therefore, the relaxation of electrons and holes by PL-emission can be investigated typically for sufficient time. This is used for the optical studies in this thesis.

Only electro-magnetic radiation of low intensity was applied for the absorption experiments. Thus, only transitions induced by the electric dipole fields are relevant. These are called the optical allowed transitions. They obey the optical selection rules: their angular momentum has to change ($\Delta l = \pm 1$) since the absorbed photon carries an angular momentum. [78, 79] The so-called forbidden optical transitions have a very minor transition probability since these higher order perturbations of the electro-magnetic field generally disappear in accordance with Fermi's golden rule when compared with the dominant electrical dipole transition.

In conclusion the absorption of electro-magnetic dipole radiation creates electrons and holes. Their dynamics can be investigated until they recombine to the ground state. The dynamics of these excited charge carriers is the topic of my thesis.

2.3.2 Radiative and Non-Radiative Decay

All physical processes are in principle reversible since typically the time inversion can be applied. Thus, if matter can absorb light it can also emit light again. Photo-excited excitons therefore decay especially via light emission. However, light absorption is not the only way to excite matter. There are hence additional decay channels for excitons other than just light emission. This means there are radiative optically allowed decay channels for excitons by emission of light. All others are called non-radiative decay channels.

Time dependent decays are described by the following differential equation:

$$\frac{dN}{dt} = -\Gamma N(t) \tag{2.8}$$

where N is the number of excited states available for decaying and Γ is a positive proportionality parameter. A general solution of equation 2.8 is:

$$N(t) = N(0)exp(-\Gamma t) \tag{2.9}$$

The spectroscopic experiments carried out for this thesis cannot directly measure the number N of excited states but only the intensity I of the photons emitted. Since I is proportional to the derivative of N in time the intensity can be expressed as

$$I(t) = I(0) \cdot exp(-\Gamma t) \tag{2.10}$$

The proportionality parameter Γ is called decay rate and defines the parameter characteristic life time τ as $\Gamma =: \frac{1}{\tau}$ where τ designs the time after which only the portion of $1/e$ is left.

Considering more decay channels, equation 2.8 becomes:

$$\frac{dN}{dt} = -\Gamma_1 \cdot N(t) - \Gamma_2 \cdot N(t) - ... = -(\Gamma_1 + \Gamma_2 + ...) \cdot N(t) \tag{2.11}$$

The solution to this equation is again equation 2.9 when we set $\Gamma = \Gamma_1 + \Gamma_2 + ...$ This means that all different decay processes can be joined together into one effective process with one effective rate or characteristic life time. Here, we obtain:

$$\frac{1}{\tau_{total}} = \frac{1}{\tau_1} + \frac{1}{\tau_2} + ... \tag{2.12}$$

The joint effects of radiative and non-radiative processes can be measured as one effective decay time τ_{total}:

$$\frac{1}{\tau_{total}} = \frac{1}{\tau_{radiate}} + \frac{1}{\tau_{nonradiative}} \tag{2.13}$$

Moreover it is possible to quantify the effect of hybrid assemblies when it induces an additional quenching compared to pure reference samples. Therefore a reference sample is required in order to investigate the usual decay characteristics of the material used. Furthermore, a hybrid sample must be measured to record the combined effect of normal decay characteristics required for the investigated material and additional quenching induced by hybrid assembly. This total quenching time τ_{Hybrid} can be expressed as:

$$\frac{1}{\tau_{Hybrid}} = \frac{1}{\tau_{Reference}} + \frac{1}{\tau_{Quenching}} \tag{2.14}$$

From equation 2.14 one can easily extract the quenching characteristics $\tau_{Quenching}$ induced by the hybrid sample. Both the reference and the hybrid sample should be measured under comparable conditions, that is the same environment or solvent, same processing method, same samples' age and history, comparable sample treatment, etc. This was ensured for the samples presented within this thesis.

In conclusion, a change of a radiative decay rate can reveal the decay rate of another non-radiative decay.

2.3.3 Charge Transfer between Nanocrystals

Charge transfer processes leading to separation of photo-excited excitons are the most important non-radiative decay channels discussed in this thesis. Chapter 4 is based on investigation of non-radiative decays to reveal charge separation by charge transfer dynamics with PL-spectroscopy. Charge transfer between the investigated isolated nano-scale quantum systems is a purely quantum mechanical phenomenon where the quantum mechanical barriers on nanometer scale are established by the isolating organic materials between localized electron states in the nanocrystals.

Charge transfer over a finite quantum mechanical tunneling barrier occurs since the electron wave function is not completely confined to one semiconductor nanoparticle. There is an overlap to the close environment. In accordance with the so-called quantum mechanical tunneling effects, charge carriers can inter-penetrate barrier-materials on the nanometer scale.

Resonant tunneling transfer of charge carriers occurs between states of the same energy level. After transfer a quick subsequent relaxation to the ground state of the neighbor particle may occur. The tunneling rate is given as [80]:

$$\Gamma = \Gamma_0 \cdot exp\left(-\sqrt{\frac{2m^*\Delta V}{\hbar^2}}b\right) \tag{2.15}$$

where b is the barrier width, ΔV the effective barrier height, m^* the effective mass (see chapter 2.2.2) and $\hbar$ the reduced Planck constant.

Non-resonant tunneling, also called hopping, occurs for transfer between different energetic states. This is especially the case in materials which are classified as disordered systems (these are for instance systems without constant periodicities or structures like those created from an ensemble of non-identical nanocrystals as it is the case for this thesis). The thermal energy and coupling energy is typically lower for hopping transfer than the spread of the energy levels involved in the charge transfer. [80] Thus an additional rate expecially for the thermal broadening (related to k_BT) and for the energetic offset ΔE between the energy has to be multiplied [80]:

$$\Gamma = \Gamma_0 \cdot exp\left(-\sqrt{\frac{2m^*\Delta V}{\hbar^2}}b\right) \cdot exp\left[-\frac{(\Delta E+\lambda)^2}{4\lambda k_BT}\right] \tag{2.16}$$

where k_B is the Boltzmann constant and λ the so-called recognition energy. [80,81] Since $\lambda << \Delta E$ is assumed for the nanocrystal assemblies studied, the thermal broadening has the shape of a Gaussian with a characteristic width of about 50 meV at T=300K. [80, 82] These considerations are especially important for hopping diffusion where the transport occurs on similar energy levels. According to Abrahams and Miller [83] the

hopping transfer to lower energy states (down-hopping) does not need to include the thermal broadening. Thus, equation 2.15 must be used. For the remainder an equation similar to equation 2.16 must be used.

Non-resonant tunneling involves that energy is absorbed and emitted at the transfer. The typical energy difference ΔE for electron transfer between CdTe and CdSe nanocrystals studied in this thesis is about 0.2 eV. This energy must be absorbed by other particles in the nanocrystal system such as the phonons and the holes. Phonons especially are important for hopping transfer since they provide the states for thermal energy broadening and may absorb or provide the necessary energy differences. However, it may be argued that the energetic level spacing in quasi zero-dimensional quantum systems can be higher than phonon energies, making single-phonon assisted processes impossible [84, 85]. However, it was shown that sub-nanosecond multi-phonon processes may break this so-called phonon bottleneck expected for semiconductor nanocrystals [86, 87]. This effect apparently did not play an important in the present thesis which was executed at about T=300K and therefore no further investigations were carried out.

To conclude, the most important dependence for the charge transfer is the exponential decay of the transfer probability with the barrier width b. It will be shown later (chapter 5.3) that an increase of the organic barrier can significantly quench the charge transfer dynamics.

2.3.4 Energy Transfer

Energy transfer between isolated systems on the nanometer scale has been investigated for many years. The relevant transfer mechanisms have been described by Förster [45] and Dexter [46]. The energy of an exciton is transferred from the so-called "donor" with the higher energy gap to the so-called "acceptor" with the smaller energy gap. Hence, the PL-emission of the donor is quenched and the PL-emission of the acceptor is enhanced.

Förster described non-radiative, optically allowed transition of excitons via dipole-dipole coupling. An exciton in the donor exhibits an electric dipole field that induces another dipole in the acceptor. Via this electro-magnetic interaction an exciton is completely transfered. A subsequent quick thermalization hinders the back transfer to the donor (in the case of hetero energy transfer). Thermalization via vibronic relaxation, for instance, may happen in nanocrystals on pico-second time scale or below. [88] The FRET-rate is according to reference [17]:

$$\Gamma_{FRET} = \frac{2\pi}{\hbar} \frac{\mu_D^2 \mu_A^2 \kappa^2}{n^4 R^6} \Theta \tag{2.17}$$

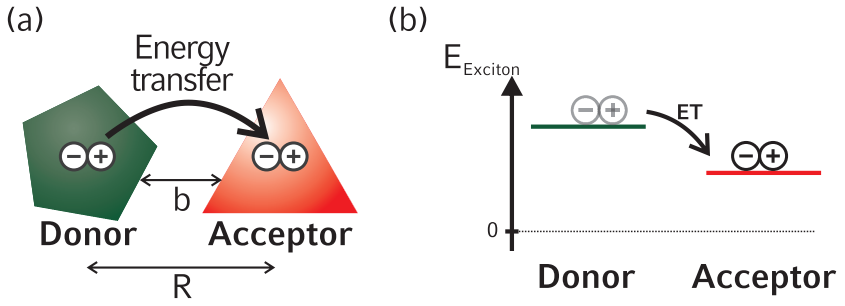

Figure 2.10: (a) Energy transfer is illustrated between two semiconductor nanoparticles with a center to center distance R. An exciton is transferred from the "donor" to the "acceptor". For comparison to electronic transfer the shorter barrier width b for electronic charge transfer is also mentioned. In the nanocrystal assemblies studied typically $R \approx 4\ nm$ and $b \approx 1\ nm$ applies. (b) Only hetero energy transfer where the exciton energy is lower on the acceptor than on the donor is illustrated and discussed. (The exciton energy comprises energy gap and exciton binding energy.)

where $\hbar$ is the reduced Planck constant, μ_D and μ_A the donor's and acceptor's transition dipoles, κ^2 an orientational average of all dipoles, n the mediums refractive index, R the transfer distance between center of the donor's particle and center of the acceptor. Θ is the spectral overlap integral (of the PL-emission of the donor and the absorption of donor. Further details can be found in other references such as [47, 89]).

Equation 2.17 depends critically on the transfer distance R as $1/R^6$ (see fig. 2.10 a), on the refractive index as $1/n^4$ and on the spectral overlap of the donor's emission and the acceptor's absorption. Förster resonant energy transfer is efficient for R in the range up to 6 nm [49, 90]. This corresponds to the length scales of the nanoparticle assemblies investigated in this thesis ($R \approx 4\ nm$).

Förster described a non-radiative energy transfer. However, although the transfer process involves no photons it still obeys the optical selection rules [58, 91]. In his publication [46] Dexter extended the theoretic discussion to include various optically forbidden transitions for energy transfer. He discussed not only electro-magnetic interaction of donor and acceptor more in detail but also added electric multipole coupling and magnetic coupling (which are basically just the Taylor expansion of the electromagnetic interaction) to Förster's theory of excitonic energy transfer. However, Dexter is known in particular for his description of electronic energy transfer [92] based on the quantum mechanical exchange interaction. Dexter found an exponentially decaying dependence on the transfer distance due to the exchange integral. [46, 92, 93]

Energy transfer is a relevant transfer mechanism in closely packed nanocrystal systems with transfer rates of up to 1/50 ps. [20] It will be shown later that energy transfer is also relevant in the type II structures studied. While charge separation by electron

transfer is supposed to cause only PL-quenching, energy transfer leads to enhancement of the energy transfer acceptor (ET-acceptor). To ensure that no energy transfer is present during studies of charge separation dynamics, only the ET-acceptor may be excited making enhancement by energy transfer from the energy transfer donor (ET-donor) impossible.

To summarize, energy transfer is relevant between closely packed nanocrystals with transfer rates of up to $1/50\ ps$. It leads to PL-quenching of the ET-donor and to enhancement of the ET-acceptor. FRET depends on the center to center distance R as $1/R^6$. The shorter tunneling barrier width b is not relevant for FRET.

2.3.5 Diffusion

In photovoltaic applications photo-generated excitons and charge carriers have to diffuse to reach the functional interfaces (like charge separating interfaces or contact electrodes). Thus, understanding diffusion processes may help to adapt thick nanocrystal systems for future applications in solar energy conversion. Diffusion processes are random walk processes of particles or charges in materials or media. Although the discussion is limited here to one dimension, diffusion can also be investigated in more dimensions.

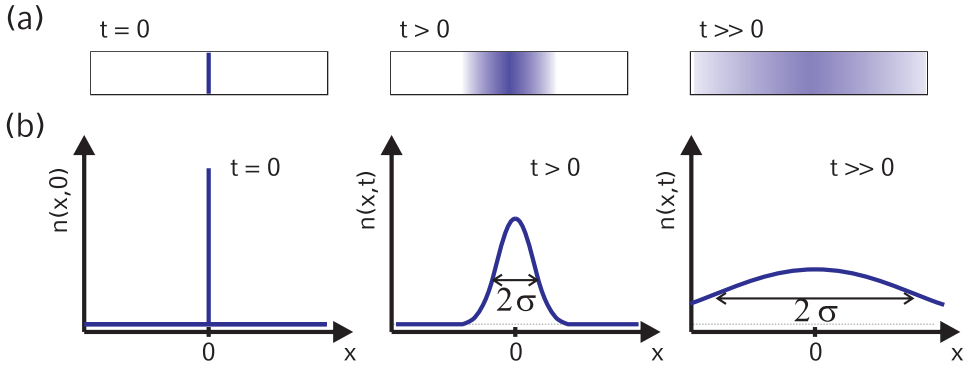

Figure 2.11: Diffusion is illustrated as evolution in time of density distribution $n(x,t)$ which is confined for $t = 0$ at $x = 0$ (a). The density distribution spreads out symmetrically in time (b,c). The standard deviation $\sigma(t)$ is illustrated in (b) and (c).

Fig. 2.11 shows an example of one dimensional diffusion. A particle density distribution $n(x,t)$ is concentrated at $t = 0$ at one point (at $x = 0$, fig. 2.11 a). Fig. 2.11 b,c illustrate the broadening of the particle density distribution $n(x,t)$ in time. The standard deviation $\sigma(t)$ of the density distribution $n(x,t)$ characterizes an average diffusion length.

Diffusion is described by Fick's laws [94, 95]. Fick's first law in one dimension (x) is:

$$J = -D \cdot \frac{\partial n}{\partial x} \tag{2.18}$$

where $J(x,t)$ is the particle flux density in x direction, D the diffusion coefficient, $n(x,t)$ the particle density distribution. Using the continuity equation $\partial n/\partial t = \partial J/\partial x$ Fick's second law can be obtained:

$$\frac{\partial n}{\partial t} = D \cdot \frac{\partial^2 n}{\partial x^2} \tag{2.19}$$

The normal distribution (also called Gaussian distribution) with the standard deviation $\sigma(t) := \sqrt{2Dt}$ is a solution of equation 2.19 as indicated in fig. 2.11:

$$n(x,t) = \frac{1}{\sqrt{2Dt} \cdot \sqrt{2\pi}} \cdot exp\left[-\frac{1}{2} \cdot \left(\frac{x}{\sqrt{2Dt}}\right)^2\right] = \frac{1}{\sigma(t) \cdot \sqrt{2\pi}} \cdot exp\left[-\frac{1}{2} \cdot \left(\frac{x}{\sigma(t)}\right)^2\right] \tag{2.20}$$

Equation 2.20 describes the evolution of the probability distribution function $n(x,t)$ for $t > 0$ for random walk of a particle starting at $t = 0$ at position $x = 0$. It is reasonable to use $\sigma(t)$ to quantify the mean diffusion length in time since the average displacement by random walk is naturally zero (the center of the distribution $n(x,t)$ remains unchanged, see also fig. 2.11). Today, the variable MSD ("mean squared displacement") is often used in literature [96, 97]:

$$MSD_{1D} := \sigma(t)^2 = 2Dt \tag{2.21}$$

The MSD shows a linear dependence in time. It is the square of the standard deviation σ. Thus, we find that any characteristic diffusion length has to be scaled to time t sublinearly as $\sqrt{t}$. Diffusing particles with a limited life time τ are often investigated. Thus, a characteristic diffusion length λ_{diff} is defined as follows according to references [98, 99]:

$$l_{diff} = \sqrt{D\tau} \tag{2.22}$$

The studies in this thesis have been performed on layered systems. Hence, diffusion is quantized by the hopping of the diffusing particles from one layer to the next with an interlayer distance l_{layer}. In analogy to reference [39] a hopping time $t_{hopping}$ can be introduced, based on equation 2.21. This provides a characteristic hopping time for one dimensional diffusion:

$$t_{hopping} = \frac{(l_{layer})^2}{2 \cdot D} \tag{2.23}$$

Diffusion of charges is related to the mobility μ of charge carriers. When the diffusion constant D is known, the mobility μ can be easily calculated according to the Einstein-

Smoluchowski-relation [100–102]:

$$D = \mu \cdot \frac{k_B T \cdot}{q} \tag{2.24}$$

where k is the Boltzmann's constant, T the absolute temperature and q the charge of the diffusing particle. This may be simplified to:

$$D \approx \mu \cdot 0.025\, V \tag{2.25}$$

for the diffusion of electrons and holes at room temperature $T \approx 300K$.

In conclusion, diffusion is a random walk process describing statistically occurring transfer processes such as hopping. Parameters have been provided that are used to quantify diffusion.

3 Experimental Details and Methods

Hybrid assemblies of colloidal CdTe and CdSe nanocrystals have been investigated experimentally in this thesis. Hence, experimental details and characteristics of the CdTe and CdSe nanocrystals are introduced before presenting the experimental methods of nano-assembly and the measurement techniques. Layered assemblies on solid and dry substrates have been prepared as well as colloidal self-organization in suspension. UV-vis extinction spectroscopy, steady state and time resolved PL-measurements and SPV-spectra and SPV-transients have been applied for the experiments in this thesis.

3.1 Experimental Details on Semiconductor Nanocrystals

3.1.1 Water Based Synthesis of CdTe and CdSe Nanocrystals

Nanocrystals can be obtained by different methods. Colloidal chemical synthesis in organic or polar solvents was used for this thesis and refers mainly to nanocrystals. Nanostructures grown by physical vapor deposition (PVD) techniques such as molecular beam epitaxy (MBE) or by chemical vapor deposition (CVD) in vacuum deposition machines are usually named quantum dots or quantum structures to differentiate between the two. [103, 104]

We concentrate here on the synthesis routine that was proposed by Gaponik et al. [63] The water-based synthesis is illustrated in fig. 3.1. This was carried out under nitrogen to avoid the presence of CO_2 or O_2. The precursor solution consists of $Cd(ClO_4)$ and thiol containing ligands (R-SH) in water. Its pH-value is adjusted to 11.2 - 11.8 by adding a solution of NaOH. The chalcogenid is added as gaseous H_2Te or H_2Se and is produced separately by dropping H_2SO_4 on Al_2Te_3 or Al_2Se_3. N_2 was used as carrier gas.

Heating the precursor solution leads to the nucleation of the nanocrystals. The ligands slow down the crystal growth so that the nanocrystals can grow as monocrystalline structures. The sulfur of the thiol groups coordinates with Cd and passivates the nanocrystal surface at least temporarily. The growth of the crystals occurs by the Ostwald ripening process where the larger nanocrystals grow while the smaller ones disappear. It is driven by minimizing the surface energy. [106] Hence, the reaction time determines the size of the nanocrystals. The nanocrystal solutions obtained from

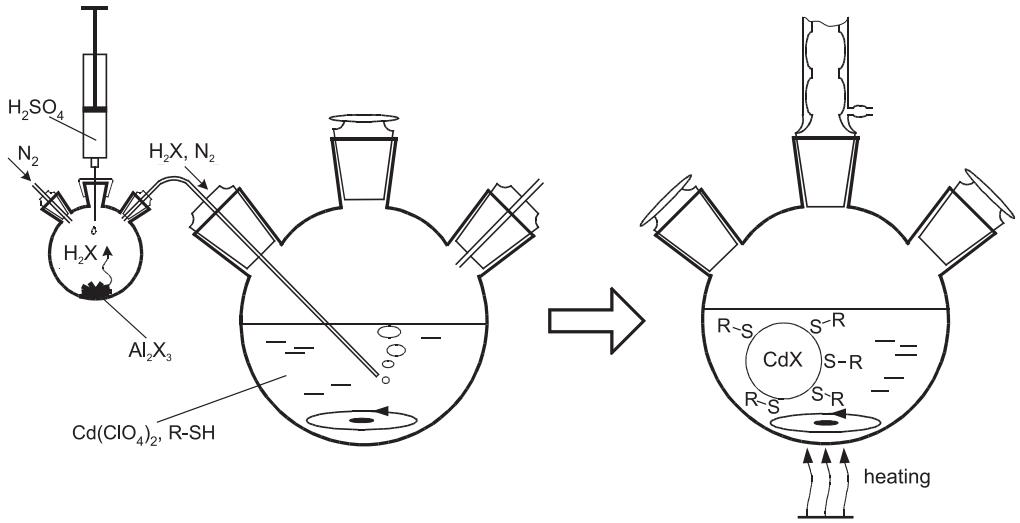

Figure 3.1: The nanocrystals are produced in a water-based chemical synthesis. The symbol "X" stands for Se or Te; R is an organic end group of the ligand. H_2X is produced from aluminum selenide or telluride and bubbled through a precursor solution containing $Cd(ClO_4)$ and ligands. The nanocrystals are formed when the solution is heated. The illustration was adapted from reference [105].

the synthesis can be further refined in size distribution by a size selection routine. By adding alcohol to the solution and by subsequent centrifugation, nanocrystals of different sizes can be precipitated step-by-step. The solubility of the nanocrystals depends on the ratio of ligands on the surface to the volume of nanocrystals. Hence, different sizes can be selectively separated. Moreover, the size selected re-dissolved nanocrystal solutions are purged from any excess reactants. For this reason parasitic effects from other materials have been excluded from my studies. [63]

Altogether the synthesis routine for TGA-capped CdTe and CdSe nanocrystals was presented. Nanocrystals grow in a heated aqueous solution. The sizes can be adjusted depending on the processing time. A precipitation from solutions can be used to fractionate the solutions in order to obtain a narrow size distribution. [63]

3.1.2 Size Characterization of CdTe and CdSe Nanocrystals

Nanocrystals are characterized by their energy gap determining their physical properties. The energy gap is related to the size of the nanocrystals. The reference fit currently used [107] is a polynomial fit and is approved for CdTe nanocrystals from 3.5 to 8.0 nm. As I used smaller nanocrystals of about 3 nm in size I would now like to introduce a new model that is based on formula equation (2.4) and evaluated on the basis of data already documented.

The energy gap of nanocrystals $E_{gap}(NC)$ consists of the bulk material's band gap $E_{gap}(Bulk)$ and the quantization energy E_{quant} of the nanocrystal. According to equation (2.4) the following relationship exists between E_{quant} and an effective nanocrystal diameter d_{eff}, where we now introduce the fitting parameter Δd:

$$E_{quant} \propto \frac{1}{d_{eff}^2} =: \frac{1}{(d_{NC} + \Delta d)^2} \tag{3.1}$$

According to the quantum mechanical tunneling effect (fig. 2.2 a) the effective diameter d_{eff} is larger for an electron wave function in a quantum well with finite barriers than it is for the geometric diameter d_{NCs} of the well. Therefore, we introduced the parameter Δd which is used in the following as a fitting parameter. A physical interpretation is that Δd characterizes an effective the penetration depth of the electron wave function into the barriers. Moreover, the proportionality constant A is needed for the fit. We obtain the following fit (with the two parameters A and Δd):

$$d_{NCs} = \sqrt{\frac{A}{(E_{gap}(NC) - E_{gap}(Bulk))}} - \Delta d \tag{3.2}$$

where d_{NCs} stands for the mean geometric diameter of the nanocrystals (in nm), $E_{gap}(NC)$ denominates the nanocrystal's energy gap (in eV) determined from the wave length of the first absorption peak, $E_{gap}(Bulk)$ is a documented value of the band gap energy for the same bulk material (in eV, see tab. 2.1) and A and Δd are the only fitting parameters (their units are nm·eV and nm respectively). All parameters are displayed in table 3.1, the fit is presented in fig. 3.2. In parallel to my work on an improved fitting model, other publications also appeared using new fitting models based on the physical relation between the quantization energy E_{quant} and the nanocrystal diameter d_{NC}. [108, 109] A four parameter fit was used.

Fig. 3.2 presents documented data on energy gap and nanocrystal diameter which have been obtained from the first absorption peaks and transmission electron microscopy photographs. [25, 107] CdTe (fig. 3.2 a) and CdSe nanocrystals (fig. 3.2 b) are illustrated. The fitting curves proposed by Yu et al. [107] by a polynomial four or five parameter fit is illustrated in gray. The best fit in accordance with the two parameter fitting of equation (3.2) is shown in dark green. The parameters shown in table 3.1 have been used for the fitting curves.

The significant difference of the fit presented (equation 3.2) and the one of Yu et al. can only be observed for the CdTe nanocrystals below 3.5 nm in size. For the rest a good agreement can be observed. Thus, the parameters obtained in table 3.1 can be discussed for their physical relevance. The proportionality parameter A can be

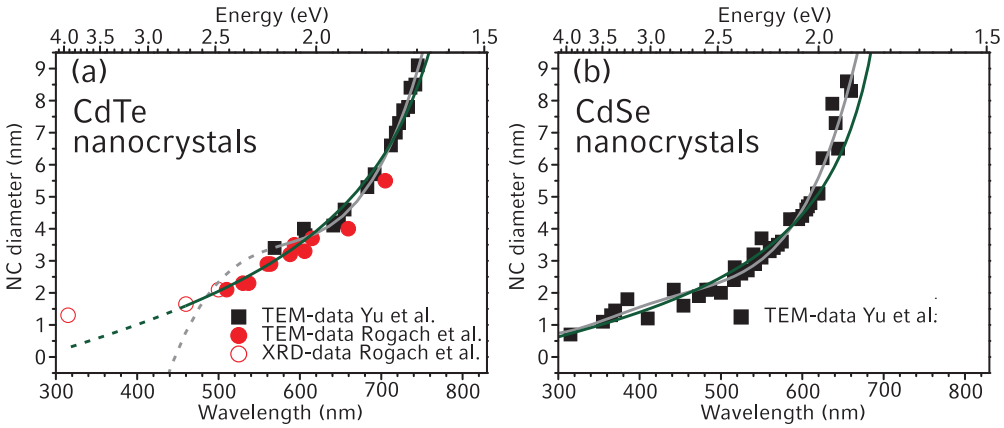

Figure 3.2: The "sizing curves" for CdTe (a) and CdSe (b) nanocrystals are displayed. They correlate the measured energy gap and nanocrystal size. The data points have been extracted from Yu et al. (reference [107], black squares) and Andrey et al. (reference [25], red circles). The fits are displayed for Yu et al. (reference [107], gray) and according to equation 3.2 with the parameters shown in table 3.1 (dark green). Broken lines are extrapolations of the fits.

	Δd	A	$E_{gap}(Bulk)$
CdTe nanocrystals	2.825 nm	23,85 nm·eV	1.477 eV
CdSe nanocrystals	1.795 nm	14.27 nm·eV	1.7 eV

Table 3.1: Fitting parameters obtained for nanocrystal sizing curves from data of references [25, 107]. The values of Δd in larger than 1 nm demonstrates the non negligible overlap of wave functions with the environment. It is attributed to the finite barrier height of the organic ligands and the solvent.

compared to the factor $3 \cdot \left(\frac{\hbar^2\pi^2}{2m_e^*} + \frac{\hbar^2\pi^2}{2m_h^*}\right)$ in equation (2.7) and A is of the same order of magnitude as the theoretic value.

The variable Δd may be more important. This parameter value is the difference between the geometric diameter of the II-VI semiconductor material of the nanocrystals and the real expansion of the electron and hole wave functions. Therefore, Δd indicates how strongly the evanescent wave functions penetrate the barrier of organic ligands and other surrounding media. This is important for tunneling transfer dynamics which is the main topic of this thesis. The fit provides a virtual broadening of the nanocrystals' diameter by 2-3 nm. Hence, there is probably still a significant evanescent electron wave function after 1 nm barrier width that may feature hopping transfer dynamics.

In conclusion a new fitting model with only two parameters was successfully introduced. The interpretation of this physical model indicates that the electronic wave functions are not just confined to the geometric nanocrystal diameter but a significant penetration beyond 1 nm around the nanocrystals may be likely. This highlights the

possibility of electronic interactions which are relevant especially for charge transfer and charge separation dynamics.

3.1.3 Stokes Shift for the CdTe Nanocrystals Used

Fig. 3.3 presents the absorption and emission data of various nanocrystal solutions in water. Only nanocrystal batches or high quality are plotted. The nanocrystal diameter is calculated according to the formula and parameters in chapter 3.1.2. We observe a Stokes shift of 50-200 meV as difference between absorption and emission of the investigated nanocrystals. A general trend of decreasing Stokes shift with increasing nanocrystal size can be seen.

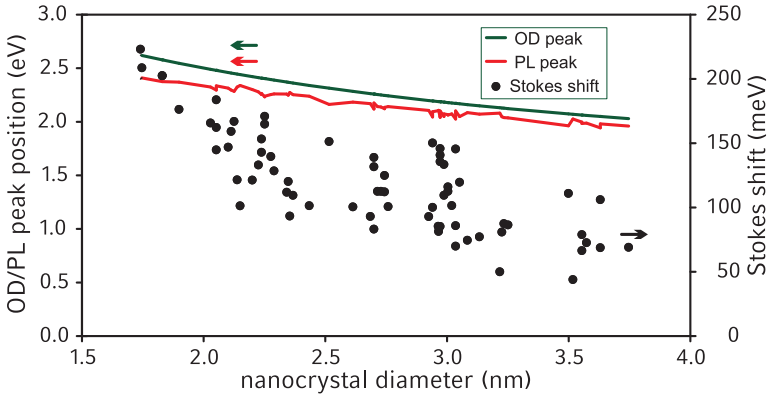

Figure 3.3: This shows data on the Stokes shift experimentally obtained in CdTe nanocrystals. The positions of the first absorption peak (dark green) and PL-emission peak (red) are correlated to the diameter of the CdTe nanocrystals. The Stokes shift (dots) was calculated from its difference (typically 50-150 meV for nanocrystals in this thesis). The nanocrystal diameter is calculated according to the formula and parameters given in chapter 3.1.2.

The Stokes shift is attributed to the exciton binding energy (by coulomb interaction; see fig. 2.9 c). This is smaller than the values expected from existing documentation. Typical exciton binding energy values are for CdSe nanoparticles of 4 nm diameter about 100 meV [76] and about 300 meV for 3 nm diameter. [74].

3.2 Assembly Methods

Most of the samples investigated have been established by the ordered layer-by-layer assembly. A nano self-assembly effect via opposite electrically charged groups was applied for this layered technique. This principle was also used for clustered assembly in solution.

3.2.1 Layer-by-Layer Assembly

The applied layer-by-layer (LBL) technique is based on electrostatic adsorption of nanocrystals (negative surface charge) and poly-electrolyte (positively charged) on substrates. Monolayers of nanocrystals are obtained in this way. [18, 19, 110]

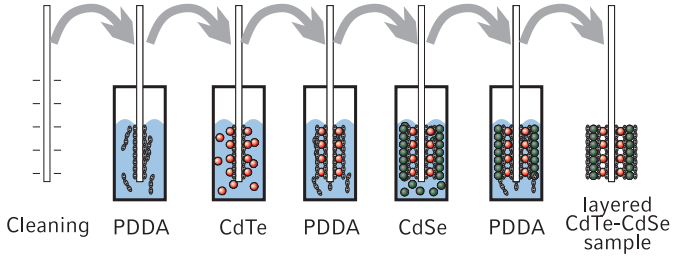

Figure 3.4: The assembly routine of LBL preparation is illustrated. Monolayers of each of the materials are grown by dipping a clean, charged substrate successively into the poly-electrolyte of positively charged PDDA and solutions of negatively charged CdTe or CdSe nanocrystals (negative charge due to TGA ligands). The LBL layers are deposited equally on all sides of the substrate.

The procedure of LBL deposition is illustrated qualitatively in fig. 3.4. The initial substrate cleaning leads to a negative surface charge. The positively charged PDDA polymer is adsorbed to the surface when this substrate is dipped in the poly-electrolyte with poly-diallyl-dimethyl-ammonium-chlorid (PDDA). As a result, the surface of the substrate becomes positively charged. Negatively charged nanoparticles are electrostaticly adsorbed into the surface in the subsequent dipping step with nanocrystal solution. The TGA-ligand shell of the nanocrystals contains a carboxylic group (-COOH) that becomes negatively charged in water ($-COO^- + H_3O^+$). Therefore, the nanocrystals become electrostaticly bound to the positively charged surface.

There are two different approaches for the cleaning: plasma-cleaning and chemical cleaning. Both lead to a negative charging of the surface. To apply plasma-cleaning the substrates have been successively pre-cleaned in an ultrasonic bath containing isopropanol, acetone, Helmanex solution (5 %) and deionized water, each time for 20 minutes. Then the samples were stored under water before being used. Shortly before LBL preparation, the substrates were dried in N_2 air flow and exposed for 5 min to a plasma cleaner (Harrick PDC-32-G2, 18W). Immediately after the plasma-cleaning the LBL deposition was started with PDDA solution.

The chemical cleaning routine does not need the pre-cleaning in ultra sonic bath. The samples were simply cleaned in a heated 1:1:3 solution of NH_3 (25 %) : H_2O_2(30 %) : H_2O at 70 °C for 1 h and cooled down for 20 - 30 min. After this treatment the surface is charged negatively (The applied mixture is softly etching SiO_2 according to

reference [111]). After rinsing the samples can be stored for about one week in water before they lose significantly their surface charge.

We used cationic and anionic polymers for self assembly of nanocrystals into monolayers. The TGA-ligands of the nanocrystals are negatively charged. Hence, the positively charged ammonium groups in the polymer PDDA monomers (fig. 3.5) attach electrostatically to the carboxyl groups of TGA ligands.

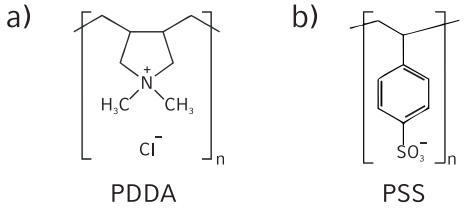

Figure 3.5: This shows the chemical structure of the monomer of PDDA (a) and PSS (b).

Poly-styrene-sulfonate (PSS) was also used in one of the experiments presented as anionic poly-electrolyte (fig 3.5 b). Both PDDA and PSS were used in a concentration of 1 mg/mL in 0.5 M NaCl solutions. Such polymers lead to a layer thickness of about 0.5 nm in layered nano-self-assembly for each polymer layer since they may interpenetrate with surrounding organic materials [19, 47]. The LBL preparation with only PDDA and nanocrystals leads to the formation of nanocrystal monolayers with an interlayer distance of about 1 nm. [19] To increase the interlayer spacing we introduced a multiple polymer layer of PDDA and PSS (1 mg/mL in a 0.5 M NaCl solution) and again PDDA for specific samples. This is supposed to increase the interlayer distance to about 2 nm.

The optimized procedure for the LBL deposition was taken from Franzl et al. [47] The LBL assembled samples were coated by alternating deposition of the positively charged PDDA (1 mg/mL in a 0.5 M NaCl solution) and negatively charged CdTe or CdSe nanocrystals from their purified stock solution (typically 10 - 100 μM for CdTe nanocrystals and 100 - 1000 μM for CdSe nanocrystals).

Typically 1 ml of nanocrystal solution and 2 ml of poly-electrolyte solution were used for the standard deposition on microscopy glasses measuring approx. 1 x 12.5 x 75 mm^3. Since we used rectangular cuvettes with a base plate of 10 x 10 mm^2 the samples could be placed diagonally into the cuvettes so that the substrates were standing in the solution without touching surfaces. Thus, a sample area of more than 1 mm^2 was coated homogeneously on both sides of the substrate.

Any excess material above one monolayer can easily be removed in washing steps after one dipping cycle since it is not electrostatically bound (not depicted in fig. 3.4). In

this way defined monolayers of nanocrystals and polymers are obtained. The surface charge of the nanocrystal coated surface is again negative in water. Thus, the next coating step with positive PDDA can be carried out to prepare the substrate for the next nanocrystal layer. Each polymer or nanocrystal layer took 15 min. All samples were finished off with a layer of PDDA also to passivate the ligands on the surface in the same way as they are passivated in the underlying layers. Effects due to different environmental conditions [73] are thus suppressed.

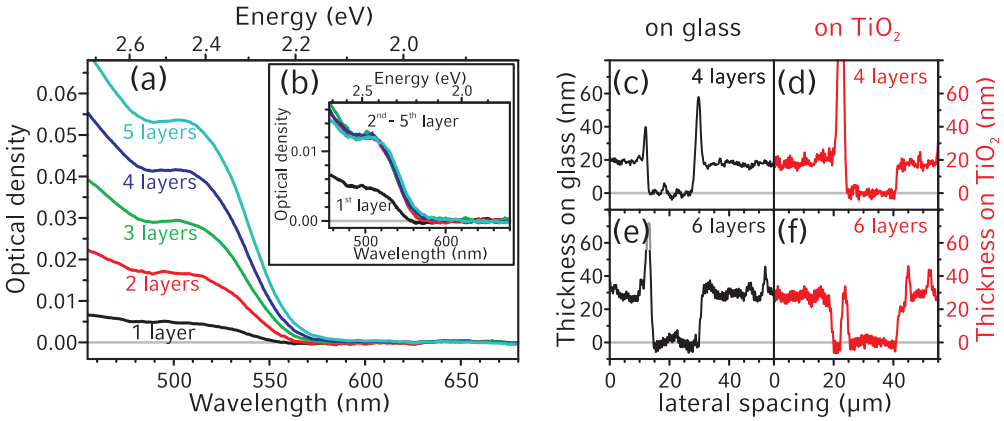

Figure 3.6: The growth and layer thickness of the nanocrystal monolayers was investigated. Transmission spectra for LBL films containing 1 - 5 layers of CdSe520 nanocrystals are displayed (a). The optical density of each single layer can be obtained from this (b). Obviously the first layer contains only 40 % of the amount of nanocrystals compared to the other layers. The film thickness was measured with a profilometer for four CdTe629 layers on glass (c) and on sputtered TiO_2 (d), as well as for six layers of CdTe629 on glass (e) and TiO_2 (f). The observed valley of about 15 μm was cut with a blade to obtain the height contrast between substrate and film.

We performed thickness measurements of LBL films with nanocrystals (fig. 3.6). Transmission spectroscopy was performed during the steps of PDDA deposition. Thus, the homogeneous increase of the optical density (OD) with each layer was monitored (fig. 3.6 a). From this we were able to deduce the OD of each single layer (fig. 3.6 b). Since the OD is proportional to the particle concentration (equation 3.4), we find that all layers are deposited with an identical amount of nanocrystals except the first nanocrystal layer which generally has a lower concentration of the order of 30 to 50 %. This is consistent with reference [19].

To measure the mechanical thickness, a Veeco Dektak 6M profilometer was applied (fig. 3.6 c-f). We used CdTe629 on two different substrates: standard microscopy glass and a compact layer of 20 nm TiO_2. A small scratch was made in the soft LBL layers with a blade (a check was made to ensure that such scratches do not damage the

substrates). In the graphs presented we observe a clear valley of 15 μm width where the nanocrystal-polymer layers have been removed. These spaces are surrounded by spikes which are attributed to the dislocated material (due to scratching). The thickness of the four layers of CdTe629 was determined to be 20 nm on both glass and TiO_2 (fig. 3.6 c,d), the six layers of CdTe629 present a thickness of 30 nm (fig. 3.6 e,f). This corresponds to an average thickness of 5 nm per PDDA-CdTe629 double layer. When we know the diameter of the nanocrystals is 4 nm we can extract the thickness of 1 nm for the organic layers composed of PDDA and the nanocrystals ligand shell.

In conclusion the LBL assembly leads to mono-layers of nanocrystals with a standard interlayer spacing of 1 nm. This layered nano-self-assembly is based on electrostatic adsorption. The nanocrystals used provide TGA-ligands which are negatively charged in water; in contrast the polymer PDDA presents positively charged groups in water. Experimental results indicate a well controlled mono-layered growth on each side of the substrates.

3.2.2 Colloidal Clustering

The colloidal clustering of nanocrystals is another method that is used to achieve closely packed nanocrystal structures. [21,22] Adding the Ca^{2+}-ions to TGA-capped nanocrystals leads to a disordered assembly of nanocrystals. Clustering offers in particular a quick tool to study effects of closely packing and an alternative hybrid assembly compared to layered assembly. It is however limited to short experiments as precipitation may occur after some hours.

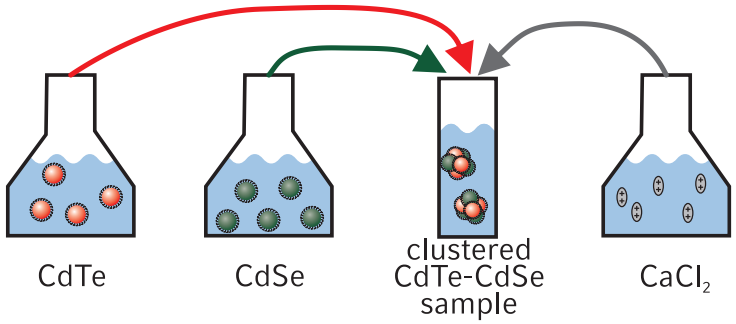

Figure 3.7: To prepare clustered samples of semiconductor nanocrystals we mix diluted nanocrystal solutions with $CaCl_2$ solution. Clusters of nanocrystals are formed within 30 min. The Ca^{2+} ions induce the clustering. [21]

We prepared a diluted solution of TGA capped nanocrystals (about 0.4 μM for each type of nanocrystals) so that the optical densities investigated did typically not exceed 0.1. The clustering is induced by adding Ca^{2+} ions (fig. 3.7). We use $CaCl_2$ in a

concentration of 100 μM. After mixing the solutions we waited 30 min before taking the measurements.

An electrostatic binding of the divalent cation with two negatively charged carboxylic groups leads to the formation of these clusters. Thus, an inter-particle distance of about 1 nm can be expected. The size of the clusters is estimated by dynamic light scattering measurements (Zetasizer Nano ZS90, Malvern) to be on the order of 100 nm.

3.3 Spectroscopy

The present work is based on optical spectroscopy. Extinction spectroscopy was used to monitor the composition of the samples. PL-signals of the samples have been monitored to study charge separation effects inducing PL-quenching. Steady state spectra and time resolved PL-graphs have been evaluated. SPV-measurements (spectroscopy and time resolved) were applied to provide direct evidence of charge separation.

3.3.1 Extinction Spectroscopy

Steady state extinction spectroscopy (fig. 3.8) was applied to obtain absorption spectra. We used a Varian Cary 50 UV-vis or a Varian Cary 5000 UV-vis-NIR spectrophotometer.

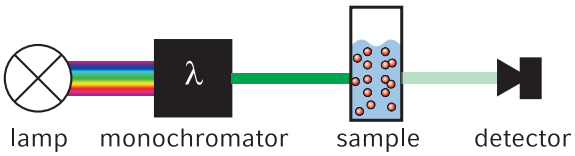

Figure 3.8: This shows the principal setup for extinction spectroscopy.

Optical Density Measurements

Monochromated light of the intensity $I_0(\lambda)$ is passed through a sample (fig. 3.8). The intensity $I(\lambda)$ transmitted through an ideal specimen is in accordance with the Beer-Lambert law [112]:

$$I(\lambda) = I_0(\lambda) \cdot e^{-\sigma(\lambda) \cdot n \cdot d} \tag{3.3}$$

where $\sigma(\lambda)$ is the wavelength dependent extinction cross section, n the particle density and d the sample thickness. Taking the logarithm of equation 3.3 we obtain the wave length dependent optical density $OD(\lambda)$:

$$OD(\lambda) = log_{10} \frac{I(\lambda)}{I_0(\lambda)} = \epsilon(\lambda) \cdot c \cdot d \tag{3.4}$$

where $\epsilon(\lambda)$ is the extinction coefficient $\epsilon(\lambda) = \sigma(\lambda)N_A/ln10$, c the particle concentration $c = n/N_A$ and N_A the Avogadro number.

Using the equation 3.4 we were easily able to compare the particle concentration c in the samples to allow precise quantitative analysis (the nanocrystal concentrations have been compared at the position of the first excitonic peak). The optical thickness of the samples in absorption was typically below 0.1 corresponding to above 80 % of light transmission.

Scattering Correction for OD-Data

We performed extinction spectroscopy of solved or dispersed samples in cuvettes or dry layered sample on glass substrates. Extinction in these real samples consists of the following contributions: Absorption by the investigated material (OD_{abs}), absorption by matrix material (substrate, impurities and solvent) (OD_{matrix}), scattering at the geometric shapes and configurations in the sample ($OD_{scat.}$) and (directed) reflection on interfaces of changing refractive interfaces ($OD_{refl.}$).

Therefore, the globally measured OD of the sample becomes:

$$OD(\lambda) = OD_{abs}(\lambda) + OD_{matrix}(\lambda) + OD_{scat.}(\lambda) + OD_{refl.}(\lambda) = log_{10}\frac{I(\lambda)}{I_0(\lambda)} \quad (3.5)$$

The absorption of the matrix material or the substrate (OD_{matrix}) can be measured. The contribution of reflection ($OD_{refl.}$) is generally a constant offset for the applied samples (except the layer thickness of material deposited on substrates becomes significant (e.g. >100 nm) so that film thickness interference pattern may occur). Thus, the intensity I_0^* of a glass substrate or cuvette with solvent was measured as reference. Equation 3.5 can be simplified to:

$$OD^*(\lambda) = OD_{abs}(\lambda) + OD_{scat.}(\lambda) = log_{10}\frac{I(\lambda)}{I_0^*(\lambda)} \quad (3.6)$$

The scattering term is supposed to dissappear in theory at small nanocrystal sizes used [47]. However, as a few samples had impurities or scratches, it seemed useful to fit the scattering. In analogy to the Mie scattering from atmospheric spectroscopy, the following simple empirical relation may be used:

$$\sigma_{scat.}(\lambda) \propto \lambda^{-\alpha_{Angström}} \quad (3.7)$$

where $\alpha_{Angström}$ is called Angström coefficient of disturbance with $0 < \alpha_{Angström} \leq 4$. [113] We also extended the OD*-measurements to the NIR-vis range where no absorption of the sample was present. This part was fitted according equation 3.7 for possible scattering. Moreover, an offset from a slightly different reflection was subtracted. In

this way, we obtained the background corrected absorption spectra OD_{abs}. An extreme example for this fit is displayed in fig. 3.9 for demonstration with low nanocrystal load (below one monolayer) and extremely high scattering background.

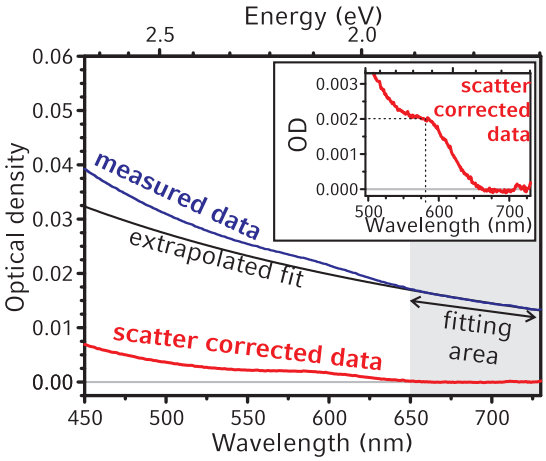

Figure 3.9: Scattering correction according to equation 3.7 is presented for the extreme example of inkjet-printed CdTe580 nanocrystals on glass corresponding to not even one monolayer of nanocrystals (blue). The best fit of the part with no absorption (from 650 nm to the infra-red) is displayed according to equation 3.7 (black). The extrapolation of this fit is subtracted from the measured data to obtain the scatter-corrected data (red). The inset shows the corrected data. After making this correction, it is now possible to extract the nanoparticle concentration. All OD data evaluated during this thesis showed nearly no scattering. The example presented was just chosen to clearly illustrate the correction method.

3.3.2 Photoluminescence Spectroscopy

PL-spectroscopy was one of the principle methods of investigation used in this thesis (fig. 3.10). Samples have been excited with a fixed wavelength. In general the excitation wavelength was about 400 nm so that all the nanocrystals were excited simultaneously. However, some experiments were also carried out, where only one component of a hybrid assembly was selectively excited.

The PL-emission was detected either as spectra or for a fixed wave length. The PL-signal was collected at an angle of 90° with respect to the excitation beam.

Samples in solution have been measured in cuvettes. To avoid reflection of the excitation light into the emission light path, the cuvettes have been oriented parallel with their surface normal to the excitation beam (fig. 3.10). Solid samples on planar glass substrates have been positioned at an angle of 54.7° to avoid polarization dependent detection of the PL-light by the monochromator. The direct reflection of the excitation light was directed away from the detection path. The OD of the samples was low to

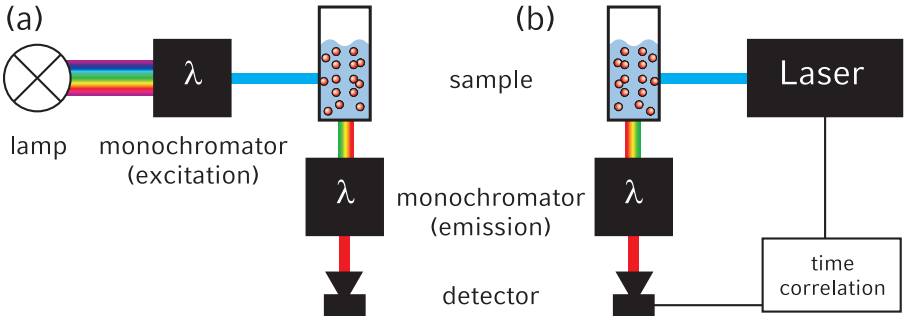

Figure 3.10: This shows the principal setups for steady state PL-spectroscopy (a) and time correlated single photon counting using a laser as excitation source (b).

avoid misleading interpretation due to re-absorption within the samples (OD < 0.1 at position of PL-emission).

Steady State Photoluminiecence

The steady-state PL-spectra were taken with a Varian Cary Eclipse spectrophotometer and a Horiba Jobin-Yvon Fluorolog-3 spectrometer. Both use as light sources Xenon lamps and apply monochromators with gratings to filter the excitation and the emission light. Thus, higher order diffractions may pass the monochromator and must be blocked by additional filters.

Spectra have been recorded in the spectral range of 300 - 1000 nm. With respect to the applied scanning settings the measurement time did not exceed 1 min for one spectrum. The excitation intensity was the same for each set of samples (containing hybrid and reference samples). Attention was paid to staying within the linear regime of the detector (photomultiplier).

Normalization of PL-Data

There may be many ways to normalize the PL-graphs depending on what should be emphasized. In the context of this thesis it was the aim to investigate how the relative quantum efficiency of the investigated nanocrystals changes when they are included in hybrid assemblies.

In the PL-experiments presented we have one hybrid sample containing two types of semiconductor nanocrystals and two reference samples for the corresponding individual nanocrystals. Thus, it makes sense to rescale the reference samples to make them comparable with the hybrid samples.

We fitted the OD-spectra of the hybrid sample by linear superposition using a least square fit (see fig. 4.4 b). In this way we obtained the relative concentration variations

between hybrid and reference samples. Moreover, we used the OD-spectra to calculate how much energy is absorbed from each component in the hybrid and the reference sample. The reference graphs have then been rescaled accordingly. The normalization corrections generally remain small and normally do not change more than about 5 %.

It is important to use comparable samples in order to exclude, for instance, additional effects originating from photo-degradation or a significantly different optical thickness. We took care to prepare all samples in parallel and the sample age did not differ by more than 1 h at measurement (for OD and steady state PL). The sample thickness was in general comparable (similar layer numbers). All samples have been prepared on a shaded laboratory space, then stored and transported in a black paper box to avoid photo-degradation.

To conclude, the PL-graphs of the references have been normalized in this thesis so that the relative quenching or enhancement of the relative PL-efficiency can be directly observed for the corresponding reference sample. We only need then to compare the peak heights of the references (colored graphs) with the black graph of the hybrid assembly.

Time Resolved Photoluminescence

Two setups have been used for time resolved PL. The PicoQuant FluoTime 200 is a setup for time correlated single photon counting to measure the time evolution at a fixed excitation and a fixed emission wave length (scheme in fig. 3.10 b). The time resolution of our slowly decaying PL-experiments was about 1 ns. Diode lasers with 405±5 nm or 470±10 nm have been used. The counting rate was limited to less than 1 % of the repetition rate of the laser to stay within the linear detection regime. The adjustment was done for the sample with the highest PL-intensity of each set of samples.

Second, a Hamamatsu C5680 streak camera was used to detect the PL-emission wavelength dependent and time resolved (fig. 3.11). The wave length resolution along one axis of the Streak camera's CCD chip is obtained by using a Chromex IS250 polychromator (40 gr/mm grating). The time resolution of the PL-emission is displayed along the second axis of a Streak picture. The spectrally resolved photons hit locally resolved the photo cathode of the Streak camera where the photons are transformed to free electrons (under vacuum). These electrons are accelerated through a grid counter electrode. Electrons passing this grid are deflected by a time-dependent electric field (perpendicular to the spectral resolution) to obtain the time resolution. Thus, the electrons now hit the screen resolved in wavelength and time. To detect this weak electron picture by the CCD chip the electrons are amplified spatially resolved in a micro channel plate. They then hit a phosphorescent screen and are transformed back to photons which are detected by the CCD chip of the Streak camera. We use the

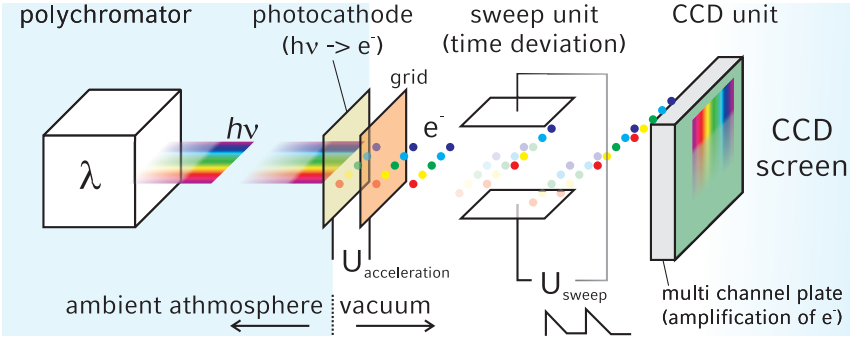

Figure 3.11: This shows the principals of the detection of a time resolved PL-signal with a streak camera. A periodically repeated time resolved PL-signal is first split spectrally by a polychromator in front of the Streak camera. The incident photons are converted to electrons in a photocathode and accelerated through a grid (under vacuum). In the sweeping unit a capacitor separates the time dependence along the vertical axis. In the end the electrons are amplified in a multi-channel plate and their impact on a phosphorescence screen was detected by a CCD chip.

streak camera with the "single sweep" plug-in (M5677) where the time window ranges from 5 ns to 10 ms and the time resolution is 50 ps in the best case.

For excitation in Streak experiments we used our femto-second laser setups. 400 nm light pulses of about 70 fs pulse width with 100 kHz repetition rate have been obtained from our amplifier setup. The 800 nm pulses of the Coherent RegA 9050 (a Ti:Sa regenerative amplifier) have been frequency doubled in a Coherent OPA (optical parametrical amplifier).

For 590 nm excitation pulses we first pumped a Coherent Mira 900-F Ti:Sa oscillator by a Coherent Verdi Nd:YAG (neodymium-doped yttrium aluminum garnet) continuous-wave solid-state laser. Thus, we obtained laser pulses of about 800 nm with 120 fs pulse duration and about 75 MHz repetition rate (this corresponds to a time window of 12 ns between the pulses). The laser pulses have been converted with a optical parametrical oscillator (OPO Advanced ring, Angewandte Physik & Elektronik GmbH) to about 590 nm wavelength. To reduce the repetition rate a pulse picker was used.

3.3.3 Surface Photovoltage

SPV experiments are quasi non-contact methods to track photo-excited charges in layered hybrid assemblies. Planar samples providing charge separating interfaces can be studied. [41–44] We used this method to clearly show directional charge separation and diffusion in layered hybrid nanocrystal assemblies.

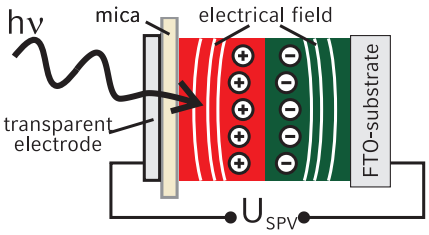

Figure 3.12: This shows the principle of SPV. A sample is excited by light ($h\nu$). Charge separation occurs across a charge selective interface. The separated charges provide an electrical field that can be measured as an SPV-signal (U_{SPV}) in an outer capacitor. To permit light absorption one electrode of the capacitor needs to be transparent. To capture significant signal the space between the capacitor needs to be small and homogeneous. Thus, a mica plate is used as spacer.

The SPV-setups are based on a "sample in capacitor" configuration (see fig. 3.12). Photo-excited electric dipoles provide electric fields which can be measured by an external capacitor. Since the capacitor is planar, only one dimensional charge separation across a large interface can be measured.

To excite the sample, at least one of the electrodes must be transparent to allow photo-excitation of the sample and subsequent charge separation in the sample. We used SnO_2:F (FTO) for both electrodes. The samples have been deposed on FTO (400 nm thickness) coated substrates by LBL assembly.

The experiments were executed under modulated excitation. This means that the measured charge separation dynamics (also including relaxation via recombination) were faster than the modulation frequency. Slower components are not resolved. All experiments have been executed in a home-made cryostat under a medium vacuum.

The measured signal U_{SPV} is proportional to the amount of separated charges Q and their averaged separation distance d (perpendicular to the capacitor plates) [42]:

$$U_{SPV} \propto Q \cdot d \tag{3.8}$$

SPV allows conclusions to be made concerning charge separation efficiency and time resolved dynamics. We use SPV-spectroscopy here to compare samples. SPV-transients have been applied to reveal details about diffusion.

The setup for SPV-spectroscopy is displayed in fig. 3.13. The light from a 250 W halogen lamp was used for excitation. It was monochromated by a prism-monochromator (intensity at 550 nm on the order of 10 W/m^2). The SPV-spectra taken have not been corrected for changing excitation flux to show the raw data. A chopper wheel (about 3 Hz) was used. We used a high impedance 500 MHz buffer (input resistance > 100 GΩ, output resistance 50 Ω) with 10 GΩ load resistance. The measurement circuit had an

RC time constant of the order of 100 ms. SPV-spectra were taken with a lock-in amplifier (Signal Recovery Model 5210). The lock-in amplifier measures the signal in phase with excitation and the 90° phase shifted signal (also called quadrature). A retardation of a positive signal results by convention in a negative quadrature signal.

SPV-transients were measured with a 300 MHz-sampling oscilloscope with readout on logarithmical time-scale using an excitation at 442.8 nm wavelength of a pulsed dye laser (pulse length 5 ns, excitation intensity at the sample 0.2 mJ/cm^2, repetition rate 1 Hz).

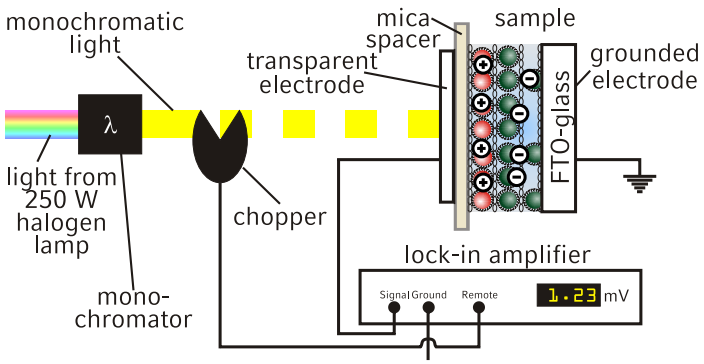

Figure 3.13: This shows the principles of SPV-spectroscopy. Light is first monochromated, then modulated by a chopper before it hits a sample. The light induced SPV-signal is measured with a lock-in amplifier.

4 Charge Separation between CdTe and CdSe Nanocrystals

The closely packed structures of CdTe and CdSe nanocrystals are studied in this chapter. We found evidence of charge separation indirectly by PL-spectroscopy which is induced by the expected type II alignment of CdTe and CdSe nanocrystals used. The PL-quenching observed of the CdTe nanocrystals is attributed to charge separation by electron transfer from CdTe to CdSe nanocrystals. It cannot be explained by energy transfer since energy transfer is shown to enhance slightly the CdTe nanocrystal's PL. Moreover, the PL-quenching correlates well to the energetic offset of the electron levels in the hybrid assembly which supports the expectation that the closely packed nanocrystals used also typically exhibit the same type II alignment as the assembly of bulk CdTe and CdSe. The effect was observed on two independent systems: colloidal clustered nanocrystals in solution and dry layered structures on glass.

4.1 Experimental System

CdTe and CdSe bulk materials exhibit a type II alignment. [54] Using CdTe and CdSe nanocrystals of comparable sizes (around 3 nm) the quantization energies for both materials can be compared since their effective electron and hole masses are comparable (chapter 2.2.2 and 2.2.3). Therefore, a type II alignment is expected for these CdTe and CdSe nanocrystals as illustrated in fig. 4.1 a,b. The type II alignment fosters the collection of photo-excited electrons in CdSe nanocrystals, whereas holes find their lowest excited state in CdTe nanocrystals.

The fundamental processes for the experiments are illustrated in fig. 4.1 b. After photo-excitation of CdTe nanocrystals, electrons and holes can decay radiatively by emission of luminescence light. The induced charge separation by electron transfer from a CdTe to a CdSe nanocrystal acts as an additional decay channel for the charge carriers. Thus, PL-quenching is an indirect indication of the charge separation in the hybrid system.

To take advantage of the interaction between nanocrystals, we used two different methods to obtain closely packing: clustered assembly in solution (fig. 4.1 c) and dry layered assembly on glass substrates of alternating CdTe and CdSe nanocrystal

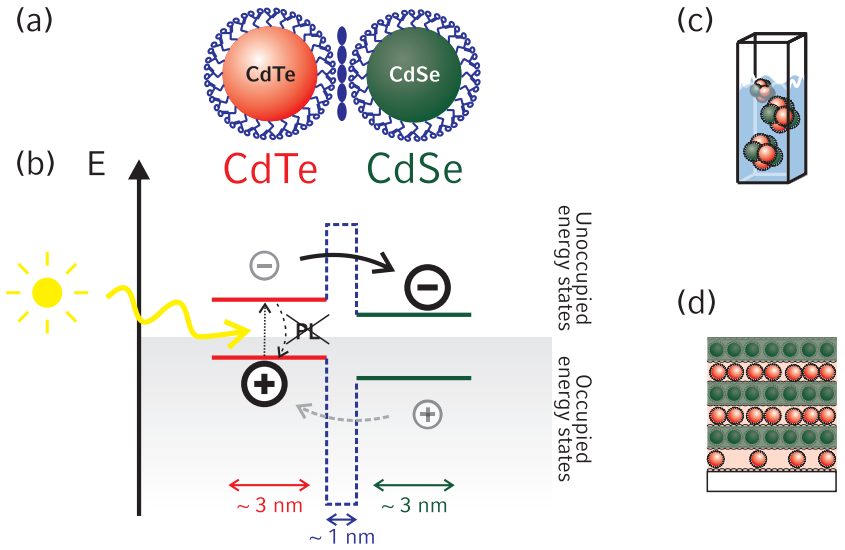

Figure 4.1: Closely packing of type II aligned CdTe and CdSe nanocrystals (a) leads to charge separation as shown in the energy scheme (b). Typical nanocrystals of about 3 nm in diameter are illustrated with the organic tunneling barrier of about 1 nm formed by ligands and polymer or ions between nanocrystals (b). The PL of CdTe nanocrystals is suppressed by electron transfer to CdSe nanocrystals. We studied hybrid assemblies by clustering (c) and of self assembled layered structures on glass (d).

monolayers or double-layers (fig. 4.1 d). Both methods result in inter-layer distances between CdTe and CdSe nanocrystals of about 1 nm. This is due to the short TGA ligands and the polymers or ions used to achieve the close packing [19,21]. The organic materials between the nanocrystals act as tunneling barriers as indicated in fig. 4.1 b.

All investigations have been executed on the decay of CdTe nanocrystals since the thiol capped CdSe nanocrystals used are bad emitters [24] and exhibit unstable and often weak PL-features in layered structures. Thus, the PL of the CdSe nanocrystals cannot be evaluated significantly within this thesis.

4.2 Photoluminescence Quenching Indicating Charge Separation

PL-measurements are presented in the following indicating charge separation between type II aligned CdTe and CdSe nanocrystals as a reason for the quenched PL of CdTe nanocrystals. First, we concentrated on a closely packed system with low order while using random clustering of nanocrystals before studying the PL-signal of layered struc-

tures in the next section. Both systems were investigated with steady state PL and time resolved PL.

4.2.1 Clustered System

PL-spectroscopy and time resolved PL-measurements have been applied to clustered assemblies of CdTe and CdSe nanocrystals. The strong PL-quenching of the CdTe nanocrystals indicates efficient charge separation by electron transfer from CdTe to CdSe nanocrystals.

The assembly of nanocrystal-clusters leads to an expected inter-particle distance of about 1 nm (chapter 3.2.2). We used CdTe567 (diameter: 2.9 nm) and CdSe529 (diameter: 2.9 nm, according equation 3.2). An offset of 0.36 eV can be calculated between the first unoccupied electron levels of CdTe567 and CdSe529 (according chapter 2.2.3). The optical densities of the samples are depicted in fig. 4.2 a. Fig. 4.2 b shows the corresponding PL-spectra taken at 400 nm excitation wavelength where both CdTe567 and CdSe529 absorb. The hybrid sample presents a quenched PL-peak at the emission of CdTe567. This indicates the expected charge separation. No PL-emission of the CdSe529 can be observed in any sample. (This is due to bad quantum efficiencies of those TGA-capped CdSe nanocrystals in water. [24])

The OD-graphs (fig. 4.2 a) have been used to determine the precise concentrations of nanocrystals in each sample. This allows for correction of the small concentration variations observed. We fitted the OD-curve of the hybrid sample with a least square fit (broken line, fig. 4.2 a) by linear superposition of both reference OD-graphs. Thus, from the fitting coefficients we obtained the relative concentration differences between hybrid and reference samples. This relative concentration variation has been applied to rescale the PL-intensities of the reference samples in fig. 4.2 b (according chapter 3.3.2).

A quenching of 63 % was obtained for the CdTe567 PL-emission in the hybrid sample (fig. 4.2 b). Hence, we can conclude that the PL of CdTe567 is quenched due to charge separation induced by electron transfer from CdTe567 to CdSe529. We can assume that energy transfer (see chapter 2.3.4) from CdTe567 to CdSe529 is very unlikely due to negligible spectral overlap and especially due to the unfavorable energy gaps, the smallest energy gap being located at CdTe567. Hence, energy transfer would lead to a PL-enhancement of the CdTe567 since it is the ET-acceptors. The quenching of steady state PL therefore strongly indicates charge separation in this type II aligned closely packed nanocrystal system.

More insight was obtained from the time resolved evolution of the PL-emission presented in fig. 4.3 a. The same samples as shown in fig. 4.2 were studied using a time correlated single photon counting setup. We used a PicoQuant FluoTime 200 at an excitation wavelength of 470 +/- 10 nm and an emission wavelength of 605 +/- 16 nm.

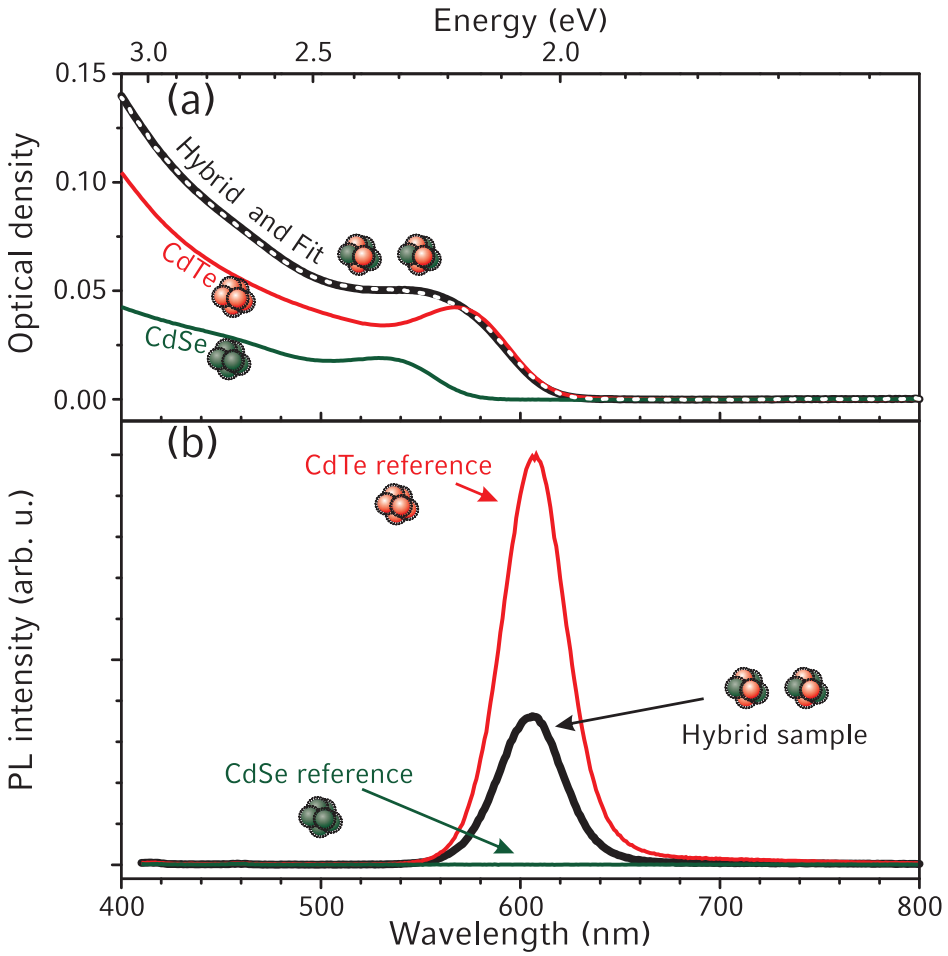

Figure 4.2: The PL-quenching data displayed shows charge separation in hybrid clustered assemblies of CdTe and CdSe nanocrystals. The OD (a) and PL-data (b) are presented for the hybrid clustered sample (black lines), CdTe567 reference (red line) and CdSe529 reference (green line). The OD of samples was fitted by linear superposition (broken line) to measure the exact content of nanocrystals. (b) The PL-graphs have been excited at 400 nm wavelength. Reference samples' PL-graphs have been normalized to the fitted concentrations. A quenching of 63 % was observed. (Data already presented in reference [114])

The same excitation intensity and measurement duration was applied so that the measured amplitudes can be compared directly. For more clarity, the normalized PL-decays have also been plotted in the inset to fig. 4.3 a.

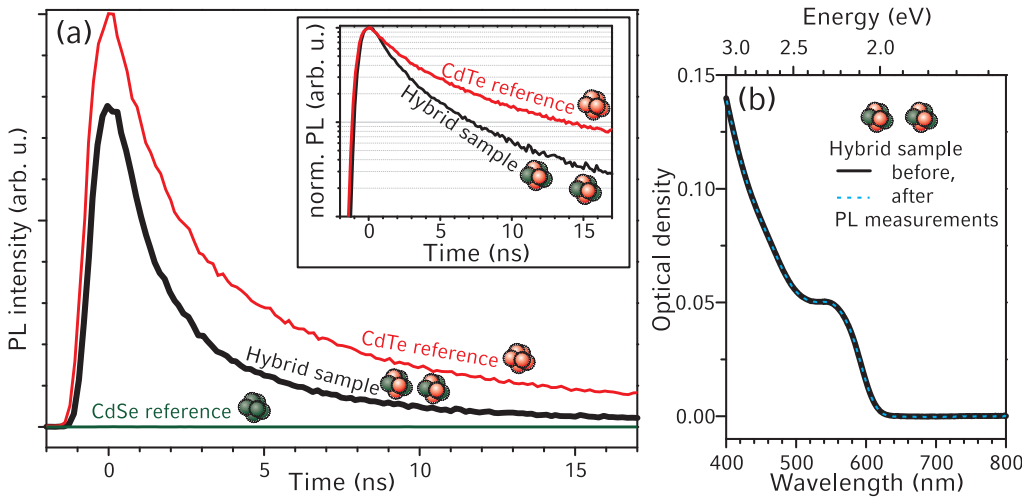

Figure 4.3: (a) Time resolved PL-data confirm the PL-quenching. The graph contains a hybrid clustered sample (bold black lines), CdTe nanocrystals reference (red line) and CdSe nanocrystals reference (green line). Excitation was at 470 +/- 10 nm, emission at CdTe nanocrystals PL-peak about 605 +/- 16 nm, time resolution was around 1 ns. The decays of the reference samples are normalized according to the fitted nanocrystal concentration in the hybrid sample. The inset shows data on logarithmic time scale normalized to their maxima. (b) The OD of the hybrid sample is displayed before (solid black line) and after (broken blue line) PL-measurements, proving no degradation. (The same data are already partially presented in reference [114])

As expected from the steady-state PL, a clear quenching of the CdTe567's PL was observed in time resolved PL-measurements for the hybrid sample. The faster PL-decay indicates the presence of a new decay channel. This is consistent with the expected charge separation via electron transfer from CdTe567 to CdSe529.

The spectra of the reference samples have been rescaled to the excitation intensity received per nanocrystal (see chapter 3.3.2). Thus, the initially reduced PL-amplitude indicates that a faster decay mechanism is present and effective on a timescale of at least 1 ns (the time resolution of the measurement).

This indicates a quick initial quenching on the nanosecond time scale caused by fast charge separation. We deduced a global quenching of 60 % (by integration of the presented PL-signals in time). This agrees with the 63 % obtained from steady state PL (fig. 4.2 b). Thus, the results of time resolved (fig. 4.3) and steady state PL (fig. 4.2) are consistent.

The inset to fig. 4.3 a shows the time resolved data normalized to their maxima on a logarithmic PL-intensity scale. A faster decay of the CdTe567's PL-emission is observed in the hybrid specimen compared to the decay of the reference sample. Furthermore, both decays are not mono-exponential. There are two major reasons: firstly, also the ensemble of one type of nanocrystals does not exhibit mono-exponential decay. Secondly, the disordered inhomogeneous clustering of nanocrystals provides a wide range of interparticle distances which at the same time induces a broad distribution of transfer times. According to formula 2.14 we obtain a rough order of magnitude value in the range of 3 - 6 ns for transfer times (depending on the evaluation of fig. 4.3 a or its inset).

The OD of the hybrid sample before and after the measurements does not change (see fig. 4.3 b). Hence, no photo-degradation effect can be observed for the studied system. Thus, we excluded other reasons for this quenching and found that only charge separation by electron transfer may explain the observations. Also environmental or solvatochromism effects as described in references [73,115] are excluded since both types of nanocrystals carry the same ligands (TGA), are solved in the same solvent and their stock solutions are size selected and purified. Hence, charge separation via electron transfer from CdTe567 to CdSe529 on nanosecond time scale is strongly indicated.

In conclusion, the experiments provide strong evidence of charge separation in a hybrid clustered system of CdTe and CdSe nanocrystals. The charge separation was monitored via the quenching of the CdTe567's PL-emission. In this way we monitored the effect of electron transfer from CdTe567 to CdSe529. We observed a quenching of about 60 % in the steady state PL for the presented nanocrystals. FRET has been excluded as a quenching mechanism since CdTe567 would normally serve in this configuration as ET-acceptor and should receive an PL-enhancement and not the observed PL-quenching. The time resolved PL-decays motivate electron transfer times on the nanosecond scale. All-in-all the measurements presented provide a strong indication of charge separation in closely packed systems of CdTe and CdSe nanocrystals of similar sizes.

4.2.2 Layered System

The results on layered hybrid samples of CdTe and CdSe nanocrystal are presented in the following and confirm the results on clustered samples presented above. The observed PL-quenching of CdTe nanocrystals indicates electron transfer from CdTe to CdSe nanocrystals leading to charge separation. Wavelength dependent measurements reveal that charge separation dynamics are obviously dominating energy transfer dynamics in the studied systems since for all measurements a strong PL-quenching of CdTe nanocrystals is observed in the hybrid samples. The LBL-method (chapter 3.2.1)

allowed better control of the nanoassembly since monolayers of nanocrystals are deposited. When we compared dry LBL-samples on glass substrates with the clustered systems in water presented above it was obvious that the environment surrounding the nanocrystals had changed significantly. This new environment affects the kinetics of the nanocrystals and the PL quantum yield for the CdTe629 decreased by at least one order of magnitude, while the quantum efficiency of CdSe nanocrystals emission rose significantly [73,116]. Nevertheless, a comparable PL-quenching behavior was observed for the CdTe nanocrystals, as reported above, in clustered assemblies. Once again, we observe PL-quenching for the CdTe nanocrystals used in hybrid CdTe629-CdSe507 and CdTe601- CdSe507 samples.

Measurements using different excitation wavelengths exhibited a small but significant contribution of energy transfer from CdSe to CdTe nanocrystals which also decreased the investigated PL-quenching of the CdTe nanocrystals. Nevertheless, the PL-quenching of CdTe nanocrystals remained dominant. In the following we present the results using steady state and time resolved PL.

Steady State PL

Fig. 4.4 presents PL-quenching of CdTe nanocrystals indicating charge separation. The optical data have been obtained on the following set of samples (fig. 4.4 a): two reference samples comprising six monolayers of CdTe629 (diameter: 4.1 nm) or CdSe507 (diameter: 2.6 nm). The hybrid sample was established with two layers of CdTe629 nanocrystals sandwiched by CdSe507 nanocrystal layers. The OD of the samples investigated is presented in fig. 4.4 b. Only the background offsets and weak scattering (see chapter 3.3.1) have been corrected for the OD-spectra. The PL-graphs of the references have been rescaled accordingly (see chapter 3.3.2). The arrows in fig. 4.4 b indicate the excitation wavelengths for the subsequent PL-measurements (fig. 4.4 c,d,e). Both CdTe629 and CdSe507 are excited with different relative intensities for excitation at (400±10) nm and (545±10) nm. At (600±8) nm excitation, only the CdTe629 nanocrystals are excited selectively; hence no PL-signal was detected for the CdSe507 reference in fig. 4.4 e. The large difference in the first excitonic absorption of CdSe507 and CdTe629 allows the selective excitation of only CdTe629 nanocrystals.

The hybrid sample exhibited a PL-quenching of the CdTe629 nanocrystals of about 60 - 70 % (fig. 4.4 c,d,e). This indicated charge separation by electron transfer from CdTe nanocrystals to CdSe nanocrystals. A clear excitonic peak of CdTe629 was observed around 660 nm for the reference sample without any significant trap emissions in the NIR range. In contrast the CdSe507 showed weak excitonic core emission at about 540 nm and a broad trap emission from 600 to 900 nm.

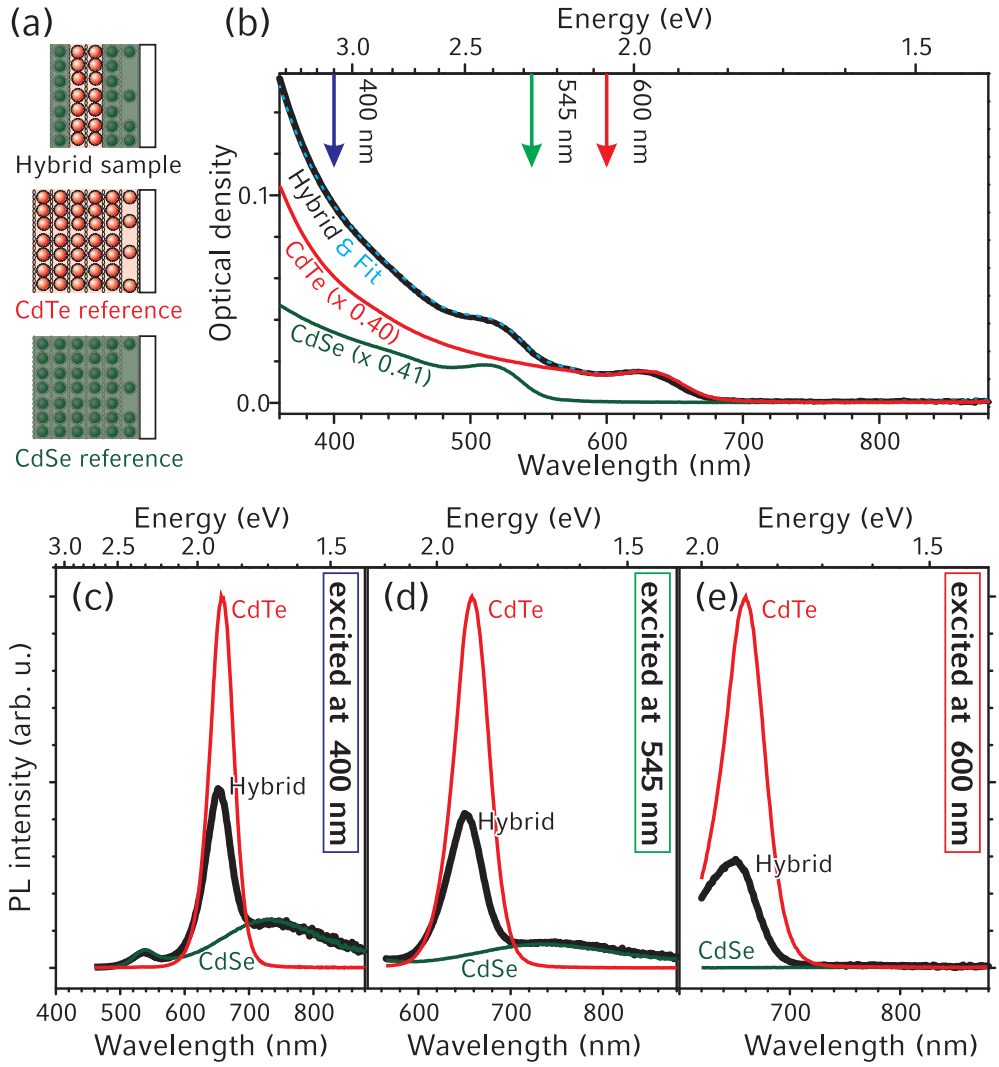

Figure 4.4: The PL-study on the CdTe629 nanocrystal's PL-quenching provides evidence of charge separation in layered nanocrystal assemblies. Studies relating to excitation wavelength exhibit the strongest quenching when only CdTe629 is excited selectively. This indicates additional energy transfer dynamics when CdSe507 is also excited. The schemes of the hybrid and reference samples are illustrated in (a). The hybrid sample consists of three CdSe507 and two CdTe629 layers (black), references of each six layers CdTe629 (red) or CdSe507 (green). The corresponding OD graphs are presented in (b) after background and scattering correction. The CdTe and CdSe OD graphs have been rescaled to achieve in linear superposition the best fit (broken blue) of the OD in the hybrid sample (b). The PL-response of the CdTe and CdSe reference sample has been rescaled accordingly. PL-measurements were carried out for the excitation wavelengths (400±10) nm (c), (545±10) nm (d) and (600±8) nm (e) as indicated in (b). Both CdTe629 and CdSe507 were excited for (c) and (d); only CdTe629 was excited for (e). CdTe is strongly quenched in all PL-graphs. No significant PL-quenching or enhancement of the CdSe507 was detected.

The PL of CdSe507 was not affected in the hybrid sample. The core emission at 540 nm and the broad trap emission from 600 to 900 nm remained unchanged. Thus, there was no evidence of hole transfer within the PL-lifetime of CdSe507 since the CdSe nanocrystals PL around 540 nm was not quenched. Moreover, there was no evidence of energy transfer from CdTe nanocrystals to the CdSe nanocrystal trap states in the NIR since no enhancement was observed in the NIR.

Further details of the differences between the excitations at 400, 545 and 600 nm can be seen from the quantitative data provided in table 4.1.

PL-excitation	400 nm	545 nm	600 nm
PL-quenching of CdTe629	59 - 60 %	62 %	68 - 71 %
$Abs_{CdSe507}$ / Abs_{Total} in hybrid sample	33 %	25 %	0 %

Table 4.1: The data evaluation of fig. 4.4 is presented in this table. The first line shows the applied excitation wavelengths. The second line presents the recorded PL-quenching for fig. 4.4 c,d,e (obtained from peak integrals and peak heights after subtracting the rescaled CdSe507 reference's PL). The portions of absorbed excitation intensity for CdSe507 in the hybrid sample relative to the total absorbed intensity of the hybrid sample are displayed in the third line. Weaker absorption of CdSe507 compared to CdTe629 is related to the significant smaller size of CdSe507 and hence to the significant lower extinction coefficient of CdSe507. [107].

The PL-quenching of CdTe629 became stronger when the excitation wavelength was increased up to 600 nm (approx. 70 %). At this position only CdTe nanocrystals were excited as there was no absorption at this wave length and no PL-emission was observed for the CdTe507 reference. Moreover, we did not see any enhancement of the hybrid sample's PL in the NIR so that energy transfer from CdTe629 to the luminescent trap states of CdSe507 can be excluded. Hence, we can conclude that the PL-quenching of about 70 % can be attributed to charge separation via electron transfer from CdTe629 to CdSe507 nanocrystals.

Furthermore, we observe that the decreased PL-quenching for excitation at 400 and 545 nm (fig. 4.4 c,d) is correlated to the absorption of the CdSe507 nanocrystals. This is a strong indication of significant energy transfer from CdSe507 to CdSe629 nanocrystals as the PL-emission of the CdTe629 nanocrystals in the hybrid sample is enhanced from about 30 to about 40 %. However, the effect of the charge separation still appears dominant compared to the energy transfer dynamics discussed.

Last but not least, a small blue shift of the CdTe629 nanocrystals' PL was observed at the hybrid sample for both the OD-spectrum (fig. 4.4 b) and the PL-spectra (fig. 4.4 c,d,e). This may be attributed to light-induced degradation of the sample at ambient air. However, this is a weak point when layered samples are studied by PL-spectroscopy. As the PL-emission of the CdTe629 nanocrystals changes, the PL-

efficiency may also decrease which may also cause the PL-quenching. However, the PL-quenching of the CdTe629 nanocrystals is the only argument relating to how charge separation can be detected by PL-spectroscopy. Thus, an independent direct proof of charge separation was required. This is described later in this thesis with SPV-techniques (chapter 5).

In conclusion, the results of the steady-state PL-spectroscopy indicate charge separation by electron transfer from CdTe to CdSe nanocrystals with a maximum quenching of about 70 % in the investigated system. Furthermore, we could observe small but significant effects of energy transfer from CdSe to CdTe nanocrystals.

Time Resolved PL

To support the conclusions from steady state PL-spectroscopy, we performed time resolved PL-measurements using different excitation wavelengths. We used CdTe601 and CdSe507 nanocrystals where an offset for the relevant electron energies is expected to be around 0.19 eV (according to chapter 2.2.1). The OD-data of the samples containing each eight nanocrystal monolayers are displayed in fig. 4.5 a together with the samples' schemes in the insets. The hybrid sample comprises alternating monolayers of CdTe601 and CdSe507.

Fig. 4.5 b,c show the PL-decay of CdTe601 for excitation at 410 nm and 590 nm respectively. Any overlap with neighboring PL-peaks of CdSe507 was avoided for the evaluation interval of the decays. The time resolution of this measurement was limited to 40 ps (full width at half maximum; FWHM) of the excitation peak as indicated in fig. 4.5 b,c by the internal response function. All time-resolved experiments were carried out with low excitation intensities and under vacuum in order to keep the single exciton regime and to prevent photo-degradation effects with atmospheric gases during measurement.

Fig. 4.5 b,c show effective quenching of CdTe601 nanocrystal's PL-emission for both excitation wavelengths. This indicates an efficient electron transfer from the CdTe601 to CdSe507 nanocrystals on a sub-nanosecond time scale.

The hybrid sample decayed faster when only CdTe601 nanocrystals were excited (fig. 4.5 c) compared to when both CdTe601 and CdSe507 nanocrystals were excited (fig. 4.5 b). The CdTe601 reference sample exhibited the same decay characteristics independent of the excitation wavelength. The characteristic PL-quenching time is extracted according to equation 2.14: the quantitative evaluation of the CdTe601 nanocrystals decays led to a quenching time constant of about 200 ps for excitation at 410 nm (fig. 4.5 b) and about 100 ps for 590 nm excitation (fig. 4.5 c).

Since both types of nanocrystals were excited at 410 nm, an energy transfer mechanism from CdSe501 to CdTe601 was supposed to enhance the CdTe601 nanocrystals'

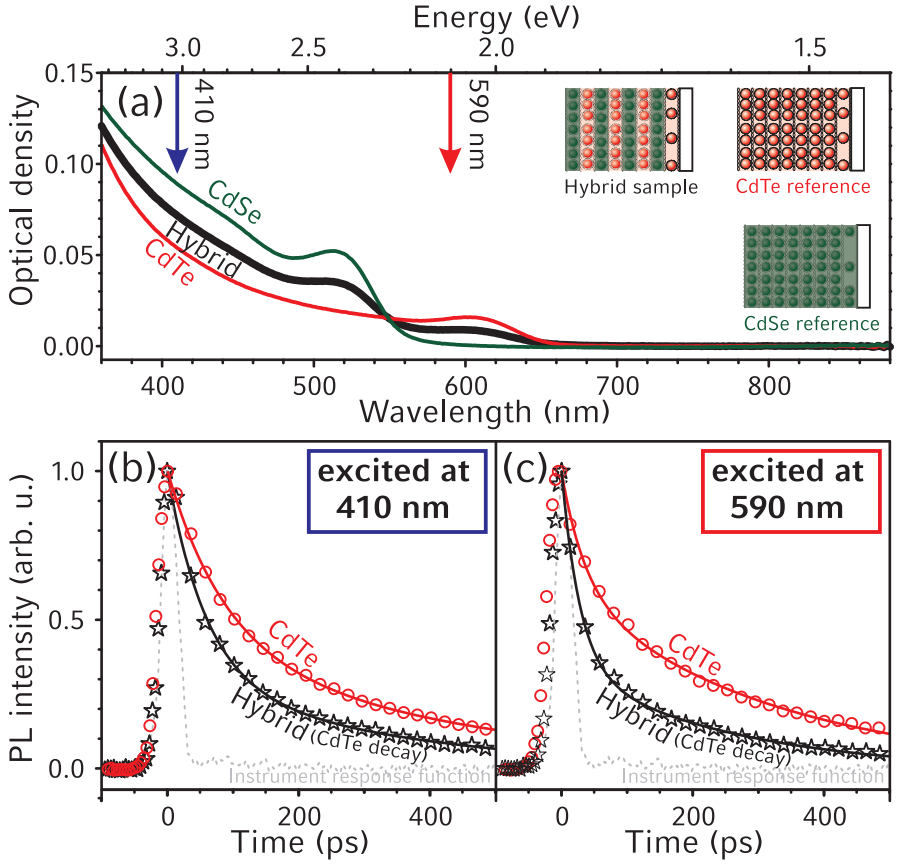

Figure 4.5: The presented time-resolved data of the PL-quenching on CdTe601 nanocrystals indicate the dominance of charge separation dynamics and also indicate weak energy transfer since PL-quenching is less pronounced when also the ET-donor CdSe507 was excited (at 410 nm). OD-graphs of eight layer samples (background and scattering corrected) are presented (a). The graphs of the hybrid sample of alternated each four layers of CdSe507 and CdTe601 are in black, the references with each eight layers of nanocrystals for CdTe601 in red and for CdSe507 in green. The arrows in (a) indicate the excitation wavelength of the PL-measurements presented below. The PL-transients for excitation wavelength 410 nm (b) and 590 nm (c) were measured at the emission of the CdTe601 nanocrystals around 645 nm. The hybrid sample is presented as black stars, the CdTe601's reference as red circles. Fitted multi-exponential decays are added as a guide. The instrument response function of the measurement setup is displayed as a broken gray line. Charge separation is indicated by the faster PL-decay of CdTe601 in the hybrid sample compared to the reference for both excitation wavelength (b,c). By selective excitation of only CdTe601 (c) the quickest decay was observed indicating the effects of excitonic energy transfer from CdSe507 to CdTe601 which prolong the decay of the CdTe601 in the hybrid sample (b). The PL-quenching rate was calculated to be about 200 ps (b) or about 100 ps (c).

PL. Nevertheless, the CdTe601 nanocrystals' PL-quenching attributed to charge separation was still dominant. The two effects resulted in a prolonged PL-quenching time. These results confirmed the findings of steady-state PL above (fig. 4.4 c,d,e).

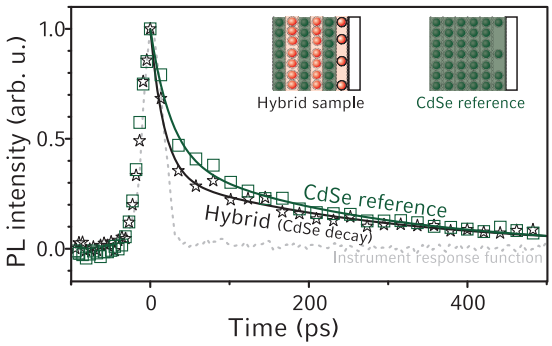

Figure 4.6: The fast time resolved decay of CdSe nanocrystals shows no significant influence from the hybrid assembly. PL-transients of CdSe507 are displayed for the excitation wavelength 410 nm and emission around the CdSe507 core of approx. 540 nm. The hybrid sample was established of three alternating CdTe601 and CdSe507 layers (black stars), the CdSe507 references with six layers (green squares). The solid lines presents a fitted multiexponential decay and is intended only as a guide, the broken gray line represents the instrument response function of the measurement setup with about 40 ps FWHM. A fast initial decay of CdSe507 appears for the hybrid sample. Nevertheless, differences between reference and hybrid sample could not be detected in the essential final decay over 200 ps. Thus, the apparent faster decay in the beginning may be attributed to a parasitic effect such as jittering of the laser, for instance.

To obtain a complete picture of the system it is generally useful not to rely on the data from just one component in the hybrid assembly. Thus, we now wish to discuss in brief the PL-decay of CdSe nanocrystals. In fig. 4.6 the decays of CdSe507 are displayed in a reference sample (six layers) and a hybrid sample of three alternating CdTe 601 and CdSe507 layers. Both are quite similar especially for the essential longer times scale above 200 ps. Initial differences around 80 ps are considered as parasitic effects from the experimentation (such as jittering of the laser). Thus, there was no significant influence from the hybrid assembly on the CdSe507's PL. This is consistent with the steady-state results of fig. 4.4. Furthermore the PL-decay of CdSe507 was much faster than the decay of CdTe601. Hence, an effect of charge separation would affect the CdSe507 used much less compared to the relatively longer living PL of CdTe601.

We conclude this section of PL-studies with the finding of an efficient PL-quenching for CdTe nanocrystals. A characteristic quenching time as low as 100 ps was revealed for the PL-emission of CdTe nanocrystals in the presented system. Due to the expected type II band alignment of the CdTe601 and CdSe507 nanocrystals selected we attribute

this fast PL-extinction to a charge separation process induced by electron transfer from CdTe601 to CdSe507. As secondary and weaker effect we obtained indication of energy transfer from CdSe to CdTe nanocrystals. There appeared to be no significant effects on the CdSe nanocrystal PL. The main effect was however the PL-quenching of the CdTe nanocrystals. Although the data presented provide strong indications of dominant charge separation dynamics, the PL-spectroscopy can only be used as indirect proof.

4.3 Correlation of PL-Quenching and Energetic Offset of Electron States

Different PL-quenching behavior was observed when studying hybrid assemblies with nanocrystals of different sizes. From the following, it can be seen that the PL-quenching efficiency and rate correlate with the offsets between the energy levels of the investigated electron transfer. These energy levels in the nanocrystals which are related to the conduction band of bulk semiconductors have been calculated using the effective mass approximation (chapter 2.2.3) The correlation further supports the theory that the investigated PL-quenching of the CdTe nanocrystals was caused by charge separation due to electron transfer from CdTe to CdSe nanocrystals. Experiments of clustered and layered samples were investigated.

PL-Experiments on Clustered Systems

Fig. 4.7 presents experimental results on different hybrid clustered CdTe-CdSe samples. Various combinations of nanocrystal measuring 2.0 - 3.6 nm in diameter have been used. In detail, we used two types of CdSe nanocrystals: CdSe462 (diameter: 2.0 nm) and CdSe507 (diameter: 2.6 nm). Moreover, we used CdTe512 (diameter: 2.2 nm), CdTe550 (diameter: 2.7 nm), CdTe570 (diameter: 3.0 nm) and CdTe585 - CdTe601 (diameter: 3.3-3.6 nm). All CdTe nanocrystals were extracted from the same synthesis at different reaction times. They were purified from excess reactants and size selected. The same applies for the CdSe nanocrystal solutions.

The offset of the energy ground levels for the first excited electrons was calculated according to chapter 2.2.3. In fig. 4.7 the offsets are set into correlation with the relative PL-efficiency of the CdTe nanocrystals in hybrid assemblies. 100 % corresponds to the PL-efficiency of the pure CdTe nanocrystal reference samples.

Clustered samples were prepared as described in chapter 3.2.2. We performed the PL-measurements using a Varian Cary Eclipse spectrophotometer and applying 400 nm excitation wave length. Thus, in all experiments, both CdTe and CdSe nanocrystals, were always excited simultaneously. Hence, we studied the competition of charge separating effects and energy transfer at the same time. The choice of 400 nm excitation

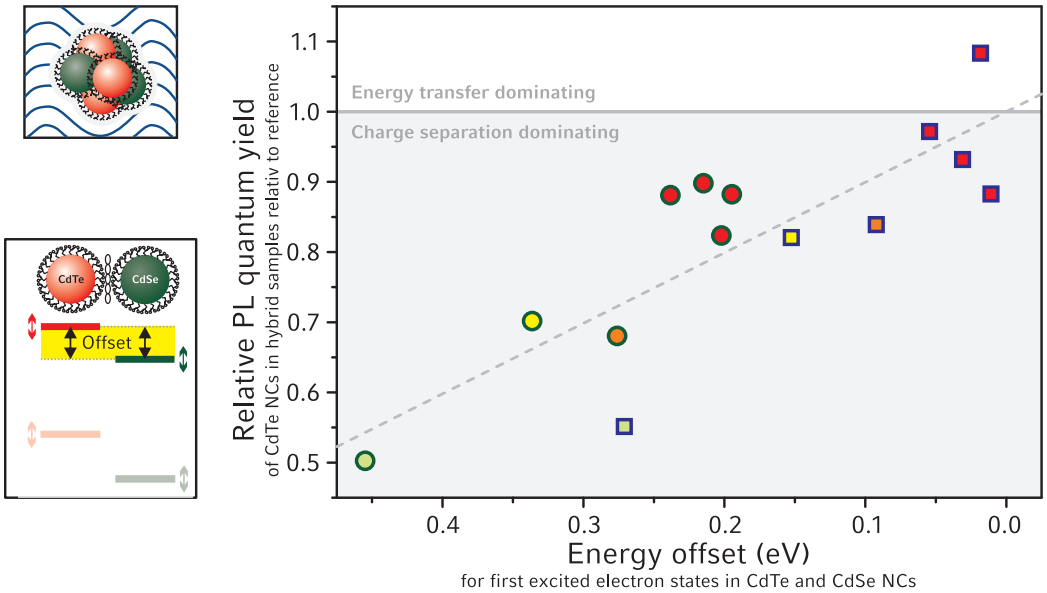

Figure 4.7: A correlation is presented between PL-quenching efficiency and energetic offset of the lowest conduction band related energy levels in the CdTe and CdSe nanocrystals. The results were obtained when using clustered samples. The PL-quantum-yield of CdTe nanocrystals in hybrid assemblies using CdSe nanocrystals is presented relative to the PL-yield of only-CdTe nanocrystal reference clusters. The x-axis presents the offset of energy levels corresponding to the conduction band states as presented in the bottom left-hand side. The broken line is provided as a guide. Squares stand for assemblies using CdSe462, circles using CdSe507. The color of the data points indicates qualitatively the energy gap of the CdTe nanocrystals.

provided comparable measurement conditions for all samples. The spectra obtained are similar to fig. 4.2 b and were evaluated similar as described there.

Fig. 4.7 shows the correlation between energetic offset of the electron states and the PL-quenching by charge separation (electronic transfers). The relative PL-emission yield in the hybrid sample recovers when the energetic offset of the levels for electron transfer decreases. This is consistent with the expectations from single charge carrier transfer dynamics where the offset is a driving force for the charge separation dynamics.

Moreover, enhancement of the PL was recorded for one data point when the calculated offset approaches 0 eV. This is interpreted as a sign of a changed regime where energy transfer from CdSe to CdTe becomes dominant over the charge separation which is supposed to quench the CdTe nanocrystals' PL.

The observed trend is consistent to expectations: the smaller the energetic offset, the lower the driving force of charge separation is and hence the quenching becomes less effective. Energy transfer should be always present (as evidenced before). Hence, the cross-over from dominant PL-quenching by charge separation to enhanced PL by energy transfer may occur even before the energetic offset crosses 0 eV. Furthermore the offsets are only roughly calculated based on literature values of bulk materials and by simple effective mass approach which does not include the exciton binding energy for instance. Thus, the real crossover between type I and type II alignment could not be determined exactly. There is a possible error of about 0.1 eV in the energetic offset, especially since the exciton binding energy revealed by the Stokes shift may be in the order of 0.1 eV (see chapter 3.1.3).

Not all data points are on a line for linear correlation. In particular, we observe that the PL-quenching behavior also correlates with the two CdSe nanocrystals used. Thus there might be an additional effect to consider (such as energy transfer or charging effects induced by the ligand shell). This was not evaluated with the two dimensional plot of only a few data points. However the general tendency of a correlation of the PL-quenching to the energetic offset can be observed.

All things considered, it has been shown that transfer dynamics can be tuned by selection of adapted sizes of both CdTe and CdSe nanocrystals. In this way it is possible to control the PL-quenching that is attributed to the charge separation between hybrid closely packed CdTe and CdSe nanocrystals.

PL-Measurements at Layered Systems

Similar results were also observed in layered systems for the dependence of the PL-quenching on a fine tuning of the energy offset (of the conduction band-related nanocrystal states). The quenching rates are presented to quantify the effect of PL-quenching.

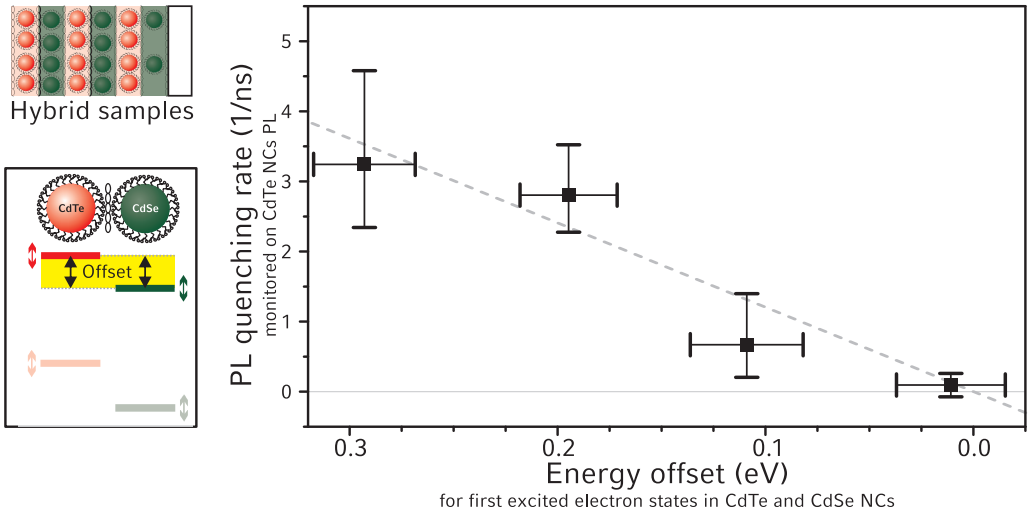

Figure 4.8: The PL-quenching rates of layered hybrid assemblies of CdTe and CdSe nanocrystals reveal a dependence on the energetic offset of the electron levels. All data have been obtained from time resolved PL-data using equation 2.14. Hybrid samples consist of six alternating CdTe-CdSe nanocrystal layers and reference samples of six CdTe nanocrystal layers. In the experiment the two types of nanocrystal were been excited using 400 nm as excitation wavelength in a decay time window of only 1 ns. The x-axis presents the energetic offset of the levels originating from the semiconductor conduction band (see scheme on the bottom at the left hand side). The broken line is provided as a guide only. Error bars have been obtained through different evaluation methods for decay times of multiexponential decay (using $T_{1/2}$ and $T_{1/e}$) and by assumption of only 5 % size distribution for both nanocrystals batches used. CdTe570, CdTe601, CdSe462 and Cd507 nanocrystals were used.

The PL-quenching rates presented are caused by the competition of charge separation and energy transfer dynamics in hybrid type II aligned structures.

Fig. 4.8 shows the effective PL-quenching rates obtained on samples of six nanocrystal layers. The choice of different nanocrystal sizes leads to the theoretically calculated offsets on the coordinate axis. To provide comparable measurement conditions an excitation wavelength of around 400 nm was applied, always exciting both CdTe and CdSe nanocrystals. Hence, fig. 4.8 presents the effective PL-quenching containing both PL-quenching effects by charge separation and PL-enhancement due to energy transfer.

The general trend of the PL-quenching rates reveals its dependence on the energetic offset. The previous findings of clustered self-assembly (fig. 4.7) were reproduced with layered samples. The PL-quenching attributed to charge separation can be determined by the choice of nanocrystals. PL-quenching disappeared when the calculated energy offset approached 0.0 eV.

The PL-quenching rate of about 1/200 ps reported in fig. 4.5 does not correspond fully with the data presented in fig. 4.8. This is because we used a different sample structure for maximal charge separation in fig. 4.5 so these samples did not come from the same monolitic experiment: the layer number of the samples is different (eight versus six nanocrystal layers). The structure is terminated once by CdSe, and a second time by CdTe nanocrystals. It should therefore be stressed that the sample structure also had a significant impact on the global PL-quenching effect which was induced by PL-quenching due to charge separation and by PL-enhancement due to energy transfer.

All together, the rates observed in fig. 4.8 and evaluated on sub-nanoseconds time scale are in good agreement with the expected dominant charge separation dynamics by electron transfer from CdTe to CdSe nanocrystals. The PL-quenching was the lowest when the calculated energy offset in nanocrystals was closest to 0.0 eV.

4.4 Discussion

The results provided strong indirect evidence that charge separation via electron transfer occurs in type II aligned, closely packed assemblies of CdTe and CdSe nanocrystals. The PL-quenching of the CdTe nanocrystals could be observed independently in two different systems. Water-based disordered colloidal clustering and dry layer-by-layer assembled structures produced the same PL-quenching effect so that quenching induced from the environment or the assembly system may be excluded. Moreover, there was a good correlation between the energetic offset of the electronic states (as driving force for the electron transfer) and the experimentally measured PL-quenching. Both observations are strong indications for the expected electron transfer process which leads to charge separation.

Other PL-quenching dynamics need to be ruled out if PL-quenching alone should be used as proof. Therefore, energy transfer dynamics have been addressed. Since CdTe is the energy transfer acceptor due to its smaller energy gap we could see that energy transfer from CdSe to CdTe nanocrystals really leads to an enhanced effect on the CdTe nanocrystal's PL. However, the presence of trap states in the NIR gives rise to ambiguous interpretation: energy transfer from CdTe to the trap states of CdSe nanocrystals might be possible which could explain the observed PL-quenching of the CdTe nanocrystals. It may be argued that the absorption spectra of CdSe show that these trap states provide no absorption at the emission of the CdTe nanocrystals. Therefore, optically allowed FRET is forbidden as there is insufficient spectral overlap so that no FRET can occur. Moreover, the PL-signal of the traps is not enhanced. However, energy transfer to dark states cannot be excluded.

The instability of the CdSe nanocrystals' PL-signal may not provide convincing proof that the PL-quenching observed on the adjacent CdTe nanocrystals is not also affected by such degradation. A blue shift of the CdTe nanocystals' PL-peak was observed in parallel to its PL-quenching on layered samples. On the other hand we may expect that separated charges induce chemical reactions on the semiconductor nanocrystals. Thus, degradation effects leading to a blue shift are, from this point of view, consistent with the expected charge separation dynamics.

Therefore, clear direct proof of the charge separation is needed. This will be discussed in the next chapter. Today, PL-quenching is also used as indication for charge separation effects that might be related to type II alignment. [117, 118] However the PL-quenching is normally not used on its own to provide clear evidence of charge separation.

Several papers already exist that relate to II-VI semiconductor nanocrystal structures making use of the size quantization effect in order to tune the effective band alignment between type I and type II. The major part of these papers is limited to directly grown nanoparticles, in particular, core-shell nanocrystals.

Both type I and type II core shell nanocrystals often exhibit a higher PL quantum yield than their "naked" cores. A major difference lies in the radiative PL decay rate: in type I core-shell nanocrystals electrons and holes are both confined to the material with the lower energy gap including some mostly evanescent wave functions into the other material. Hence, there is perfect overlap of electron and hole wave functions and a high radiative rate can be seen. In type II nanocrystals in contrast, electrons and holes are each mostly confined to the different spatial places that correspond to the different II-VI semiconductor materials. Thus, the overlap between electron and hole wave function is small and the radiative rate is significantly lower. [31] Zeng et al. and Nonoguchi et al. demonstrated the possibility of tuning type I nanocrystals to type II

nanocrystals [119] as well as the crossover from type II to type I [120] while monitoring the radiative rate of nanocrystals having different shell coating thickness

Another way to distinguish between type I and type II nanocrystals in the cited literature is the appearance of the absorption spectra. Type I core-shell nanocrystals exhibit sharp absorption and PL-peaks. In contrast type II core-shell nanocrystals present a broad onset of the absorption due to weak oscillator strength of cross-over-excitons together with a relatively sharp PL-emission peak guaranteeing monodisperse nanocrystals size distribution. Thus, Ivanov et al. were able to provide evidence of cross-over from type I to type II and back again to type I alignment in $ZnSe/CdSe$ core/shell nanocrystals [121]. Similar observations were also found in reference [119].

Recently Wu et al. worked on clustered aggregates of CdTe and CdSe nanocrystals directly assembled via positively and negatively charged nanocrystals [122]. Studying the influence of various parameters on the PL-quenching they also tried to tune the band alignment by applying the size quantization effect. When employing large CdTe nanocrystals of 1.9 eV energy gap (first OD peak at 660 nm, diameter 4.6 nm, ligands positively charged) and small CdSe nanocrystals (2.7 eV energy gap, OD peak at 456 nm, diameter 1.9 nm, ligands negatively charged) he was unable to observe any significant PL-quenching due to charge separation. However, he was also unable to observe any PL-enhancement by energy transfer.

However, there seems to be interest in engineering the band positions and the absorption independently. Ternary nanocrystals alloys like CdS_xTe_{1-x} [123] or $CdSe_xTe_{1-x}$ [62] may be used for this purpose.

Last but not least we may discuss the transfer rates observed. A transfer rate of up to 1/100 ps was revealed for layered assembly in this chapter whereas charge separation with a rate in the nanosecond range was indicated for clustered assembly. The difference might be explained by the following facts: the rate in the layered structures was revealed without the energy transfer from CdSe to CdTe nanocrystals. The transfer distance could be different for clustered assembly. Moreover, the PL life time was different for nanocrystals in solutions.

The electron transfer rate of about 1/100 ps in layered type II aligned assemblies compares well to the energy transfer rate in layered assemblies of type I aligned CdTe nanocrystal assemblies. [19] A characteristic energy transfer time of 134 - 254 ps was reported by the PL-quenching on the ET-donor. An offset of 0.23 eV can be calculated for the relevant electron states in this reported type I system. This compares well to the 0.19 eV which was calculated for the type II system studied in this thesis. It appears that energy transfer dynamics and charge separation dynamics are competing on the same time scale or that both are related to each other. However, for the investigated hybrid type II system of CdSe-CdTe nanocrystals we might discuss why a dominance

of the electronic transfer was observed: since the CdSe PL is quickly decaying there might not be enough time for efficient energy transfer.

To summarize, efficient PL-quenching provided a strong indication of charge separation by electron transfer from CdTe nanocrystals to CdSe nanocrystals. It was observed in both clustered and layered nanocrystal assemblies. Time resolved spectroscopy showed a maximum transfer rate in the order of 1/100 ps which is attributed to electron transfer in layered hybrid nanocrystal structures. Moreover, a correlation was revealed between the PL-quenching and the offset between the energy levels of conduction band-related energy states. This correlation is valid for both layered and clustered assemblies. This supports expectation that the energy levels of nanocrystals may be easily approximated by effective mass approach. However, the PL-quenching data presented provided only indirect indications of charge separation by electron transfer from CdTe to CdSe nanocrystals.

5 Directional Charge Separation and Diffusion for Layered CdTe and CdSe Nanocrystals

In this chapter SPV-techniques clearly show the charge selectivity of the CdTe-CdSe nanocrystal interface since we directly measure the dipolar field of the separated electron hole pairs. An inversion of the layer structure leads to a sign change for the SPV-voltage. The charge separation can be suppressed when the interlayer spacing is doubled. This proves that in reality the measured charge separation originates from the layered nanocrystal assemblies. Moreover, it is consistent with the assumed transfer mechanism of tunneling.

The studies presented in the previous chapter provided indirect evidence of charge separation between CdTe and CdSe nanocrystals based on PL-quenching of time and spectrally resolved PL-data. The presence of trap dynamics for instance also gives rise to ambiguous interpretations. Hence, solid direct proof of charge separation in hybrid assemblies of CdTe and CdSe nanocrystal was needed and established by SPV-techniques that allow the detection of separated charges by sensing externally induced electric dipole fields (chapter 3.3.3).

Moreover, here is evidence of diffusion in layered CdTe and CdSe nanocrystal assemblies. Since the nanocrystal layers are separated by about 1 nm of an organic barrier we report on hopping diffusion of electrons and holes at the end of this chapter.

5.1 Experimental System

SPV-spectroscopy (see chapter 3.3.3) was applied on samples containing several layers of CdTe or CdSe nanocrystals topped by one single layer of the complementary nanocrystals to obtain the charge separating interface of CdTe and CdSe nanocrystals on the top of the sample (fig. 5.1). The measurement was only sensitive in the direction perpendicular to the electrodes of the SPV-setup. Hence, only the contribution of charge separation perpendicular to the CdTe-CdSe nanocrystal interface plain was measured. All samples were prepared by LBL-assembly on cleaned FTO substrates

(thickness about 400 nm on glass) activated by the chemical cleaning procedure using NH_3 and H_2O_2 (see chapter 3.2.1).

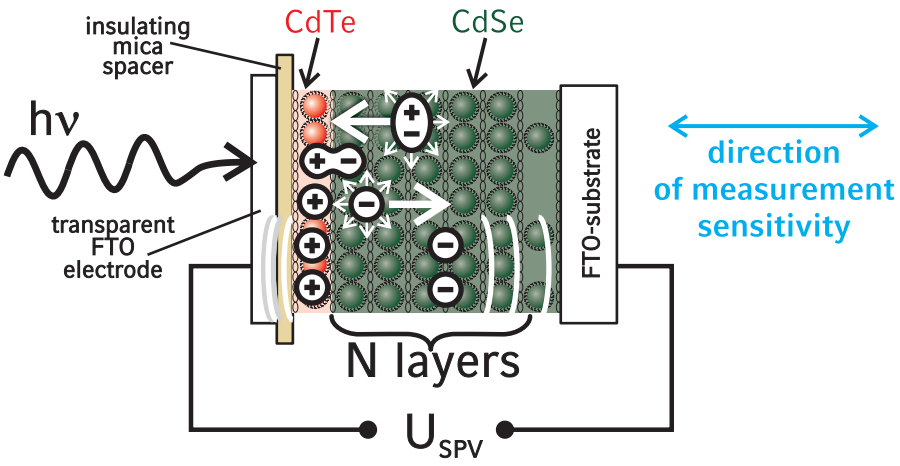

Figure 5.1: This shows a typical sample in a SPV-setup with the expected physical processes. Photo-excited excitons may diffuse to the charge separating interface of the type II aligned CdTe and CdSe nanocrystals at the point where they separate. The separated charges, which may diffuse, exhibit an electrical field that is measured in the capacitor configuration of the SPV-setup. SPV is only sensitive for charge separation perpendicular to the capacitor plain. (The figure have already been presented similarly in reference [124].)

As well as the measurement of pure charge separation, the effects of diffusion can also be seen (fig. 5.1). Exciton diffusion is supposed to increase the number of excitons that get separated on the type II interface. Charge diffusion increases the average charge separation distance. Hence, the SPV-signal increases in the case of diffusion because the SPV-signal depends linearly on both the number of created charges and the average separation distance (see equation 3.8).

5.2 Directional Charge Separation

This section presents data on the directionality of charge separation on a CdTe-CdSe nanocrystal interface. Spectrally resolved SPV-data are presented before the time evolution of the SPV-signal is discussed. We observe that the sign of the SPV-signal depends only on the layer order of the CdTe-CdSe nanocrystal interface proving the directionality of the charge separation where electrons get concentrated on CdSe nanocrystals and holes on CdTe nanocrystals.

Fig. 5.2 a,b present SPV-data on two complementary samples inverted with the respect to the positions of CdTe578 and CdSe529 nanocrystals. Therefore, fig. 5.2 a presents data from a sample with six layers of CdSe529 topped by one monolayer of

CdTe578, fig. 5.2 b shows six layers of CdTe578 topped with one CdSe529 layer. The nanocrystal diameters are 3.1 nm for CdTe578 and 2.9 nm for CdSe52 (according to equation 3.2).

The positive (in-phase) signal shown in fig. 5.2 a proves the collection of positive charges on the top of the sample in CdTe578 and negative charges in CdSe529. The SPV-signal and, hence, the directionality of the charge separation is inverted for the complementary sample in fig. 5.2 b. The comparison of fig. 5.2 a,b reveals a sign-change of the SPV-signal when the layer order of CdTe578 and CdSe529 is changed. This clearly confirms the directionality of the charge separation as expected from the type II alignment of CdTe and CdSe bulk materials (see fig. 4.1).

No SPV-signal was detected in the NIR-range where there was no absorption of the nanocrystals. The onset of the graphs (fig. 5.2 a,b) leading to a shoulder at around 600 nm corresponds to the absorption of CdTe578, a second peak around 530 nm corresponds to the absorption of CdSe529 nanocrystals. The decrease of the SPV-signal to the bluish wavelengths is caused by the decreasing excitation intensity (fig. 5.2 c).

A positive in-phase signal was observed across the whole spectrum in fig. 5.2 a, a negative one in fig. 5.2 b. The presented 90° phase-shifted signals are inverted with respect to the in-phase signal. This indicates that the build-up and decay of the SPV-signal show some retardation with respect to the chopped excitation light. (By convention for the lock-in-amplifier used the 90° phase-shifted signal is inverted in the case of a retarded SPV-signal.) This indicates a long life time of the charge separation and is discussed later with time resolved SPV-measurements.

The shape of the 90° phase-shifted signals in fig. 5.2 a,b is very similar to the in-phase signal indicating a similar, constant phase shift of the SPV-signal in both samples across the spectrum. Hence, the charge separation dynamics are independent of the excitation wavelength and the SPV-spectra show a complete sign change (corresponding to a phase shift of 180°). This confirms the collection of positive charges (holes) in CdTe578 and electrons in CdSe529 nanocrystals.

A significant SPV-signal rises at wavelength where only CdTe578 absorb. Hence, the charge separation obviously starts when only CdTe578 is excited and no electron-hole pair is present in CdSe529. The sign of the SPV-signals does not change for different wavelengths indicating that the directional charge separation on the CdTe578-CdSe529 interface is the only significant charge separation mechanism which can be observed. Other potential charge separation dynamics on other interfaces are insignificant.

Fig. 5.2 c presents the OD of the nanocrystals used and the light intensity of the excitation light in the setup. Since the excitation intensity is not constant and decaying to the UV-range, the SPV-signals presented in fig. 5.2 a,b are also decreasing to the shorter wavelength. The SPV-signal is proportional to the created free charges (equa-

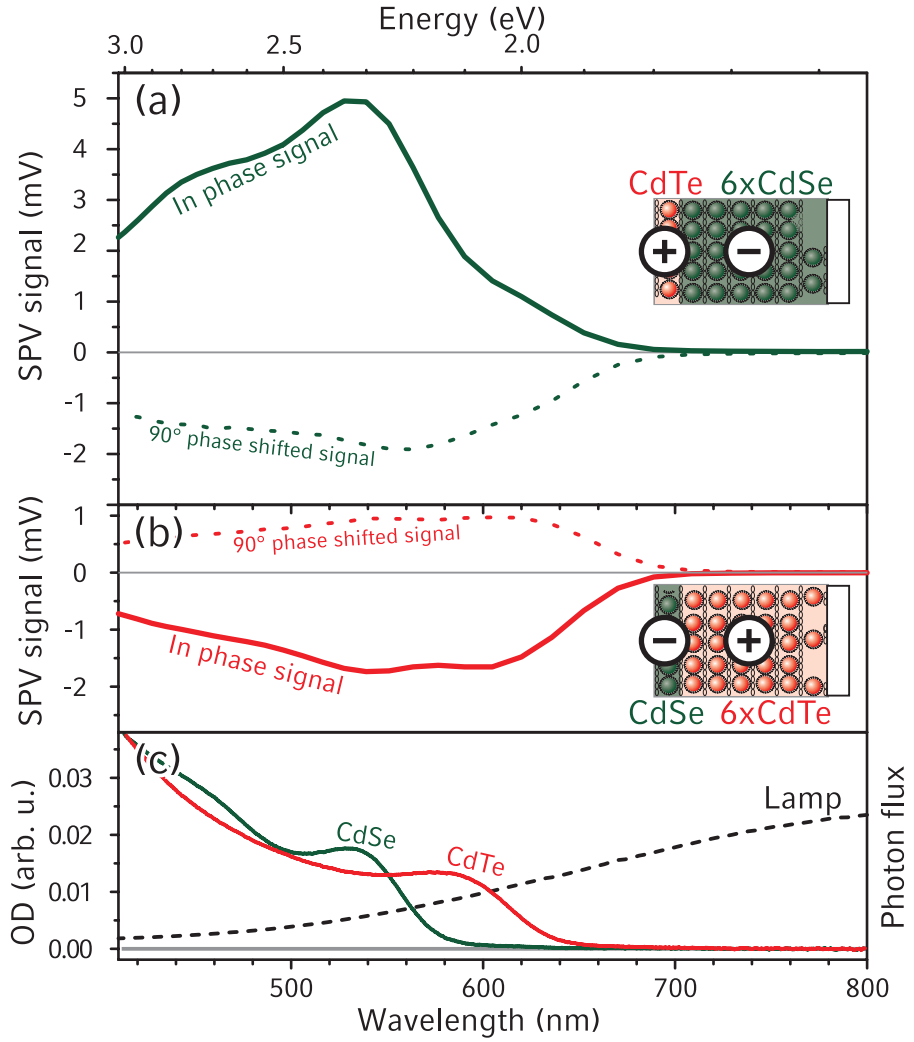

Figure 5.2: SPV provides experimental evidence about the directionality of charge separation. The SPV-spectra are displayed for two hybrid samples (a,b). The sample of (a) comprises six layers of CdSe529 topped by one layer of CdTe578 (green graphs). The sample of (b) is an inverted sample by replacing CdSe529 with CdTe578 vice versa. SPV-signals are displayed in-phase with excitation light (solid line) and 90° phase-shifted (broken line, by convention inverted if signal is a retarded signal). (c) OD-spectra of CdTe578 (red) and CdSe529 (green) in three layer LBL samples on glass and excitation intensity of SPV-experiments (broken black) are provided for comparison with SPV-spectra. The sign of the SPV-signal is inverted when the layer order is inverted proving directional charge separation. (The data have already been presented in reference [124].)

tion 3.8). Thus, a check was made to ensure that the shape of the SPV-curves can be reproduced by multiplying the excitation intensity with the OD of the samples (data not shown). The peaks occurring in the spectra correspond to the first absorption peaks of the nanocrystals. The presented SPV-graphs show the measured raw data. Hence, the graphs in fig. 5.2 a,b,c can be fully understood and prove the expected directional charge separation.

As already mentioned, time-resolved SPV-measurements (fig. 5.3) were performed on the same sample as presented in fig. 5.2. These measurements confirm the directionality of charge separation since the signs stays either positive (fig. 5.3 a) or negative (fig. 5.3 b) for the whole time range investigated. The time-resolved transient measurements are plotted on a logarithmic time scale. Fig. 5.3 a shows the sample of six CdSe529 layers topped by one CdTe578 layer and we can see an all-over positive signal with the peak maximum delayed by about 0.5 μs after the excitation pulse. Fig. 5.3 b presents the complementary sample with six CdTe578 layers topped by one layer of CdSe529. Here we recorded an all over negative signal and a much longer delay of the peak maximum with about 100-400 μs. The different delay times of the peaks in fig. 5.3 provide evidence of significant differences in the charge carrier dynamics. This topic is addressed in more detail in section 5.4 where diffusion is discussed on samples having different numbers of nanocrystal layers.

SPV-transients have been obtained for different wavelengths. The orange graphs present excitation of only CdTe578 at 604.8 nm laser wavelength. The blue graphs present excitation of both CdTe578 and CdSe529 nanocrystals at an excitation wavelength of 442.8 nm. The initial shape of the graphs shown in fig. 5.3 is almost identical for both excitation wavelengths although the amplitude varies in fig. 5.3 a. This is an indication that the same diffusion processes are active for both excitations in fig. 5.3 a. Hence, there is apparently no difference in the diffusion dynamics depending on absorption in CdTe nanocrystals or in CdSe nanocrystals. In fig. 5.3 b a difference in both excitations can be observed for the time scales over 10 μs indicating slightly different recombination dynamics.

The sign of the SPV-signal does not change for the whole investigated time range (fig. 5.3). This means that all charge separation dynamics of this hybrid multilayer sample exhibit only one dominant charge separation direction. Other interfaces such as nanocrystals to FTO do not contribute significantly to the SPV charge separation signal. Parasitic charge separation at the boundaries should always present the same directionality in these complementary samples. Thus, a sign change during the decay of one sample would be a clear indication of additional parasitic charge separation dynamics. As it is shown with the directionality of the SPV-sign for the whole measurement

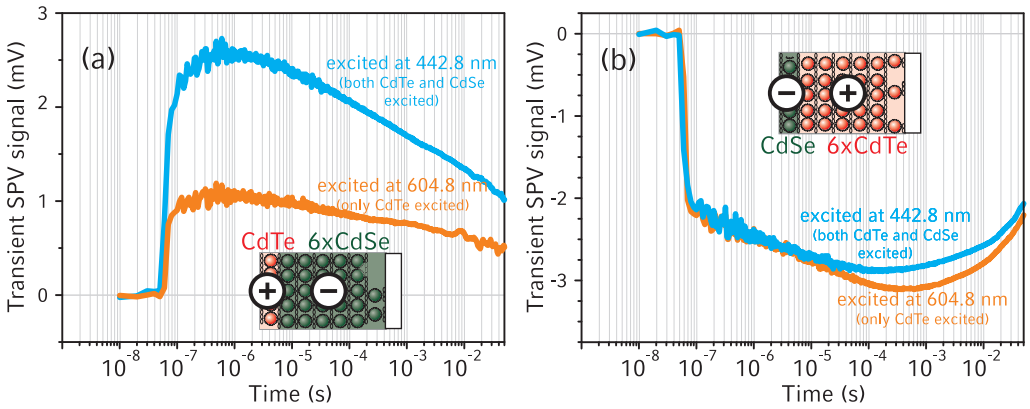

Figure 5.3: Time resolved SPV-signals confirm the experimental evidence for the directionality of charge separation. SPV-transient spectra are given on a logarithmic time scale. The first sample (a) comprises six layers of CdSe529 topped by one layer of CdTe578 (green) and the second sample (b) complements the first sample when the positions of CdTe578 and CdSe529 nanocrystals are exchanged. Inverting the nanocrystal position changes the signal's sign. Different amplitude, build-up and decay characteristics in (a) and (b) are apparent. The data are consistent with fig 5.2. The shape and sign of the transient graphs prove only significant contribution to SPV-signal by charge separation dynamics going to the indicated direction in the small sample schemes. No significant dependence of the SPV-graphs on the excitation wavelength was observed. The SPV-transients were recorded when only CdTe578 is excited (wavelength 604.8 nm, orange) and when both CdTe578 and CdSe529 were excited (wavelength 442.8 nm, blue). The graphs are not normalized but the measurements have been recorded at different excitation intensities to provide roughly the same SPV-amplitudes. (The onset of the laser pulse was shifted to 16 ns on both graphs.)

range we cannot find any evidence of other strong charge separating interfaces on these samples except the type II interface of CdTe578 and CdSe529 nanocrystals.

The data presented in fig. 5.3 confirm the findings given above for fig. 5.2: electrons are collected in layers of CdSe529 and positively charged holes in CdTe578. Hence, the time-resolved data also confirm the charge separation direction expected from the type II alignment of CdSe and CdTe semiconductors.

In conclusion, we have used SPV-spectroscopy and transients to clearly demonstrate the directionality of the charge separation in hybrid multilayered structures of CdTe578 and CdSe529 separated by a single PDDA-polymer spacer inducing an inter-layer distance of about 1 nm. Holes accumulate in CdTe nanocrystal layers, and electrons in CdSe nanocrystal layers. The observed charge selective separation supports the expected type II alignment between suitable CdTe and CdSe nanocrystals.

5.3 Suppression of Charge Separation at Increased Barrier Width

This section proves the strong sensitivity of the charge separation process to the barrier width in LBL assembled nanocrystal structures. We observed that the SPV-signal is suppressed when the barrier between the nanocrystal layers was doubled. This proves the strong distance dependence of the charge transfer process conform to the expected transfer mechanisms of tunneling.

Fig. 5.4 a presents schemes of the investigated samples of four layers CdTe578 topped by one layer of CdSe529 to induce charge separation. The sample called a "spacer sample" was prepared with additional double polymer layers that increase the inter-nanocrystal-distance from about 1 nm to about 2 nm (see chapter 3.2.1). Both samples (spacer and reference) contain the same amount of the individual nanocrystal species.

Fig. 5.4 clearly shows that the SPV-signal of the spacer sample is almost completely quenched. This indicates the strong distance dependence of the transfer mechanism. Considering tunneling as a mechanism for charge separation, an exponentially decaying dependence on the inverse of the transfer distance (i.e. barrier width) is expected (chapter 2.3.3). This is consistent with the findings in a nearly complete quenching of the SPV-signal presented above. Moreover, the almost complete quenching of the SPV-signal confirms that the investigated charge separation dynamics are only caused by tunneling transfer between adjacent nanocrystal layers. This excludes parasitic effects of other interfaces at the sample to explain the measured charge separation effect.

Fig. 5.4 b presents in detail the in-phase SPV-signal and fig. 5.4 c the 90° phase-shifted signal. Practically no signal can be observed for the blue plotted spacer sample when we compare it to the red reference sample graphs. The in-phase signal of the

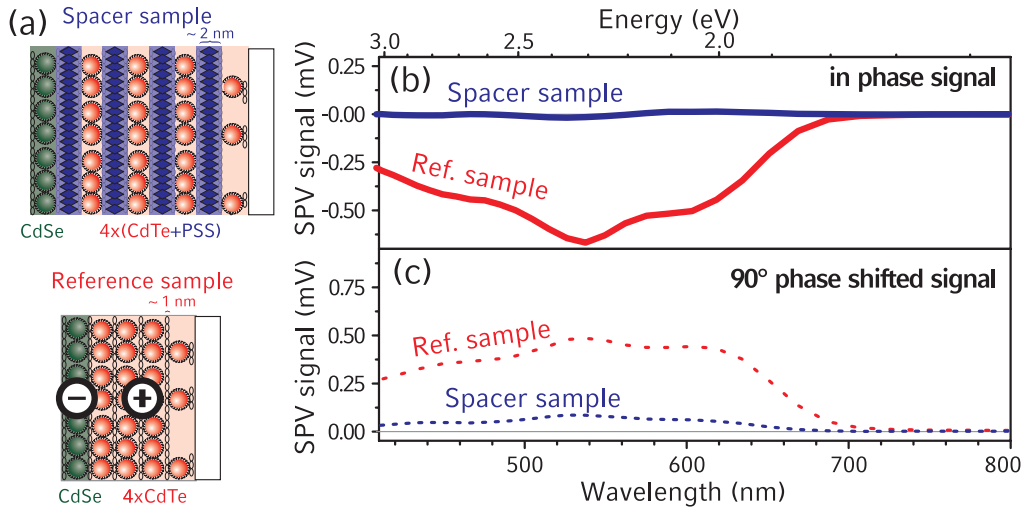

Figure 5.4: An increased barrier width leads to suppression of the SPV-signal. The samples' schemes are illustrated with two different interlayer barrier widths as indicated (a). Both samples comprise four CdTe578 layers topped by one CdSe529 layer. The spacer sample contains an extra double layer of isolating polymers between each nanocrystal layer increasing barrier width from about 1 nm to about 2 nm. The corresponding SPV-signals are presented in-phase with excitation (b) and 90° phase-shifted for the out-of-phase contributions (c). The spacer sample is strongly quenched (blue lines) whereas the reference sample shows signal (red). Thus, the increased inter-layer barrier significantly decreases the efficiency of the charge separation. (The data are already presented in reference [124].)

spacer sample (blue) with the increased barrier width is almost zero, the 90° phase-shifted signal rises a little bit indicating that a weak retarded charge separation is taking place. Hence, the charge separation signal in SPV is mostly suppressed by the increased inter-layer distance.

To conclude this section we found a strong dependence of the charge transfer processes on the barrier width. We observed a nearly complete quenching of the SPV-signal. The barrier between the nanocrystal layers consists of the organics of ligands and polymer layers. The organic inter-layer barrier was increased from about 1 nm to 2 nm in the layered assembly of CdTe and CdSe studied. The result is consistent with transfer dynamics such as inter-layer-tunneling of single charge carriers. Moreover, the experiment confirms that no charge transfer dynamics at interfaces other than nanocrystal layers lead to the observed strong charge separation signal.

5.4 Diffusion in Layered Semiconductor Nanocrystal Assemblies

It is necessary to ensure the creation of separated single charges in order to study the diffusion of single charges. Thus, to guarantee this, we made use of the type II aligned interface between the CdTe and CdSe nanocrystalsused. The type II interface confines holes to CdTe nanocrystal layers and electrons to CdSe nanocrystal layers. This is illustrated in fig. 5.1. The samples shown consists of some multilayers of CdSe nanocrystals topped by one layer of CdTe nanocrystal. Thus, the holes remain confined to the CdTe top-layer and electron diffusion may be studied over CdSe layers. Separated electrons and holes exhibit an electrical field which is dependent on the separation distance. Thus, SPV-techniques can be applied to reveal diffusion. To study diffusion in CdTe layers, analog samples of CdTe multilayer with one CdSe top-layer were produced.

Let us assume that charge separation would only occur for charges which are excited directly on the interface of one CdTe and one CdSe nanocrystal monolayer. Thus, it would not make any difference to the SPV-signal if more layers of the same nanocrystals were added on one side. However, it can be observed that the SPV-signal increases when the number of layers is increased. Therefore, we must assume that diffusion processes do take place. Our observations concerning diffusion are presented in the following.

SPV-spectroscopy and time-resolved SPV have been applied to reveal diffusion processes. Data are presented for samples with different numbers of nanocrystal layers to provide evidence of diffusion processes. SPV-spectra are analyzed indicating diffusion dynamics for electrons, holes and propablyexcitons. SPV-transients are consistent with the experiment showing that diffusion in CdSe layers is faster than in CdTe layers.

The experimental results presented in this section have been obtained using samples with 2, 4, 6 and 10 layers of CdSe529 topped by one layer of CdTe578 nanocrystals to study electron diffusion over CdSe529 layers (see insert in fig. 5.5 a). To obtain indications on hole diffusion dynamics over CdTe578 layers the structures consist of 2-10 CdTe578 nanocrystal layers topped with one CdSe529 layer (see insert in fig. 5.5 b). A strong correlation of the number of nanocrystal layers N to the SPV-intensity and SPV-peak position was observed which indicates diffusion processes.

Steady State SPV Results

SPV-spectroscopy provides indications of diffusion processes on up to ten nanocrystal layers since the SPV-amplitude is correlated to the layer number in the samples. Without any diffusion process only a constant SPV-signal would be expected from the type II interface of CdTe and CdSe nanocrystals. In this subsection we present separate analyses of the contributions of the CdTe and the CdSe nanocrystals. We evaluated the contribution of the CdTe and CdSe nanocrystals in relation to the overall SPV-spectra in correlation with the number N of the nanocrystal layers in the samples (fig. 5.5 a,b). Fig. 5.5 c demonstrates the fit of the SPV-spectra required to obtain the contributions α_{CdSe} and β_{CdTe} presented in fig. 5.5 a,b. A linear superposition of the SPV-references of single materials was used.

First of all, we find that the contributions of both types of nanocrystal always increases in relation to the global SPV-amplitude. No contribution remains constant, which would indicate that the separated charges remain only on the CdTe-CdSe interface. We observe that the contribution on both the CdTe and the CdSe nanocrystals follows a power-law. This is a clear indication of diffusion processes over the nanocrystal layers since without diffusion we cannot expect any change to the SPV-spectra.

We now analyze the strong increase in the SPV-amplitude with increasing number of layers N in the context of charge carrier dynamics. We know from chapter 3.3.3 that the relation $SPV \propto Q \cdot d$ applies with Q as amount of separated charges and the average separation distance d. Thus, we can expect the following two contributions. firstly, the average separation distance d increases linearly in accordance with a growing layer number N since the room for free diffusion becomes larger. Secondly, the absorption in the material or the multilayers may increase linearly with the layer number since the amount of separated charges Q may increase if photo-excited excitons from all nanocrystal layers contribute to charge separation. Thus, a linear increase of the SPV-amplitude of the top layer's contribution in correlation to the layer thickness N can be expected. This linear increase may be attributed to diffusion processes of separated charges. A quadratic dependence on the layer number N may therefore be expected for the multilayers, indicating that both the diffusion of the separated charge carriers

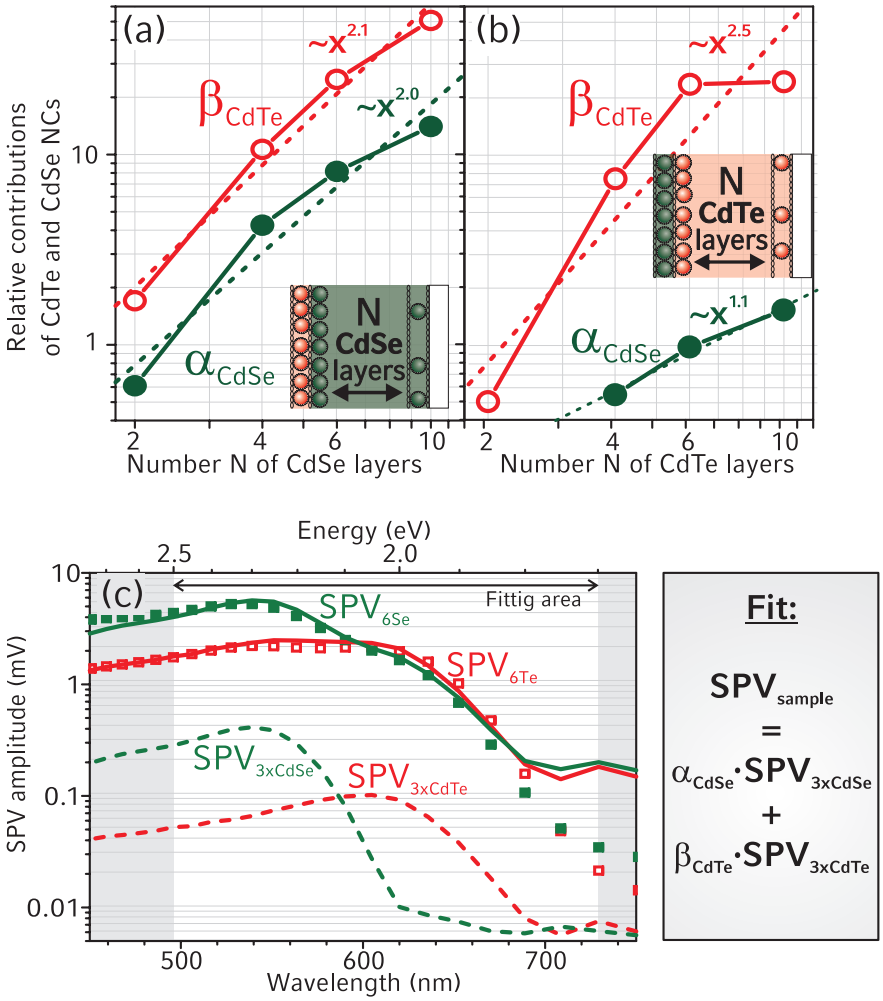

Figure 5.5: The SPV-amplitude increases when the number of (a) CdSe or (b) CdTe nanocrystal monolayers increases, indicating that diffusion processes occur also in the layers furthest away from the charge separating interface of CdTe-CdSe nanocrystals. A power-law dependence is revealed for the contributions of CdTe and CdSe nanocrystals to the SPV-amplitude. The fitted contribution values have been plotted for the samples of N CdSe layers topped by one layer of CdTe (a) and N CdTe layers topped by CdSe (b). The corresponding sample's schemes are shown in the figure insets. The spectra are fitted to the fit-formula of linear superposition to reveal the contributions α_{CdSe} and β_{CdTe} in (a) and (b). An example of the fit is displayed in (c). The SPV-spectra of hybrid assemblies (squares) are fitted (solid line) by linear superposition of SPV reference spectra (broken lines). SPV_{6Se} (dark green) represents a sample of six CdSe nanocrystal layers topped by one CdTe layer and SPV_{6Te} red for a sample of six CdTe nanocrystal layers topped by one CdSe layer. The weak reference signals (broken lines) were obtained from samples of three layers of CdTe (red) or CdSe nanocrystal (dark green) on FTO of about 400 nm thick. (The data have already been presented in reference [125].)

and the photo-excited charges from all nanocrystal layers contribute significantly to the SPV-signal.

These expectations are confirmed exactly for the plotted contributions α_{CdSe} in fig. 5.5 a,b. Fig. 5.5 a reveals a quadratic dependence of the CdSe nanocrystal's contribution α_{CdSe} to the SPV-signals when the CdSe529 layer number N is increased. Fig. 5.5 b shows only a linear dependence of the CdSe nanocrystals contribution α_{CdSe} on the CdTe layer number N. This corresponds exactly to the above stated expectations and proves charge diffusion in the CdSe layers.

The CdTe nanocrystal's contribution β_{CdTe} to the SPV-signals does not follow exactly the above discussed expectations. Fig. 5.5 a shows a quadratic dependence on the layer number N of CdSe529 although the number of CdTe578 layers is constant. Fig. 5.5 b indicates a nearly cubic dependence at the beginning with an apparent saturation at ten CdTe578 layers. It cannot be clearly explained why a quadratic and cubic dependence is observed instead of a linear and quadratic dependence.

In any case, the difference between quadratic and cubic contribution of β_{CdTe} indicates that the multilayered CdTe nanocrystals provide a higher contribution than the CdSe nanocrystal topping layer. This is interpreted as a weak indication for exciton diffusion or other charge separation and diffusion processes. However, the strong increase for all contributions in fig. 5.5 a,b provides a clear indication of charge diffusion in the layers.

Last but not least, a general tendency can be seen for starting saturation for ten nanocrystal layers. It appears that all the plotted contributions run slowly into saturation with its strongest expression for β_{CdTe} in fig. 5.5 b.

The tendencies of fig. 5.5 a,b have been reproduced using different nanocrystals (not shown) indicating the general validity of the findings. Also the unexpected behavior of CdTe nanocrystal's contribution is reproducible. The dependencies of the CdTe and CdSe contributions in fig. 5.5 a,b can therefore be motivated especially for CdSe by the correlation of the higher separation distance d induced by charge carrier diffusion and to higher absorption caused by higher layer thickness. The higher absorption obviously leads to the creation of more separated charges Q. Thus, the tendencies of fig. 5.5 a,b indicate diffusion dynamics in fair agreement with the relation $SPV \propto Q \cdot d$.

Time-Resolved Experiments

Fig. 5.6 presents transient graphs for the varied layer number N of CdSe529 layers (fig. 5.6 a) or CdTe578 layers (fig. 5.6 b). We observe that the peak positions of the transients shift to longer times when the number N of nanocrystal layers is increased. Moreover, the SPV-amplitude increases for growing layer number N as expected from the evaluation of the SPV-spectra presented above. These effects indicate not only that

the two nanocrystal layers of the type II interface alone are responsible for the observed signal but also that the charges from nanocrystals that are not in direct contact with this type II interface contribute to the SPV-signal. Hence, diffusion processes are obvious in the structures presented. Since SPV detects the field of separated charges we attribute the observed effects in fig. 5.6 to diffusion of single charge carriers over the layers of the same type of nanocrystals.

The diffusion observed by transient SPV on multilayered CdSe samples with CdTe topping layer may be attributed to electron diffusion over CdSe layers. In the excitation wavelength dependent measurements of fig. 5.3 we observed no significant difference in the build-up of the time-resolved signal. When the CdTe top-layer is excited selectively (fig. 5.3 a) excitons are created only in the top-layer. Hence, an with the time increasing SPV-signal indicates the electron diffusion over the CdSe layers since the holes are supposed to stay in the type II aligned CdTe nanocrystals. As there is no obvious difference between the excitation of CdTe578 only and the excitation of both CdSe529 and CdTe578 in fig. 5.3 a it can be assumed that the contribution from the CdSe529 nanocrystals is also related to the same diffusion process which is electron diffusion when only the CdTe578 top layer is excited.

Furthermore, it should be pointed out that the samples in fig. 5.6 a show in general a faster increase in the SPV-amplitude compared to fig. 5.6 b. Hence, diffusion processes in CdSe nanocrystal multilayers appear to be faster than in CdTe nanocrystal multilayers.

Last but not least, reference spectra are shown with either the three layers of CdSe529 (fig. 5.6 a) or CdTe578 nanocrystals (fig. 5.6 b) on FTO-substrates. A significant signal is observed there with its peak right at the beginning and a quite quick decay. This may be an indication of photogeneration of free charge carriers instead of excitons in nanocrystal layers as proposed in reference [126]. This signal of the reference samples has the same sign for both CdTe578 and CdSe529 since no controlled directionality for charge separation was induced by an interface such as CdTe578-CdSe529.

To summarize, both SPV-spectra and time-resolved SPV provide a strong indication of diffusion dynamics in the presented sample series. It appears that charge diffusion is faster in CdSe than in CdTe nanocrystal layers. Moreover, we found indications that electron-hole pairs created in layers without direct contact to the type II interface also contribute significantly to an enhanced SPV-signal.

5.5 Discussion

The SPV-measurements given at the start of this chapter showed the directionality of the charge separation on the CdTe-CdSe nanocrystal interface. A positive SPV-

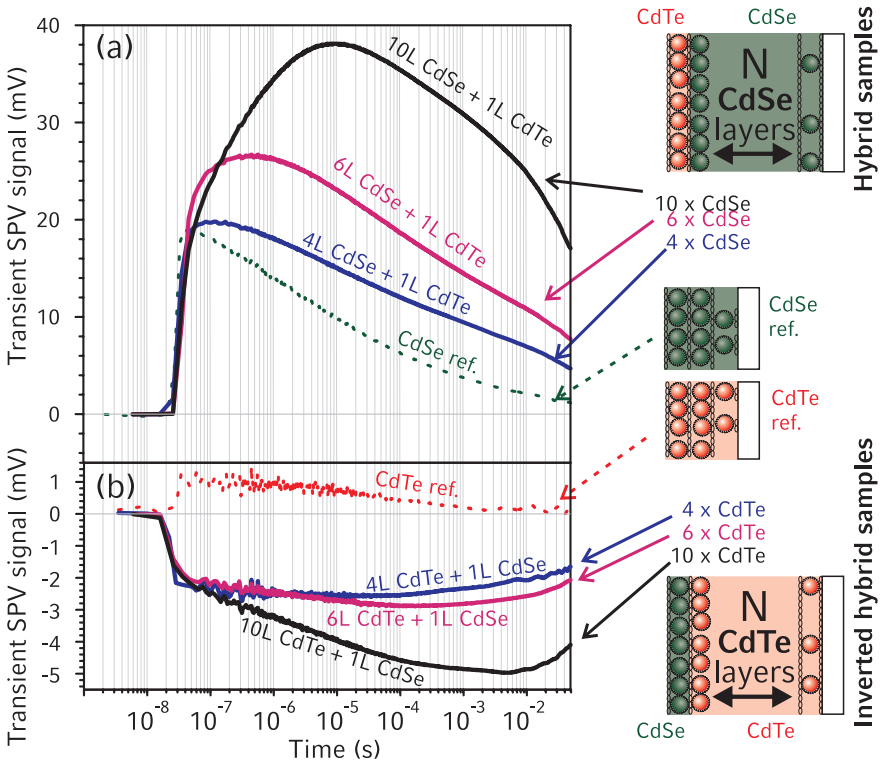

Figure 5.6: SPV-transient spectra show charge diffusion processes due to the different build-up times of the SPV-signal. The plots are presented on a logarithmic time scale. The samples contain a varying number N of CdSe529 layers topped by one layer of CdTe578(a). The measurements on complementary samples with respect to replacing CdSe529 with CdTe578 vice versa are also displayed (b). The transients in (a) show a faster build-up and a higher amplitude than in (b). The peaks shift to longer times for higher layer numbers (in both (a) and (b)). The onset of the laser pulse has been shifted to 16 ns in both graphs to better illustrate this (excitation wavelength: 442.8 nm; the data are already presented in reference [124]).

signal was obtained for a structure of CdSe nanocrystals topped by CdTe nanocrystals indicating the collection of holes in the CdTe top-layer. By reversing the structure of the sample and using CdTe nanocrystals topped by CdSe nanocrystals we were able to prove by negative SPV-signal the collection of electrons in the CdSe top-layer. The sign of the SPV-signal was only dependent on the order of the CdTe-CdSe nanocrystal layers and no spectral influence or time dependencies could alter the SPV-sign. This proves the collection of electrons in the CdSe and the holes in CdTe nanocrystals as expected from the intrinsic type II alignment of bulk CdTe and bulk CdSe. [54]

The SPV-signal was almost completely quenched when the inter-layer distance was doubled (from 1 nm to 2 nm). This confirms that the SPV-signal observed has to be attributed to charge separation effects in the layered nanocrystal structure since no other interface such as nanocrystals-mica or nanocrystals-FTO caused any significant additional charge separation. There are thus two possibilities of obtaining charge separation: first, the expected charge separation at the type II interface of CdTe and CdSe nanocrystals and second, the photoexciation creates free charge carriers that are diffusing in the heterostructures and lead to an SPV-signal in analogy to reference [126]. Reference samples of three CdTe or three CdSe layers on FTO substrates indicate in fact that there are photogenerated free charge carriers available in the investigated films (fig. 5.6). However, these photoexcited charges in all reference samples always lead to a charge separation with the same sign. Therefore, the presence of photoexcited free charge carriers does not contradict the charge selectivity of the type II alignment between CdTe and CdSe nanocrystals. We observe that the sign of the SPV-signal depends only on the orientation of the CdTe-CdSe interface. Thus, the charge separating properties of this type II interface is proven.

The experiment with increased barrier width between the nanocrystals conforms to the expected tunneling / hopping transfer dynamics. Tunneling depends exponentially on the barrier width. Thus, doubling the barrier width is expected to decrease the transfer rate substantially. Moreover, optical measurements with LBL samples containing PSS did not indicate additional quenching due to the presence of the PSS polymers. Hence, the presented closely packed assemblies of CdTe578 and CdSe529 nanocrystals can therefore really be called type II tunneling structures.

The distance dependence of the SPV-signal reveals diffusion phenomena in layered nanocrystal structures. We took advantage of the charge selectivity of the type II alignment to separate the charges at a well-located interface so that one type of charge carriers could be confined to a specific layer. This concept obviously works as we can clearly attribute the increase in the SPV-signal in multilayered CdSe samples to electron diffusion over an increased number of CdSe layers. On the one hand, the study provides evidence of how much each layer contributes to the SPV-signal in dependence

on the multilayer thickness. On the other hand, time-resolved measurements showed that, with selective excitation of only the top-layer compared to excitation of both top and multilayers, no significant differences could be detected in the signal shape. This indicates that charges created in the CdTe top layer produce the same signal as charges created in the whole sample. Since holes are confined to the CdTe top-layer of the structure in question, the increase in the SPV-signal must be attributed to electron diffusion in the CdSe multilayers.

The diffusion dynamics found in the CdTe multilayers cannot be attributed so clearly to hole diffusion since excitation intensity dependent time resolved measurements show some differences after a delay. Only the evaluation of the contribution of CdSe to the SPV-spectrum indicates hole diffusion dynamics. All-in-all the diffusion process in CdTe multilayers was shown to be slower than in CdSe multilayers. This is well in agreement with the expectation that hole diffusion is much slower than electron diffusion in closely packed nanocrystal structures with an organic tunneling barrier of about 1 nm. [36]

To quantify the diffusion a rough estimate can be obtained with an approximation in analogy to reference [127]. Diffusion was studied there with SPV and Monte-Carlo simulation. The system investigated was similar with regard to the asymmetry: Photoexcitation on a top layer leads to charge injection in a thick layer and subsequent diffusion in the thick layer. Diffusion starts from one side of the boundaries and its development is evaluated in the sample area where the diffusion takes place. The following correlation of the peak time t_{peak} of SPV-transients, diffusion constant D and a dielectric screening length λ_S was obtained (by Monte-Carlo simulation with diffusion coefficients varying from 10^{-3} to 10^{-8} cm^2/s):

$$\lambda_S \approx \frac{2}{2.5} \cdot D \cdot t_{peak} \tag{5.1}$$

Apart from the factor $\frac{2}{2.5}$ this is the same as the characteristic diffusion length distance l_{diff} for free diffusion in unlimited space for one dimension (equation 2.22). The finding of reference [127] is that the diffusion distance in such asymmetric structures is correlated to the characteristic diffusion length l_{diff} (of a symmetric structure) which may be comprehensive in some way. Thus, the above mentioned equation may deliver a rough estimate of the diffusion process until further theoretic description or simulation provides more precise formula.

This formula (equation 5.1) may be applied to the peak delay times t_{peak} shown in fig. 5.6. The expected layer thickness can be used instead of the screening length λ_S. In this way, a rough estimate can be obtained for the order of magnitude of the diffusion parameters which may be compared with literature values. Thus, a mobility of the order of $10^{-4} - 10^{-6}(\frac{cm^2}{Vs})$ can be estimated in CdSe529 multilayers and of

$10^{-6} - 10^{-8}(\frac{cm^2}{Vs})$ in CdTe nanocrystal multilayers. This corresponds to an inter-layer hopping time (equation 2.23) of about 10 ns to 100μs.

The value assumed for diffusion in CdSe529 compares well to the studies of references [36,37] which reported an electron mobility of $10^{-4} - 10^{-6} cm^2/Vs$ [36] over CdSe nanocrystal layers separated by about 1 nm of organics. Publications for nanocrystal assemblies with decreased inter-particle distance or changed chemistry or ligands showed much higher electron mobilities in the order of $10^{-2}\frac{cm^2}{Vs}$ [39,40,126,128] and up to $10^{-1}\frac{cm^2}{Vs}$ [129]. Thermal sintering which is supposed to destroy the nanocrystaline nature of CdSe nanocrystals provided a conductivity of $1\frac{cm^2}{Vs}$ [38]. Since Ginger et al. [36] and Hikmet et al. [37] reported electron diffusion values similar to the values we obtained for comparable closely packed nanocrystal systems, this highlights the fact that SPV can be used to obtain information on the charge carrier diffusion dynamics. However, before SPV can be used for diffusion studies, the model mentioned above must be refined using, for example, Monte-Carlo simulation.

Moreover we found that light which was absorbed at a significant distance from the charge separating interface contributes similary to the charge separation signal as light absorbed in the adjacent CdTe-CdSe layers. This may be an indication of exciton diffusion or for photo-creation of free charge carriers in the nanocrystal layers (in analogy to reference [126]). Let us assume a significant creation of free charges in the multilayer part. Then electrons and holes may diffuse independently. Thus, when one of them reach the type II interface, one type of charge carriers gets "trapped" in the top layer. The diffusion of this trapped charge species is hence causing an SPV-signal. The other type of charge carrier continues its diffusion in the multilayers. If however charges created at the type II interface diffuse, they get directly separated and it is the other type of charge carriers which enhances the SPV-signal due to diffusion. This would imply that electrons and holes diffuse at a comparable speed since we cannot distinguish a significant difference for excitation in the monolayers or in the multilayers. Ginger et al. however reported a strong difference between electrons and holes for diffusion. [36] Exciton diffusion on the other hand might transfer the excitons to the type II interface where charge separation provides the free charge carriers for diffusion. Since the lifetime of bright excitons is typically below 1 ns this diffusion must be fast. However, initial preliminary experiments on exciton diffusion did not reveal fast exciton diffusion and no such indications have been found in existing literature. Diffusion of dark excitons is mentioned rarely in literature. However, it was reported that dark excitons could be recycled in energy transfer over CdTe nanocrystal layers. [48]

Although the mechanism of the observed diffusion cannot be determined exactly the charge separating properties of the type II alignment have been approved and used in other applications. Talgorn et al. found evidence of an increase in photoconductivity

in multilayered CdTe-CdSe films. [130] Moreover the photovoltaic effect was approved in closely packed films of CdTe-CdS or CdTe-CdSe nanocrystal devices. [131, 132]

In conclusion, the directionality of the charge separation of the CdTe578-CdSe529 interface studied was proven. Electrons are collected in CdSe, holes in CdTe nanocrystals. A strong dependence of the transfer on the inter-layer distance is shown which is consistent with the expected tunneling transfer dynamics. There is evidence of diffusion in layered CdTe and CdSe nanocrystal assemblies. The charge separating interface of CdTe and CdSe nanocrystals is used to ensure the creation of free charge carriers which diffuse over several nanocrystal layers. The exact mechanism for diffusion, especially in relation to the diffusing particles, could not be seen. However, diffusion of electrons over CdSe multilayers appears faster than diffusion of the charge carriers in CdTe multilayers.

6 Conclusions and Outlook

Closely packed nanocrystal systems have been investigated in this thesis with respect to charge separation by charge carrier tunneling. Clustered and layered samples have been analyzed using PL-measurements and SPV-methods. The most important findings are reviewed in the following. A short outlook is also provided for potential further aspects and application of the presented results.

The main purpose of this thesis was to find and quantify electronic tunneling transfer in closely packed self-assembled nanocrystal structures presenting quantum mechanical barriers of about 1 nm width. We successfully used hybrid assemblies of CdTe and CdSe nanocrystals where the expected type II alignment between CdTe and CdSe typically leads to a concentration of electrons in CdSe and holes in CdTe nanocrystals. We were able to prove the charge selectivity of the CdTe-CdSe nanocrystal interface which induces charge separation. We mainly investigated the effects related to the electron transfer from CdTe to CdSe nanocrystals. Closely packing was achieved by two independent methods: the disordered colloidal clustering in solution and the layered assembly on dry glass substrates. Both methods lead to an inter-particle distance of about 1 nm of mainly organic material which acts as a tunneling barrier.

PL-spectroscopy was applied. The PL-quenching of the CdTe nanocrystals in hybrid assemblies indicates charge separation by electron transfer from CdTe to CdSe nanocrystals. A maximum quenching rate of up to 1/100 ps was measured leading to a significant global PL-quenching of up to about 70 % for the CdTe nanocrystals. It was shown that charge separation dynamics compete with energy transfer dynamics and that charge separation typically dominates. The quantum confinement effect was used to tune the energetic offset between the CdTe and CdSe nanocrystals. We thus observe a correlation of PL-quenching and offset of the energy states for the electron transfer. The investigated PL-quenching vanishes when this offset approaches 0.0 eV. The fact that PL-quenching and its correlation with the energetic offset was observed for both clustered and layered assembly provides a strong indirect indication of charge separation via electron transfer from CdTe to CdSe nanocrystals.

The main result of this thesis is the direct proof of the charge separation on the type II interface of CdTe and CdSe nanocrystal layers. SPV-measurements as a direct measurement methode showed clearly the directionality of charge separation since the SPV measures the electric field of the separated charges. Electrons are collected on CdSe nanocrystal layers, holes on CdTe nanocrystal layers. A change in the order between CdSe and CdTe therefore leads to a change in the sign of the SPV-signal. Both SPV-spectra and time-resolved SPV-measurements support this finding and showed that the charge selectivity of the CdTe-CdSe interface is unidirectional for the whole excitation spectrum and the entire investigated time range. This indicates that the directionality of the CdTe-CdSe interface is the only dominant charge separation mechanism that was observed. Hence, the type II alignment of the self-assembled nanocrystals used was clearly proven. Introducing an additional barrier between the nanocrystal layers doubled the barrier width so that the SPV-signal is quenched. This is consistent with tunneling transfer which is exponentially dependent on barrier width. Moreover, we learned that both absorption in CdTe and CdSe nanocrystals and the sample thickness contribute to the SPV-signal. Thus, we could observe electron diffusion in CdSe multilayers which was faster than the charge carrier diffusion dynamics in CdTe nanocrystal multilayers.

Future research may address the combination of energy transfer dynamics with the charge separation processes presented in this thesis. On the one hand, this may provide a better understanding of their fundamental processes and differentiate between excitonic FRET and electronic Dexter energy transfer. On the other hand, it may pave the way for imitation of the natural photosynthesis where both energy transfer and charge separation are realized on the nanoscale. The nanocrystals may be used as building blocks to replace the organic molecules of natural processes. The closely packed self-assembly of type II aligned nanocrystals may find application in solid state devices such as extremely thin absorber solar cells with surface enhanced substrates. Also colloidal application for water splitting may be an option, where semiconductor nanocrystals may provide both energy transfer and charge separation. The organic barrier around the particles may help to protect the semiconductor nanocrystals against degradation during photo-catalytic water splitting. Moreover, the semiconductor nanocrystals may be used as a tape rule for sensing the relative energetic alignment to other nanoparticles or molecules. The PL-quenching rate correlates with the offset of the energy levels which can be tuned due to the quantum confinement effect. PL-quenching studies may reveal the relative energetic alignment of other nanoparticles when experimental series of their closely packed hybrid assemblies with different nanocrystal sizes are analyzed.

Bibliography

[1] Ilan Gur, Neil A. Fromer, Michael L. Geier, and A. Paul Alivisatos. Air-stable all-inorganic nanocrystal solar cells processed from solution. *Science*, 310(5747):462–465, 2005.

[2] Prashant V. Kamat. Quantum dot solar cells. Semiconductor nanocrystals as light harvesters. *The Journal of Physical Chemistry C*, 112(48):18737–18753, 2008.

[3] Jin Ho Bang and Prashant V. Kamat. Quantum dot sensitized solar cells. A tale of two semiconductor nanocrystals: CdSe and CdTe. *ACS Nano*, 3(6):1467–1476, 2009.

[4] Joseph M. Luther, Matt Law, Matthew C. Beard, Qing Song, Matthew O. Reese, Randy J. Ellingson, and Arthur J. Nozik. Schottky solar cells based on colloidal nanocrystal films. *Nano Letters*, 8(10):3488–3492, 2008.

[5] Lili Han, Donghuan Qin, Xi Jiang, Yanshan Liu, Li Wang, Junwu Chen, and Yong Cao. Synthesis of high quality zinc-blende CdSe nanocrystals and their application in hybrid solar cells. *Nanotechnology*, 17(18):4736, 2006.

[6] Yi Zhou, Yunchao Li, Haizheng Zhong, Jianhui Hou, Yuqin Ding, Chunhe Yang, and Yongfang Li. Hybrid nanocrystal/polymer solar cells based on tetrapod-shaped $CdSe_x$ Te_{1-x} nanocrystals. *Nanotechnology*, 17(16):4041, 2006.

[7] Brian R. Saunders and Michael L. Turner. Nanoparticle-polymer photovoltaic cells. *Advances in Colloid and Interface Science*, 138(1):1 – 23, 2008.

[8] Sandeep Kumar and Gregory D. Scholes. Colloidal nanocrystal solar cells. *Microchimica Acta*, 160:315–325, 2008.

[9] Thomas Dittrich, Abdelhak Belaidi, and Ahmed Ennaoui. Concepts of inorganic solid-state nanostructured solar cells. *Solar Energy Materials and Solar Cells*, 95(6):1527 – 1536, 2011. [Special Issue : Thin film and nanostructured solar cells].

[10] A. P. Alivisatos. Semiconductor clusters, nanocrystals, and quantum dots. *Science*, 271(5251):933–937, 1996.

[11] Seth Coe, Wing-Keung Woo, Moungi Bawendi, and Vladimir Bulovic. Electroluminescence from single monolayers of nanocrystals in molecular organic devices. *Nature*, 420:800, 2002.

[12] Andreas Biebersdorf, Roland Dietmüller, Andrei S. Susha, Andrey L. Rogach, Sergey K. Poznyak, Dmitri V. Talapin, Horst Weller, Thomas A. Klar, and Jochen Feldmann. Semiconductor nanocrystals photosensitize C_{60} crystals. *Nano Letters*, 6(7):1559–1563, 2006.

[13] Mingyuan Gao, Junqi Sun, Eric Dulkeith, Nicolai Gaponik, Uli Lemmer, and Jochen Feldmann. Lateral patterning of CdTe nanocrystal films by the electric field directed layer-by-layer assembly method. *Langmuir*, 18(10):4098–4102, 2002.

[14] Hans-Juergen Eisler, Vikram C. Sundar, Moungi G. Bawendi, Michael Walsh, Henry I. Smith, and Victor Klimov. Color-selective semiconductor nanocrystal laser. *Applied Physics Letters*, 80(24):4614–4616, 2002.

[15] Y. Chan, J.-Michel Caruge, P. T. Snee, and M. G. Bawendi. Multiexcitonic two-state lasing in a CdSe nanocrystal laser. *Applied Physics Letters*, 85(13):2460–2462, 2004.

[16] Y.-W. Lin, W.-L. Tseng, and H.-T. Chang. Using a layer-by-layer assembly technique to fabricate multicolored-light-emitting films of CdSe@CdS and CdTe quantum dots. *Advanced Materials*, 18(11):1381–1386, 2006.

[17] S. A. Crooker, J. A. Hollingsworth, S. Tretiak, and V. I. Klimov. Spectrally resolved dynamics of energy transfer in quantum-dot assemblies: Towards engineered energy flows in artificial materials. *Phys. Rev. Lett.*, 89(18):186802, 2002.

[18] A. L. Rogach, D. S. Koktysh, M. Harrison, and N. A. Kotov. Layer-by-layer assembled films of HgTe nanocrystals with strong infrared emission. *Chemistry of Materials*, 12(6):1526–1528, 2000.

[19] T. Franzl, D. S. Koktysh, T. A. Klar, A. L. Rogach, J. Feldmann, and N. Gaponik. Fast energy transfer in layer-by-layer assembled CdTe nanocrystal bilayers. *Applied Physics Letters*, 84(15):2904–2906, 2004.

[20] T. Franzl, A. Shavel, A. L. Rogach, N. Gaponik, T. A. Klar, A. Eychmüller, and J. Feldmann. High-rate unidirectional energy transfer in directly assembled CdTe nanocrystal bilayers. *Small*, 1(4):392–395, 2005.

[21] S. Mayilo, J. Hilhorst, A. S. Susha, C. Hohl, T. Franzl, T. A. Klar, A. L. Rogach, and J. Feldmann. Energy transfer in solution-based clusters of CdTe nanocrys-

tals electrostatically bound by calcium ions. *Journal of Physical Chemistry C*, 112(37):14589–14594, 2008.

[22] Andrei S. Susha, Almudena Munoz Javier, Wolfgang J. Parak, and Andrey L. Rogach. Luminescent CdTe nanocrystals as ion probes and pH sensors in aqueous solutions. *Colloids and Surfaces A: Physicochemical and Engineering Aspects*, 281:40 – 43, 2006.

[23] T. Vossmeyer, L. Katsikas, M. Giersig, I. G. Popovic, K. Diesner, A. Chemseddine, A. Eychmueller, and H. Weller. CdS nanoclusters: Synthesis, characterization, size dependent oscillator strength, temperature shift of the excitonic transition energy, and reversible absorbance shift. *The Journal of Physical Chemistry*, 98(31):7665–7673, 1994.

[24] Andrey L. Rogach, Andreas Kornowski, Mingyuan Gao, Alexander Eychmüller, and Horst Weller. Synthesis and characterization of a size series of extremely small thiol-stabilized CdSe nanocrystals. *The Journal of Physical Chemistry B*, 103(16):3065–3069, 1999.

[25] Andrey L. Rogach, Thomas Franzl, Thomas A. Klar, Jochen Feldmann, Nikolai Gaponik, Vladimir Lesnyak, Alexey Shavel, Alexander Eychmüller, Yuri P. Rakovich, and John F. Donegan. Aqueous synthesis of thiol-capped CdTe nanocrystals: state-of-the-art. *The Journal of Physical Chemistry C*, 111(40):14628–14637, 2007.

[26] Andrey Rogach, Stephen V. Kershaw, Mike Burt, Mike T. Harrison, Andreas Kornowski, Alexander Eychmüller, and Horst Weller. Colloidally prepared HgTe nanocrystals with strong room-temperature infrared luminescence. *Advanced Materials*, 11(7):552–555, 1999.

[27] C. B. Murray, D. J. Norris, and M. G. Bawendi. Synthesis and characterization of nearly monodisperse CdE (E = sulfur, selenium, tellurium) semiconductor nanocrystallites. *Journal of the American Chemical Society*, 115(19):8706–8715, 1993.

[28] O. I. Micic, J. R. Sprague, C. J. Curtis, K. M. Jones, J. L Machol, A. J. Nozik, H. Giessen, B. Fluegel, G. Mohs, and N. Peyghambarian. Synthesis and characterization of InP, GaP, and $GaInP_2$ quantum dots. *The Journal of Physical Chemistry*, 99(19):7754–7759, 1995.

[29] James R. Heath. Covalency in semiconductor quantum dots. *Chem. Soc. Rev.*, 27:65–71, 1998.

[30] H. Lee, S.W. Yoon, J.P. Ahn, Y.D. Suh, J.S. Lee, H. Lim, and D. Kim. Synthesis of type II CdTe/CdSe heterostructure tetrapod nanocrystals for PV applications. *Solar Energy Materials and Solar Cells*, 93(6-7):779 – 782, 2009.

[31] Dirk Dorfs, Thomas Franzl, Ruth Osovsky, Maya Brumer, Efrat Lifshitz, Thomas A. Klar, and Alexander Eychmüller. Type-I and type-II nanoscale heterostructures based on CdTe nanocrystals: A comparative study. *Small*, 4(8):1148–1152, 2008.

[32] Sergei A. Ivanov, Andrei Piryatinski, Jagjit Nanda, Sergei Tretiak, Kevin R. Zavadil, William O. Wallace, Don Werder, and Victor I. Klimov. Type-II core/shell CdS/ZnSe nanocrystals: Synthesis, electronic structures, and spectroscopic properties. *Journal of the American Chemical Society*, 129(38):11708–11719, 2007.

[33] Jonathan E. Halpert, Venda J. Porter, John P. Zimmer, and Moungi G. Bawendi. Synthesis of CdSe/CdTe nanobarbells. *Journal of the American Chemical Society*, 128(39):12590–12591, 2006.

[34] Sandeep Kumar, Marcus Jones, Shun S. Lo, and Gregory D. Scholes. Nanorod heterostructures showing photoinduced charge separation. *Small*, 3(9):1633–1639, 2007.

[35] A. Biebersdorf, R. Dietmüller, A. Ohlinger, T. Klar, J. Feldmann, D. Talapin, and H. Weller. Photodoping with CdSe nanocrystals as a tool to probe trap-state distributions in C_{60} crystals. *Applied Physics B: Lasers and Optics*, 93:239–243, 2008.

[36] D. S. Ginger and N. C. Greenham. Charge injection and transport in films of CdSe nanocrystals. *Journal of Applied Physics*, 87(3):1361–1368, 2000.

[37] R. A. M. Hikmet, D. V. Talapin, and H. Weller. Study of conduction mechanism and electroluminescence in CdSe/ZnS quantum dot composites. *Journal of Applied Physics*, 93(6):3509–3514, 2003.

[38] Brent A. Ridley, Babak Nivi, and Joseph M. Jacobson. All-inorganic field effect transistors fabricated by printing. *Science*, 286(5440):746–749, 1999.

[39] Dong Yu, Congjun Wang, and Philippe Guyot-Sionnest. n-type conducting CdSe nanocrystal solids. *Science*, 300(5623):1277–1280, 2003.

[40] Dong Yu, Brian L. Wehrenberg, Praket Jha, Jiasen Ma, and Philippe Guyot-Sionnest. Electronic transport of n-type CdSe quantum dot films: Effect of film treatment. *Journal of Applied Physics*, 99(10):104315, 2006.

[41] Leeor Kronik and Yoram Shapira. Surface photovoltage phenomena: theory, experiment, and applications. *Surface Science Reports*, 37:1 – 206, 1999.

[42] Iván Mora-Seró, Thomas Dittrich, Germà Garcia-Belmonte, and Juan Bisquert. Determination of spatial charge separation of diffusing electrons by transient photovoltage measurements. *Journal of Applied Physics*, 100(10):103705, 2006.

[43] Iván Mora-Seró, Thomas Dittrich, Andrei S. Susha, Andrey L. Rogach, and Juan Bisquert. Large improvement of electron extraction from CdSe quantum dots into a TiO_2 thin layer by N3 dye coabsorption. *Thin Solid Films*, 516(20):6994 – 6998, 2008. Proceedings on Advanced Materials and Concepts for Photovoltaics EMRS 2007 Conference, Strasbourg, France.

[44] I. Mora-Sero, J. Bisquert, Th. Dittrich, A. Belaidi, A. S. Susha, and A. L. Rogach. Photosensitization of TiO_2 layers with CdSe quantum dots: Correlation between light absorption and photoinjection. *The Journal of Physical Chemistry C*, 111(40):14889–14892, 2007.

[45] Th. Förster. Zwischenmolekulare Energiewanderung und Fluoreszenz. *Annalen der Physik*, 437(1-2):55–75, 1948.

[46] D. L. Dexter. A theory of sensitized luminescence in solids. *The Journal of Chemical Physics*, 21(5):836–850, 1953.

[47] Thomas Franzl. *Energietransfer in Nanokristall-Kaskadenstrukturen*. PhD thesis, Ludwig-Maximilians-Universität München, 2007.

[48] Thomas Franzl, Thomas A. Klar, Stefan Schietinger, Andrey L. Rogach, and Jochen Feldmann. Exciton recycling in graded gap nanocrystal structures. *Nano Letters*, 4(9):1599–1603, 2004.

[49] Andrey A. Lutich, Guoxin Jiang, Andrei S. Susha, Andrey L. Rogach, Fernando D. Stefani, and Jochen Feldmann. Energy transfer versus charge separation in type-II hybrid organic-inorganic nanocomposites. *Nano Letters*, 9(7):2636–2640, 2009.

[50] T. Franzl, D. S. Koktysh, T. A. Klar, A. L. Rogach, J. Feldmann, and N. Gaponik. Fast energy transfer in layer-by-layer assembled CdTe nanocrystal bilayers. *Applied Physics Letters*, 84(15):2904–2906, 2004.

[51] H. Ibach and H. Lueth. *Festkörperphysik: Einführung in die Grundlagen*. Springer-Lehrbuch. Springer, 2008.

[52] P. Würfel. *Physik der Solarzellen*. Spektrum Hochschultaschenbuecher. Spektrum Akademischer Verlag, 2000.

[53] Steven C. Erwin, Lijun Zu, Michael I. Haftel, Alexander L. Efros, Thomas A. Kennedy, and David J. Norris. Doping semiconductor nanocrystals. *Nature*, 436:91, 2005.

[54] S. H. Wei, S. B. Zhang, and A. Zunger. First-principles calculation of band offsets, optical bowings, and defects in CdS, CdSe, CdTe, and their alloys. *Journal of Applied Physics*, 87(3):1304–1311, 2000.

[55] L. Weinhardt, O. Fuchs, D. Gross, G. Storch, E. Umbach, N. G. Dhere, A. A. Kadam, S. S. Kulkarni, and C. Heske. Band alignment at the CdS/Cu(In,Ga)S_2 interface in thin-film solar cells. *Applied Physics Letters*, 86(6):062109, 2005.

[56] Charles Kittel (editors:Jochen Mattias Gress and Anne Lessard). *Einführung in die Festkörperphysik*. Oldenbourg Verlag, 12th. edition, 1999.

[57] C. Cohen-Tannoudji, B. Diu, and F. Laloë. *Quantenmechanik*. Number Bd. 1 in Quantenmechanik. De Gruyter, 2007.

[58] F. Schwabl. *Quantenmechanik*. Springer, 2005.

[59] Wikipedia. Teilchen im Kasten — Wikipedia, Die freie Enzyklopädie, 2012. [Online; accessed 17-November-2012].

[60] W. Heisenberg. Über den anschaulichen Inhalt der quantentheoretischen Kinematik und Mechanik. *Zeitschrift für Physik*, 43:172–198, 1927.

[61] E. Schrödinger. An undulatory theory of the mechanics of atoms and molecules. *Phys. Rev.*, 28:1049–1070, 1926.

[62] Nataliya Piven, Andrei S. Susha, Markus Döblinger, and Andrey L. Rogach. Aqueous synthesis of alloyed $CdSe_xTe_{1-x}$ nanocrystals. *The Journal of Physical Chemistry C*, 112(39):15253–15259, 2008.

[63] Nikolai Gaponik, Dmitri V. Talapin, Andrey L. Rogach, Kathrin Hoppe, Elena V. Shevchenko, Andreas Kornowski, Alexander Eychmüller, and Horst Weller. Thiol-capping of CdTe nanocrystals: an alternative to organometallic synthetic routes. *The Journal of Physical Chemistry B*, 106(29):7177–7185, 2002.

[64] Zhiyong Tang, Zhenli Zhang, Ying Wang, Sharon C. Glotzer, and Nicholas A. Kotov. Self-assembly of CdTe nanocrystals into free-floating sheets. *Science*, 314(5797):274–278, 2006.

[65] Christian Mauser. *Ladungsträgerdynamik und Coulombeffekte in Halbleiter-Tetrapods*. PhD thesis, Fakultät für Physik der Ludwig-Maximilians-Universität München, 2010.

[66] Wikipedia. Cubic crystal system — wikipedia, the free encyclopedia, 2012. [Online; accessed 25-November-2012].

[67] Yasuaki Masumoto and Koji Sonobe. Size-dependent energy levels of CdTe quantum dots. *Phys. Rev. B*, 56:9734–9737, 1997.

[68] Landolt-Börnstein (editor: W. Martienssen). *Landolt-Börnstein - Numerical Data and Functional Relationships in Science and Technology*. Springer, 1999.

[69] D. J. Chadi, John P. Walter, Marvin L. Cohen, Y. Petroff, and M. Balkanski. Reflectivities and electronic band structures of CdTe and HgTe. *Phys. Rev. B*, 5:3058–3064, 1972.

[70] Xiaojie Chen, Xinlei Hua, Jinsong Hu, Jean-Marc Langlois, and William A. Goddard. Band structures of II-VI semiconductors using Gaussian basis functions with separable ab initio pseudopotentials: Application to prediction of band offsets. *Phys. Rev. B*, 53:1377–1387, 1996.

[71] Dmitri V. Talapin. *Experimental and theoretical studies on the formation of highly luminescent II-VI, III-V and core-shell semiconductor nanocrystals*. PhD thesis, University of Hamburg, 2002.

[72] A. I. Ekimov, F. Hache, M. C. Schanne-Klein, D. Ricard, C. Flytzanis, I. A. Kurdryavtsev, T. V. Yazeva, A. V. Rodina, and Al. I. Efros. Absorption and intensity-dependent photoluminescence measurements on CdSe quantum dots: assignment of the first electronic transitions. *J. Opt. Soc. Am. B*, 10:100, 1993.

[73] Herwig Döllefeld, Horst Weller, and Alexander Eychmüller. Semiconductor nanocrystal assemblies: Experimental pitfalls and a simple model of particle-particle interaction. *The Journal of Physical Chemistry B*, 106(22):5604–5608, 2002.

[74] Robert W. Meulenberg, Jonathan R.I. Lee, Abraham Wolcott, Jin Z. Zhang, Louis J. Terminello, and Tony van Buuren. Determination of the exciton binding energy in CdSe quantum dots. *ACS Nano*, 3(2):325–330, 2009.

[75] Gregory D. Scholes and Garry Rumbles. Excitons in nanoscale systems. *Nature Materials*, 5:683, 2006.

[76] Andreas Biebersdorf. *Photosensibilisierung von C_{60} durch halbleitende Nanokristalle*. PhD thesis, Ludwig-Maximilians-Universität München, 2007.

[77] H.M. Schmidt and H. Weller. Quantum size effects in semiconductor crystallites: Calculation of the energy spectrum for the confined exciton. *Chemical Physics Letters*, 129(6):615 – 618, 1986.

[78] W. Demtröder. *Molekülphysik: Theoretische Grundlagen und experimentelle Methoden*. Oldenbourg Wissensch.Vlg, 2003.

[79] Wikipedia. Selection rule — wikipedia, the free encyclopedia, 2012. [Online; accessed 18-November-2012].

[80] Arjan Jeroen Houtepen. *Charge injection and transpoert in quantum confined and disordered systems.* PhD thesis, Universiteit Utrecht, 2007.

[81] R A Marcus. Chemical and electrochemical electron-transfer theory. *Annual Review of Physical Chemistry*, 15(1):155–196, 1964.

[82] J. Müller, J. M. Lupton, A. L. Rogach, J. Feldmann, D. V. Talapin, and H. Weller. Monitoring surface charge movement in single elongated semiconductor nanocrystals. *Phys. Rev. Lett.*, 93:167402, Oct 2004.

[83] Allen Miller and Elihu Abrahams. Impurity conduction at low concentrations. *Phys. Rev.*, 120:745–755, Nov 1960.

[84] U. Bockelmann and G. Bastard. Phonon scattering and energy relaxation in two-, one-, and zero-dimensional electron gases. *Phys. Rev. B*, 42(14):8947–8951, 1990.

[85] H. Benisty, C. M. Sotomayor-Torrès, and C. Weisbuch. Intrinsic mechanism for the poor luminescence properties of quantum-box systems. *Phys. Rev. B*, 44(19):10945–10948, 1991.

[86] T. Inoshita and H. Sakaki. Electron relaxation in a quantum dot: Significance of multiphonon processes. *Phys. Rev. B*, 46(11):7260–7263, 1992.

[87] Richard D. Schaller, Jeffrey M. Pietryga, Serguei V. Goupalov, Melissa A. Petruska, Sergei A. Ivanov, and Victor I. Klimov. Breaking the phonon bottleneck in semiconductor nanocrystals via multiphonon emission induced by intrinsic nonadiabatic interactions. *Phys. Rev. Lett.*, 95(19):196401, 2005.

[88] D. M. Mittleman, R. W. Schoenlein, J. J. Shiang, V. L. Colvin, A. P. Alivisatos, and C. V. Shank. Quantum size dependence of femtosecond electronic dephasing and vibrational dynamics in CdSe nanocrystals. *Phys. Rev. B*, 49(20):14435–14447, 1994.

[89] Gregory D. Scholes. Long-range resonance energy transfer in molecular systems. *Annual Review of Physical Chemistry*, 54(1):57–87, 2003.

[90] L. Stryer and R. P. Haugland. Energy transfer: a spectroscopic ruler. *The Proceedings of the National Academy of Sciences (USA)*, 58:719–726, 1967.

[91] Hans C. Wolf Hermann Haken. *Atom- und Quantenphysik: Einführung in die experimentellen und theoretischen Grundlagen*. Springer, 2004.

[92] Mitio Inokuti and Fumio Hirayama. Influence of energy transfer by the exchange mechanism on donor luminescence. *The Journal of Chemical Physics*, 43(6):1978–1989, 1965.

[93] A. Monguzzi, R. Tubino, and F. Meinardi. Upconversion-induced delayed fluorescence in multicomponent organic systems: Role of dexter energy transfer. *Phys. Rev. B*, 77(15):155122, Apr 2008.

[94] Adolf Fick. Über Diffusion. *Annalen der Physik*, 170(1):59–86, 1855.

[95] Adolf Fick. V. on liquid diffusion. *Philosophical Magazine Series 4*, 10:30–39, 1855.

[96] S. Chandrasekhar. Stochastic problems in physics and astronomy. *Rev. Mod. Phys.*, 15(1):1–89, 1943.

[97] Michael J. Saxton and Jacobson Ken. Single-particle tracking: Applications to membrane dynamics. *Annual Review of Biophysics and Biomolecular Structure*, 26:373–399, 1997.

[98] Kwog K. Ng S. M. Sze. *Physics of Semiconductor Devices (Third Edition)*. John Wiley and Sons, 2007.

[99] Paul E. Shaw, Arvydas Ruseckas, and Ifor D. W. Samuel. Exciton diffusion measurements in poly(3-hexylthiophene). *Advanced Materials*, 20(18):3516–3520, 2008.

[100] Albert Einstein. Über die von der molekularkinetischen Theorie der Wärme geforderte Bewegung von in ruhenden Flüssigkeiten suspendierten Teilchen. *Annalen der Physik (Leipzig)*, 17:549 – 560, 1905.

[101] Albert Einstein. Zur Theorie der Brownschen Bewegung. *Annalen der Physik (Leipzig)*, 19:371, 1906.

[102] Marian von Smoluchowski. Zur kinetischen Theorie der Brownschen Molekularbewegung und der Suspensionen. *Annalen der Physik (Leipzig)*, 21:756–780, 1906.

[103] M. Nishioka, S. Tsukamoto, Y. Nagamune, T. Tanaka, and Y. Arakawa. Fabrication of InGaAs strained quantum wires using selective MOCVD growth on SiO_2-patterned GaAs substrate. *Journal of Crystal Growth*, 124(1-4):502 – 506, 1992.

[104] W. Wegscheider, G. Schedelbeck, G. Abstreiter, M. Rother, and M. Bichler. Atomically precise GaAs/AlGaAs quantum dots fabricated by twofold cleaved edge overgrowth. *Phys. Rev. Lett.*, 79:1917–1920, 1997.

[105] Stefan Schietinger. Gerichteter Energie Transfer in Halbleiter-Quantenpunkt-Schichtsystemen. *Diploma thesis*, 2003.

[106] Dmitri V. Talapin, Andrey L. Rogach, Elena V. Shevchenko, Andreas Kornowski, Markus Haase, and Horst Weller. Dynamic distribution of growth rates within the ensembles of colloidal II-VI and III-V semiconductor nanocrystals as a factor governing their photoluminescence efficiency. *Journal of the American Chemical Society*, 124(20):5782–5790, 2002.

[107] W. William Yu, Lianhua Qu, Wenzhuo Guo, and Xiaogang Peng. Experimental determination of the extinction coefficient of CdTe, CdSe, and CdS nanocrystals. *Chemistry of Materials*, 15(14):2854–2860, 2003.

[108] Celso de Mello Donega and Rolf Koole. Size dependence of the spontaneous emission rate and absorption cross section of CdSe and CdTe quantum dots. *The Journal of Physical Chemistry C*, 113(16):6511–6520, 2009.

[109] Iwan Moreels, Karel Lambert, David De Muynck, Frank Vanhaecke, Dirk Poelman, José C. Martins, Guy Allan, and Zeger Hens. Composition and size-dependent extinction coefficient of colloidal PbSe quantum dots. *Chemistry of Materials*, 19(25):6101–6106, 2007.

[110] Gero Decher. Fuzzy nanoassemblies: Toward layered polymeric multicomposites. *Science*, 277(5330):1232–1237, 1997.

[111] Hiroyuki Kaigawa, Koji Yamamoto, and Yasuhiro Shigematsu. Etching of thermally grown SiO_2 by NH_4OH in mixture of NH_4OH and H_2O_2 cleaning solution. *Japanese Journal of Applied Physics*, 33(Part 1, No. 7A):4080–4085, 1994.

[112] Wikipedia. Beer-lambert law — wikipedia, the free encyclopedia, 2012. [Online; accessed 9-December-2012].

[113] Alain Chiron de la Casinière. *Le Rayonnement solaire dans l'environnement terrestre*. EPU, Editions Publibook universite. Publibook Societe des ecrivains, 2003.

[114] Dieter Gross, Andrei S. Susha, Thomas A. Klar, Enrico Da Como, Andrey L. Rogach, and Jochen Feldmann. Charge separation in type II tunneling structures of close-packed CdTe and CdSe nanocrystals. *Nano Letters*, 8(5):1482–1485, 2008.

[115] C. A. Leatherdale and M. G. Bawendi. Observation of solvatochromism in CdSe colloidal quantum dots. *Phys. Rev. B*, 63(16):165315, 2001.

[116] Ying Wang, Zhiyong Tang, Miguel A. Correa-Duarte, Isabel Pastoriza-Santos, Michael Giersig, Nicholas A. Kotov, and Luis M. Liz-Marzán. Mechanism of strong luminescence photoactivation of citrate-stabilized water-soluble nanoparticles with CdSe cores. *The Journal of Physical Chemistry B*, 108(40):15461–15469, 2004.

[117] Iván Mora-Seró, Dieter Gross, Tobias Mittereder, Andrey A. Lutich, Andrei S. Susha, Thomas Dittrich, Abdelhak Belaidi, Ruben Caballero, Fernando Langa, Juan Bisquert, and Andrey L. Rogach. Nanoscale interaction between CdSe or CdTe nanocrystals and molecular dyes fostering or hindering directional charge separation. *Small*, 6(2):221–225, 2010.

[118] Sixto Giménez, Andrey L. Rogach, Andrey A. Lutich, Dieter Gross, Andreas Pöschl, Andrei S. Susha, Iván Mora-Seró, Teresa Lana-Villarreal, and Juan Bisquert. Energy transfer versus charge separation in hybrid systems of semiconductor quantum dots and Ru-dyes as potential co-sensitizers of TiO_2-based solar cells. *Journal of Applied Physics*, 110(1):014314, 2011.

[119] Qinghui Zeng, Xianggui Kong, Yajuan Sun, Youlin Zhang, Langping Tu, Jialong Zhao, and Hong Zhang. Synthesis and optical properties of type II CdTe/CdS core/shell quantum dots in aqueous solution via successive ion layer adsorption and reaction. *The Journal of Physical Chemistry C*, 112(23):8587–8593, 2008.

[120] Yoshiyuki Nonoguchi, Takuya Nakashima, and Tsuyoshi Kawai. Tuning band offsets of core/shell CdS/CdTe nanocrystals. *Small*, 5(21):2403–2406, 2009.

[121] Sergei A. Ivanov, Jagjit Nanda, Andrei Piryatinski, Marc Achermann, Laurent P. Balet, Ilia V. Bezel, Polina O. Anikeeva, Sergei Tretiak, and Victor I. Klimov. Light amplification using inverted core/shell nanocrystals: Towards lasing in the single-exciton regime. *The Journal of Physical Chemistry B*, 108(30):10625–10630, 2004.

[122] Mingyan Wu, Prasun Mukherjee, Daniel N. Lamont, and David H. Waldeck. Electron transfer and fluorescence quenching of nanoparticle assemblies. *The Journal of Physical Chemistry C*, 114(13):5751–5759, 2010.

[123] Nilanka P. Gurusinghe, Nishshanka N. Hewa-Kasakarage, and Mikhail Zamkov. Composition-tunable properties of CdS_xTe_{1-x} alloy nanocrystals. *The Journal of Physical Chemistry C*, 112(33):12795–12800, 2008.

[124] Dieter Gross, Ivan Mora-Sero, Thomas Dittrich, Abdelhak Belaidi, Christian Mauser, Arjan J. Houtepen, Enrico Da Como, Andrey L. Rogach, and Jochen Feldmann. Charge separation in type II tunneling multilayered structures of CdTe and CdSe nanocrystals directly proven by surface photovoltage spectroscopy. *Journal of the American Chemical Society*, 132(17):5981–5983, 2010.

[125] Dieter Gross, Ivan Mora-Sero, Thomas Dittrich, Andrey S. Susha, Enrico Da Como, Andrey L. Rogach, and Jochen Feldmann. Charge separation in self-assembeled type-II tunneling structures of CdTe and CdSe nanocrystals. In *Spie Optics+Photonics*, number 7303-01 in Session 1 of Nanophotonic Materials VI, 2009.

[126] Elise Talgorn, Elli Moysidou, Ruben D. Abellon, Tom J. Savenije, Albert Goossens, Arjan J. Houtepen, and Laurens D. A. Siebbeles. Highly photoconductive CdSe quantum-dot films: Influence of capping molecules and film preparation procedure. *The Journal of Physical Chemistry C*, 114(8):3441–3447, 2010.

[127] Thomas Dittrich, Iván Mora-Seró, Germà García-Belmonte, and Juan Bisquert. Temperature dependent normal and anomalous electron diffusion in porous TiO_2 studied by transient surface photovoltage. *Phys. Rev. B*, 73(4):045407, 2006.

[128] Maksym V. Kovalenko, Marcus Scheele, and Dmitri V. Talapin. Colloidal nanocrystals with molecular metal chalcogenide surface ligands. *Science*, 324(5933):1417–1420, 2009.

[129] Elise Talgorn, Ruben D. Abellon, Patricia J. Kooyman, Jorge Piris, Tom J. Savenije, Albert Goossens, Arjan J. Houtepen, and Laurens D. A. Siebbeles. Supercrystals of CdSe quantum dots with high charge mobility and efficient electron transfer to TiO_2. *ACS Nano*, 4(3):1723–1731, 2010.

[130] Elise Talgorn, Marnix A. de Vries, Laurens D. A. Siebbeles, and Arjan J. Houtepen. Photoconductivity enhancement in multilayers of CdSe and CdTe quantum dots. *ACS Nano*, 5(5):3552–3558, 2011.

[131] Rajesh K. Katiyar, Satyaprakash Sahoo, A.P.S. Gaur, Arun Singh, G. Morell, and R.S. Katiyar. Studies of photovoltaic properties of nanocrystalline thin films of CdS-CdTe. *Journal of Alloys and Compounds*, 509(41):10003 – 10006, 2011.

[132] Nir Yaacobi-Gross, Natalia Garphunkin, Olga Solomeshch, Aleksandar Vaneski, Andrei S. Susha, Andrey L. Rogach, and Nir Tessler. Combining ligand-induced quantum-confined stark effect with type II heterojunction bilayer structure in CdTe and CdSe nanocrystal-based solar cells. *ACS Nano*, 6(4):3128–3133, 2012.

Acknowledgments

The research for this thesis was carried out at the Photonics and Optoelectronics Group of the Ludwig-Maximilians-Universität München under the supervision of Prof. Jochen Feldmann. Many people have been involved and I would like to thank everybody for their help, time, enthusiasm, patience and understanding.

First of all, I thank my supervisor Prof. Jochen Feldmann who gave me the opportunity to work in his group on research projects for the preparation of my PhD-thesis. The combination of freedom to realize scientific research projects and discussion where we broke down the experimental outcome to their essential scientific results provided me together with the well equipped labs and the highly skilled, international, interdisciplinary group an optimal surrounding to conduct my research under his supervision. Moreover, I am very grateful for the opportunities to present my work on international conferences and workshops where I gained more experience in science and presenting.

I want to thank Prof. Andrey Rogach as my principle advisor for this thesis. It was a pleasure for me to work in his nanocrystal team. I would like thank him particularly for his uncomplicated support although he has now moved to Hong Kong. I am also very grateful to Prof. Thomas Klar, Dr. Enrico Da Como and Dr. Andrey Lutich who contributed considerably with valuable advice, ideas, critics, discussion and practical support.

I am deeply thankful to PD. Thomas Dittrich for the cooperation on SPV techniques. I share with him the idealisme for photovoltaics. The discussions and his advices have been very helpful. Moreover I thank him for his participation during my final exam. I thank Dr. Andrei Susha for his support with chemistry particularly with regard to the production of nanocrystals and the introduction into the nano-selfassembly techniques of layer-by-layer and clustering. It was also a pleasure for me to meet Dr. Iván Mora-Seró and Dr. Sixto Giménez in Berlin and Munich for research on hybrid systems of nanocrystals with dyes and to assist in writing some papers. In the cooperation with Dr. Arjan Houtepen we studied especially diffusion processes. This was a great support and pleasure for me.

I thank the students who worked with me for their studies: Regis Cahours, Gözde Tütüncüoglu and Olga Paseka for their internship in Munich, Tobias Mittereder for his work during his bachelor thesis and Alexander Ohlinger and Andreas Pöschl who did their diploma thesis. It was a good time to work with you as part of a small research

team and an important support to this thesis. I have had also a good time with my colleagues in our office, Ilka Kriegel, Alexander Urban, Christian Mauser, Sergiy Mayilo, Alexander Biebersdorf and I thank also the all rest of Feldmann's workgroup for their support in lab and the time we spend together.

Moreover, I thank my current colleagues from Leybold Optics who are pushing me to finalize this thesis. Especially I am grateful to Ms Avril Lang for her support with my English.

Of course, I want to thank my parents and the rest of my family who supported me during my studies and made it possible. Last but not least I thank Mariam Gross, my wife, for her support, encouragement and patience especially during the phase of writing the thesis.